



max planck institute
of biochemistry



Dissertation

DER FAKULTÄT FÜR BIOLOGIE
DER LUDWIG-MAXIMILIANS-UNIVERSITÄT MÜNCHEN
ZUR ERLANGUNG DES AKADEMISCHEN GRADES
DOCTOR RERUM NATURALIUM (DR. RER. NAT.)

In vitro reconstitution of the autophagic membrane scaffold

vorgelegt von

Anna Kaufmann

aus Dresden

AUGUST 2015

Eidesstattliche Erklärung

Ich versichere hiermit an Eides statt, dass die vorgelegte Dissertation von mir selbständig und ohne unerlaubte Hilfe angefertigt ist.

München, den 19. Februar 2016

Anna Kaufmann

Diese Dissertation wurde unter der Leitung von Dr. T. Wollert am Max-Planck-Institut für Biochemie in der Forschungsgruppe Molekulare Membran- und Organell-Biologie angefertigt.

ERSTGUTACHTERIN: PROF. DR. BARBARA CONRADT

ZWEITGUTACHTER: PROF. DR. THOMAS OTT

EINGEREICHT AM: 11. AUGUST 2015

TAG DER MÜNDLICHEN PRÜFUNG: 8. FEBRUAR 2016

Table of Contents

Abstract	1
Zusammenfassung	3
1. Introduction	5
1.1. General processes of autophagy	5
1.2. Regulation of macroautophagy	7
1.3. Molecular mechanisms of autophagy	9
1.3.1. Autophagy initiation	9
1.3.2. The role of PROPPINs in phagophore assembly	10
1.4. Ubiquitin-like (UBL) conjugation systems in autophagy	10
1.4.1. Molecular mechanism of UBL conjugation systems	10
1.4.2. ATG12–ATG5 complexes	12
1.5. Atg8/ATG8 specificities	13
1.5.1. Atg8/ATG8 in autophagosome formation	14
1.5.2. Involvement of Atg8/ATG8 proteins in sealing, tethering and fusion	15
1.5.3. Specificities of Atg8/ATG8-interacting proteins	17
1.6. Objectives of this study	18
2. Materials and Methods	21
2.1. Reagents	21
2.2. AFM experiments with yeast UBL proteins	24
2.2.1. Sample preparation	24
2.2.2. LSM (Laser Scanning Microscopy)	25
2.2.3. AFM (Atomic Force Microscopy)	25
2.3. Electron Microscopy of yeast cells	26
2.4. Cloning of human ATG proteins	28
2.5. Protein expression and purification	33
2.5.1. Test expressions	33
2.5.2. Large scale expression and purification	34
2.6. Protein and lipid labeling	36
2.7. Gel electrophoresis and Western Blotting	37
2.8. Preparation of Liposomes	39
2.9. <i>In vitro</i> lipidation reaction	39

2.10. Confocal microscopy	40
2.11. Primers	41
3. Results	47
3.1. Characterization of the yeast Atg8-scaffold by AFM	47
3.2. Electron microscopy of yeast cells	55
3.3. The human UBL protein toolbox	57
3.3.1. Expression and purification of human ATG8 proteins	57
3.3.2. Expression and purification of ATG3	60
3.3.3. Expression and purification of ATG12–ATG5	60
3.3.4. Expression and purification of ATG7	63
3.3.5. Detection of thioester intermediates	64
3.3.6. Expression and purification of ATG16L1 full-length and truncated forms	66
3.4. Conjugation of hATG8s to Giant Unilamellar Vesicles (GUVs)	71
3.4.1. ATG16L1 is necessary for hATG8 lipidation	71
3.4.2. Lipidation efficiency depends on labeling and Atg8 homolog	73
3.5. FRAP experiments on GUVs	75
4. Discussion	79
4.1. The autophagic scaffold in yeast	79
4.1.1. The autophagic scaffold in comparison to canonical membrane coats	81
4.1.2. Previous discussions about a possible autophagosomal membrane scaffold	84
4.2. Varying roles for Atg18 and Atg21 in autophagosome formation	85
4.3. The autophagic scaffold in humans	86
4.3.1. Reconstituted lipidation reaction with hATG8s	87
4.3.2. Possible scaffold formation with human UBL autophagic proteins	88
5. Outlook	91
A. Appendix	93
A.1. ATG12–ATG5 production attempts	93
A.2. Testexpression of ATG7 in insect cells	94
A.3. Testexpression of ATG16L1 in insect cells	95
A.4. Additional lipidation experiments	96
A.5. Non-starved yeast cells imaged with electron microscopy	98

Table of Contents

References	99
Acknowledgements	111
Curriculum vitae	113
Publications	115

Abstract

Autophagy is a cellular recycling process where cytoplasmic material is delivered to the lysosome for degradation. It is fundamental for the homeostasis of cells, but is also involved in various diseases. During autophagy, cytoplasmic components are sequestered by a cup-shaped membrane cistern, which closes to form a double-membrane vesicle, the autophagosome. Upon fusion of the autophagosome with the lysosome its contents are degraded and can be recycled. Numerous proteins cooperate for autophagosome formation, including two intertwined Ubiquitin-like (UBL) systems: the first UBL protein, Atg12, is conjugated to Atg5, and the conjugate further associates with Atg16. The second UBL protein, Atg8, is conjugated to phosphatidylethanolamine (PE) in the autophagosomal membrane, which is catalyzed by Atg12–Atg5–Atg16. These systems are conserved in mammals, albeit more diverse. The human system possesses several ATG12–ATG5 binding proteins, as well as at least seven homologs of Atg8.

Previous work revealed that the components of the *S. cerevisiae* UBL systems self-assemble on membranes to form an immobile structure. Based on these results the hypothesis emerged, that the UBL proteins constitute the building blocks of a new kind of membrane scaffold. The first aim of this thesis was to verify this hypothesis with Atomic Force Microscopy (AFM). Therefore, Atg8 conjugation to PE was reconstituted on supported lipid bilayers. AFM demonstrated, that indeed Atg8–PE forms together with Atg12–Atg5–Atg16 a so far undescribed membrane scaffold. Atg12–Atg5 associates with Atg8–PE on the membrane and forms homogeneous complexes. These complexes are connected by Atg16 antiparallel tetramers, which constitute the edges of the scaffold.

The second aim of this thesis was to reconstitute the two human UBL systems *in vitro*. In a first step, all participating proteins were expressed and purified. This complete set of essential components was the prerequisite for further experiments and its reconstitution was achieved for the first time in this thesis. The interaction of recombinantly expressed human ATG proteins on liposomes was characterized with fluorescence microscopy, including fluorescence recovery after photo-bleaching (FRAP) experiments. These experiments demonstrated that the conjugation efficiency of hATG8s was homolog dependent. Furthermore, these experiments indicated that also in the human system a membrane scaffold is assembled. These findings pave the way towards a better understanding of the molecular basis of autophagy-related diseases.

Zusammenfassung

Autophagozytose ist ein zellulärer Recyclingprozess, bei dem zytoplasmatisches Material zum Lysosom transportiert wird um dort abgebaut zu werden. Dieser Prozess ist fundamental für das zelluläre Gleichgewicht, spielt aber auch bei verschiedenen Krankheiten eine Rolle. Während der Autophagozytose umschließt eine becherförmige Membran zytoplasmatische Komponenten. Diese Membran schließt sich und bildet ein Doppelmembranvesikel, das Autophagosom, welches mit dem Lysosom fusioniert. Zwei gekoppelte Ubiquitin-like (UBL) Proteinsysteme sind an der Entstehung des Autophagosomes beteiligt: Atg12, das erste UBL Protein, wird an sein Zielprotein Atg5 konjugiert und dieses Konjugat bindet an Atg16. Das zweite UBL Protein, Atg8, wird an Phosphatidylethanolamin (PE) in der autophagosomalen Membran konjugiert. Diese Konjugationsreaktion wird durch Atg12–Atg5–Atg16 katalysiert. Beide UBL Systeme sind beim Menschen konserviert, allerdings komplexer mit mindestens sieben Atg8 Homologen.

Vorausgegangene Experimente mit *S. cerevisiae* Atg Proteinen deuteten darauf hin, dass sich die Proteine der UBL Systeme zu einer immobilen Struktur zusammenfügen. Basierend auf diesen Ergebnissen wurde die Hypothese entwickelt, dass die UBL Proteine die Bausteine für ein neuartiges Membrangerüst bilden. Das erste Ziel dieser Arbeit bestand darin, dieses Membrangerüst mittels Kraftmikroskopie nachzuweisen. Dafür wurde die Konjugation von Atg8 auf oberflächengebundenen Lipiddoppelschichten *in vitro* rekonstituiert. Tatsächlich konnte gezeigt werden, dass sich aus Atg8–PE und Atg12–Atg5–Atg16 ein bis dahin noch nicht beschriebenes Membrangerüst zusammensetzt. Dieses besteht aus homogenen Atg8–PE/Atg12–Atg5 Komplexen, die über antiparallele Atg16 Tetramere verbunden sind.

Die zweite Aufgabe dieser Arbeit bestand darin, die humanen UBL Systeme *in vitro* zu rekonstituieren. Die rekombinante Expression und Reinigung aller beteiligten Proteine war die Voraussetzung für nachfolgenden Experimente und wurde zum ersten Mal in dieser Arbeit erreicht. Die Wechselwirkungen der humanen ATG Proteine wurden mittels konfokaler Fluoreszenzmikroskopie an Liposomen untersucht, einschließlich Fluoreszenz Recovery (FRAP). Es konnte nachgewiesen werden, dass die Konjugationseffizienz von hATG8 an die Liposomenmembran homolog-abhängig erfolgte. Darüber hinaus lieferten die Experimente Hinweise darauf, dass sich beim Menschen ebenfalls ein Membrangerüst aus ATG Proteinen zusammenfügt. Diese Erkenntnisse legen den Grundstein für ein besseres molekulares Verständnis von Krankheiten, die mit Autophagozytose in Zusammenhang stehen.

1

Introduction

In eukaryotic cells, proteins undergo a constant turnover, which is mediated by either one of two major degradative pathways: (1) the proteasomal pathway, which selectively degrades mostly cytoplasmic proteins marked by ubiquitin in the cytosol, or (2) the lysosomal pathway, which is responsible for degrading membrane proteins, endocytosed material, and composite structures such as ribosomes or entire organelles. Cargo delivery to the lysosome is mediated through vesicular carriers, derived by either endocytosis or autophagy [Tai et al. 2008]. Autophagy (“self-eating”) describes the delivery of cytoplasmic materials and organelles to the lysosome and was discovered in the 1960s [De Duve et al. 1966]. Since protein degradation is part of cellular homeostasis, autophagy plays important and often opposing roles in immune defense, ageing, cancer, and neurodegeneration [Mizushima et al. 2008]. Despite its early description, the molecular players of autophagy were not unraveled until several screens in yeast identified the genes involved in autophagy [Tsukada et al. 1993; Thumm et al. 1994; Harding et al. 1995]. To unify the nomenclature, the genes involved in autophagy were later termed “*ATG*” (**autophagy**-related) [Klionsky et al. 2003]. The identification of *ATG*-genes and the characterization of related Atg proteins (‘ATG’ for human protein nomenclature) led to a better understanding of the molecular mechanism of autophagy.

1.1. General processes of autophagy

Autophagy can be subdivided into three distinct mechanisms: macroautophagy, microautophagy, and chaperone-mediated autophagy (CMA), see Fig.1.1 for an overview. During macroautophagy, the most predominant and morphologically distinct form of autophagy, a new cellular compartment - the autophagosome - is formed. The autophagosome contains sequestered cytoplasmic components, which are delivered to and degraded in the lysosome (vacuole in yeast) [Klionsky et al. 1999]. At the onset of macroautophagy, a small cup-shaped membrane sack is being

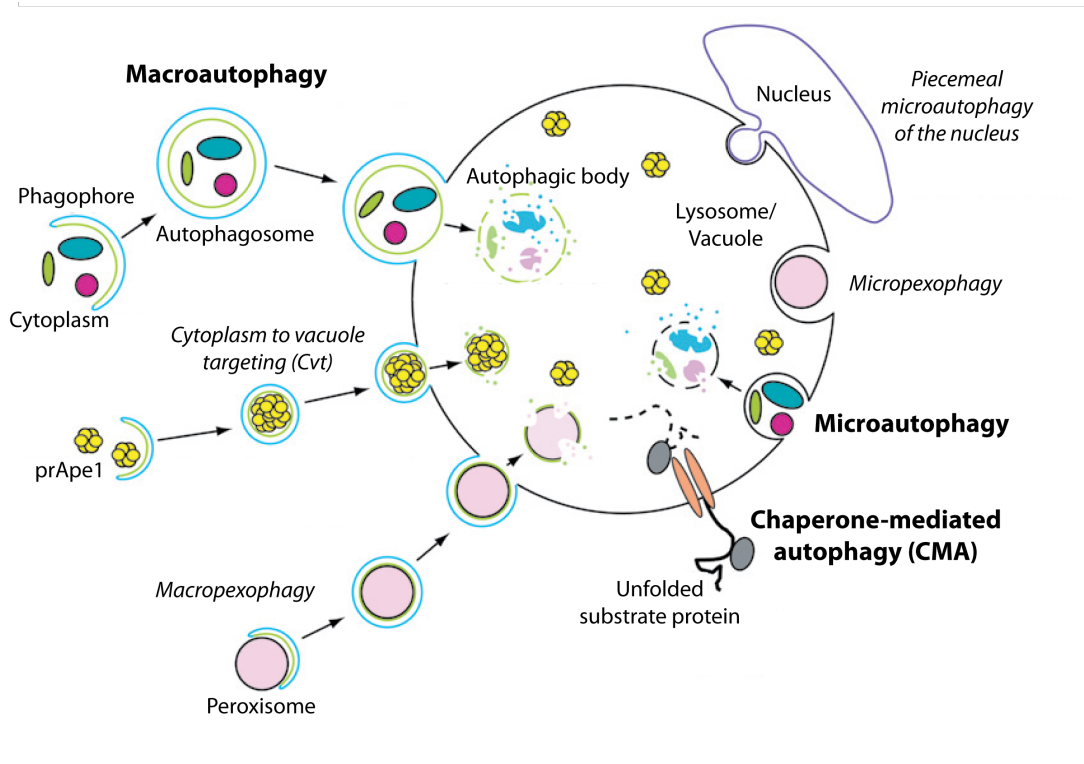


Figure 1.1.: Overview of the main autophagic pathways, adapted from [Huang et al. 2007]. The three principal modes of autophagy are macroautophagy, microautophagy, and chaperone-mediated autophagy, with specific degradation of selected cargo in macro- and microautophagy. All pathways deliver cargo to the lysosome/vacuole in yeast. The outer membrane of the autophagosome in macroautophagy is depicted in blue, the inner membrane in light green. Macro- and micropexophagy are specific forms of macro- and microautophagy, respectively. The Cvt pathway is a specific variant of macroautophagy in yeast. It delivers the peptidase prApe1 to the vacuole and uses the same components as other forms of specific macroautophagy (see also Chapter 1.5.3).

formed, which has been termed ‘phagophore’ in yeast or ‘isolation membrane’ (IM) in higher eukaryotes. For simplicity, the term phagophore will be used in this thesis. To sequester cytoplasmic material, the autophagic precursor membrane expands, which occurs by fusion of small vesicles with the phagophore [Moreau et al. 2011]. Such vesicles are thought to be derived from various donor organelles, such as the endoplasmatic reticulum (ER), the Golgi complex, or mitochondria [Juhász et al. 2006]. The membrane edges of the expanded phagophore fuse, giving rise to a double-membrane surrounded autophagosome. The autophagosomal outer membrane fuses with the lysosome to form an ‘autolysosome’ and the contents of the autophagosome, as well as the inner membrane, are degraded [Nakatogawa et al. 2009].

Regarding the mechanism of cargo selection, unspecific and specific macroautophagy can be distinguished. Under vegetative conditions, unspecific macroautophagy occurs at a low rate and is responsible for a constant turnover of cytosol, but is induced by starvation or cytotoxic stress. This non-selective degradation of cytoplasmic components mainly serves to recycle biopolymers, replenishing pools of building blocks and in case of starvation providing nutrients to the cell.

In specific macroautophagy, particular cargoes including damaged mitochondria (mitophagy, [Lemasters 2005]), pexosomes (pexophagy, [Dunn et al. 2005]) or invasive bacteria (xenophagy, [Nakagawa et al. 2004]) are enclosed by an autophagosomal membrane. Also, insoluble ubiquitinated protein aggregates can be selectively degraded through autophagy [Pankiv et al. 2007]. In yeast, the Cvt (Cytoplasm-to-vacuole-targeting) pathway transports hydrolases to the vacuole, utilizing a similar sequestration strategy. This pathway is therefore regarded as a specialized variant of specific macroautophagy [Baba et al. 1997].

Microautophagy describes a process in which the lysosomal membrane directly encloses cytosole [Mijaljica et al. 2011], and can be divided into non-selective and selective forms as well. While in non-selective microautophagy portions of the cytoplasm are engulfed by the lysosome, selective microautophagy degrades specific organelles, such as parts of the nucleus (piecemeal microautophagy [Roberts et al. 2003]).

During chaperone-mediated autophagy, the third form of autophagy, proteins are selectively bound by the hsc70 chaperone that further binds to a receptor on the lysosomal membrane (lamp2a). Proteins which possess a lysosomal targeting motif are unfolded and translocated into the lysosomal lumen [Dice 1990]. So far, this process has only been found in higher eukaryotes but not in yeast [Massey et al. 2004].

1.2. Regulation of macroautophagy

Under vegetative growing conditions, a low level of ‘basal’ unspecific macroautophagy, hereafter referred to as ‘autophagy’, constantly recycles cytoplasmic components. Together with specific autophagy, which also occurs under these conditions, this form of autophagy is essential for cellular homeostasis [Mizushima 2005].

However, autophagy can also be ‘induced’, e. g. by nutrient deprivation or other cellular stresses. In yeast, the main purpose of induced autophagy is the protection of the cell against starvation conditions by replenishing building blocks, such as amino

acids or fatty acids, to maintain vital cellular function. The induction of autophagy is regulated by two major pathways, TORC1 and PKA, depending on the limiting nutrient. The protein kinase target of rapamycin complex 1 (TORC1) responds to the levels of nitrogen in the environment, whereas cAMP-dependent protein kinase A (PKA) responds to carbon sources [Stephan et al. 2010]. Both kinases phosphorylate the Atg1/Atg13 kinase complex, the earliest acting Atg complex, independently, and therefore regulate autophagy depending on nutritional conditions [Stephan et al. 2009]. TORC1 and PKA are inhibited upon starvation, which leads to an activation of the Atg1 kinase complex, and thereby bulk autophagy is initiated [Suzuki et al. 2007].

The regulation of autophagy in mammalian cells is more complex, since in multicellular organisms, starvation conditions are not immediately detrimental for a cell. Nevertheless, starvation induces a tissue specific autophagy response. For instance, autophagy is highly upregulated in fast-twitching muscles upon starvation, but is constantly active in other tissues even under non-starvation conditions, such as thymic epithelial cells. Also, the magnitude of the autophagic response is tissue specific [Mizushima et al. 2004]. Besides starvation, other regulatory factors include insulin signaling [Neely et al. 1974], hormones, or growth factors [Lum et al. 2005]. Comparable to yeast, the two parallel pathways of PKA and TORC1 are responsible for starvation induction of autophagy in mammalian cells, with crosstalk between these pathways [Chen et al. 2011]. E. g. PKA activates TORC1, inhibiting autophagy [Mavrikakis et al. 2006], or inactivates upstream AMPK and thereby activating TORC1 [Djouder et al. 2010]. Also, other factors can influence autophagy independent of mTOR signaling, e. g. Bcl-2 [Pattingre et al. 2005]. Bulk autophagy in mammals is initiated by the counterpart to the Atg1 kinase complex, ULK1/2, together with ATG13, FIP200, and ATG101 [Mizushima 2010].

In summary, autophagy is induced by nutrient deprivation, but its regulation in mammalian cells is more complex and its full regulatory network, especially for basal autophagy, is still unknown [Chen et al. 2011]. Certainly, a tight regulation of autophagy is essential. Too much degradation results in autophagic cell death (type II programmed cell death), that is morphologically distinct from apoptosis or necrosis [Levine et al. 2005]. Yet, too little degradation would lead to an accumulation of defective proteins and organelles in the cell [Mizushima et al. 2008].

1.3. Molecular mechanisms of autophagy

1.3.1. Autophagy initiation

During autophagy, Atg proteins cooperate with canonical membrane remodeling factors to orchestrate the biogenesis of autophagosomes. At least 20 ‘core’ *ATG* genes are involved in all types of autophagy (Cvt, specific, and non-specific autophagy) and participate in the formation, expansion and sealing of the phagophore. Autophagy is induced at a specific location within the cell, which in yeast is in close proximity to the vacuole and the ER, termed pre-autophagosomal structure (PAS) [Suzuki et al. 2001]. In mammals, autophagosomes are generated at multiple sites simultaneously. These sites are close to ER membrane compartments enriched in Phosphatidylinositol 3-phosphate, termed omegasomes, where part of the ER membrane enwraps the phagophore [Axe et al. 2008; Hayashi-Nishino et al. 2009]. Atg proteins are recruited to the PAS in an hierarchic manner in yeast and humans, meaning that the protein complexes involved act successively during autophagosome formation [Suzuki et al. 2007].

The first protein complex that is activated upon starvation in yeast is the Atg1 complex, which consists of Atg1, Atg13, and the constitutive Atg17-Atg31-Atg29 complex. Atg13 is the substrate for phosphorylation by TOR in yeast [Scott et al. 2000]. In humans, the ULK1 complex corresponds to the Atg1 complex and is regulated by mTOR as well [Jung et al. 2009]. Upon starvation, TOR is inhibited and Atg13 dephosphorylation is thought to trigger the assembly of the pentameric Atg1 complex. Atg17 is an arc-shaped protein, which lead to the assumption that Atg17 is involved in tethering highly curved vesicles [Ragusa et al. 2012]. Also, Atg17 interacts with Atg9, the only essential integral membrane protein in autophagy [Noda et al. 2000; Sekito et al. 2009]. Atg9 vesicles show a cytoplasmic distribution in yeast and are regarded as membrane source to initiate the formation of the phagophore [Yamamoto et al. 2012]. However, the exact molecular mechanism of this crucial step in autophagy is still poorly understood [Hurley et al. 2014].

In the second step of autophagy the activated Atg1 kinase complex recruits class III phosphatidylinositol 3-kinase (PI3K) complex to the PAS. PI3K exists in a macromolecular complex consisting of the catalytic subunit protein Vps34, a lipid kinase, together with the protein kinase Vps15, Atg6/Beclin 1 in humans, and either Atg14 or Vps38/UVRAG [Kihara et al. 2001]. The Atg14 containing complex is involved in autophagy, whereas the Vps38/UVRAG containing complex regulates maturation of endosomes [Kang et al. 2011]. The PI3K complex generates phosphatidylinositol-

3-phosphate (PI(3)P) at the PAS [Obara et al. 2008], which recruits downstream Atg proteins. Additionally, PI(3)P production is tightly regulated by phosphatases and those phosphatases are recruited to the PAS as well at this early stage of autophagosome formation [Cebollero et al. 2012].

1.3.2. The role of PROPPINs in phagophore assembly

PI(3)P at the phagophore recruits autophagy specific PROPPINs (β -propellers that bind polyphosphoinositides), including yeast Atg18 and Atg21 [Krick et al. 2006], as well as human WIPI-proteins 1-4 (WD-repeat protein interacting with phosphoinositides [Mauthe et al. 2011; Polson et al. 2010; Proikas-Cezanne et al. 2015]). Atg18 forms a complex with Atg2 that localizes to the edges of the phagophore and is therefore assumed to play a role during phagophore expansion or closure [Guan et al. 2001; Graef et al. 2013; Suzuki et al. 2013]. The human homolog of Atg18, WIPI2b, interacts directly with proteins of the Ubiquitin-like conjugation systems [Dooley et al. 2014]. This direct interaction was also demonstrated in vegetative conditions for yeast Atg21 [Juris et al. 2015]. However, the molecular functions of Atg18 and Atg21 are still largely unknown.

1.4. Ubiquitin-like (UBL) conjugation systems in autophagy

1.4.1. Molecular mechanism of UBL conjugation systems

In autophagy, two ubiquitin-like conjugation systems exist, which act downstream in autophagosome biogenesis, and are recruited by yeast Atg21/human WIPI2b [Juris et al. 2015; Dooley et al. 2014]. For an overview of the two conjugation systems see Fig. 1.2. Both are associated with autophagosomal membranes and involved in membrane remodeling [Kirisako et al. 1999; Mizushima et al. 2001].

In yeast, two ubiquitin-like proteins, Atg12 and Atg8, are activated and conjugated to their targets by two UBL conjugation systems. The first step in the conjugation reaction of Atg12 is its activation by Atg7, an E1-like enzyme, in an ATP-dependent manner. Atg7 forms a thioester bond between the C-terminal Glycine of Atg12 and an active cysteine residue of Atg7. The activated Atg12 is then transferred to an active cysteine residue of Atg10, which acts as an E2-like enzyme. Finally, Atg12 is permanently conjugated to its sole target Atg5 [Mizushima et al. 1998b]. Atg8

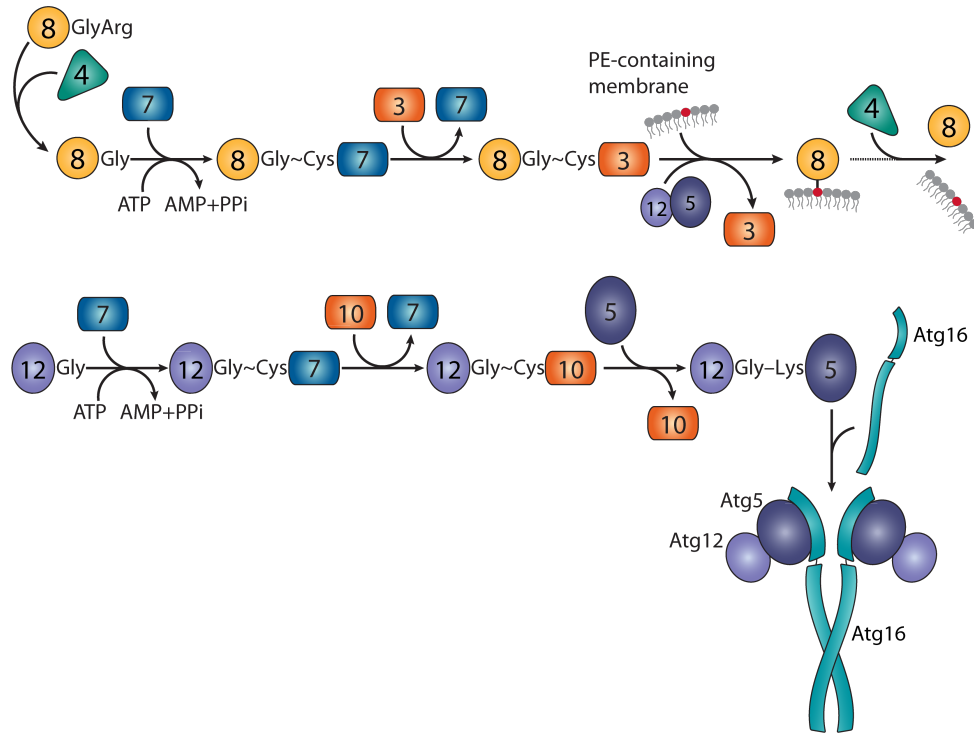


Figure 1.2.: The two Ubiquitin-like (UBL) protein systems in yeast that are part of the autophagic core machinery. The hallmark of macroautophagy is the conjugation of the UBL protein Atg8 to the autophagosome, also referred as the ‘lipidation’. The last step of Atg8-lipidation is catalyzed by the protein conjugate Atg12–Atg5. This complex is the result of the second UBL conjugation process, in which Atg12 is conjugated to its sole target Atg5. Atg12–Atg5 further associates with Atg16, a coiled-coil protein that forms the multimeric Atg12–Atg5–Atg16 complex.

undergoes a similar process. After the cleavage of its last amino acid by Atg4, a C-terminal Glycine is exposed. Atg8 is then activated by Atg7 at this C-terminal Glycine and is subsequently transferred to Atg3, the E2-like enzyme for Atg8. Intriguingly, the conjugation partner for Atg8 is the phospholipid Phosphatidylethanolamine (PE), and not a protein [Ichimura et al. 2000]. Therefore, the conjugation reaction of Atg8 is also referred to as its ‘lipidation’. This lipidation reaction is catalyzed by Atg12–Atg5, which acts as an E3-like enzyme through direct interaction with Atg3 [Hanada et al. 2007]. Thus, the two UBL systems in autophagy are interconnected. Furthermore, Atg16 binds to Atg12–Atg5 via an N-terminal Atg5-binding domain of Atg16. Atg12–Atg5–Atg16 dimerizes by coiled-coil formation of Atg16 and forms a constitutive complex of ~350 kDa [Kuma et al. 2002]. The lipidation reaction of Atg8 is organized by Atg21, a member of the PROPPIN protein family, through direct interaction with the coiled-coil domain of Atg16 [Juris et al. 2015]. In an *ATG8Δ* mutant, Atg12–Atg5–Atg16 localizes normally to the PAS. Hence, Atg12–Atg5–Atg16

acts before Atg8 [Suzuki et al. 2007]. After closure of the autophagosome, Atg8 is deconjugated from the autophagosomal membrane by Atg4 [Nair et al. 2012], whereas the conjugate Atg12–Atg5 is permanently present in the cell.

The two ubiquitin-like systems are conserved in mammals. The ATG12–ATG5 conjugate is formed by E1- and E2-like enzymes, and also functions as an E3-like enzyme for the conjugation of mammalian ATG8 homologs to PE in membranes [Mizushima et al. 1998a]. ATG3, ATG5, ATG7, and ATG16L1 knockout mice are autophagy defective and neonatal lethal due to a lack of amino acids after disruption of placental nutrient supply [Sou et al. 2008; Kuma et al. 2004; Komatsu et al. 2005; Saitoh et al. 2008]. In contrast to yeast, at least seven human ATG8s exist, which can be divided in two subfamilies, LC3s and GABARAPs, but so far only LC3B is well studied [Shpilka et al. 2011]. LC3B and GABARAP knockout mice show a normal phenotype, which hints to either redundant functions of some ATG8s or the capacity to compensate for one another [Cann et al. 2008; O’Sullivan et al. 2005].

In general, the molecular mechanisms of UBL systems in autophagy are well understood. Nevertheless, while serving as cargo adaptors on the inner membrane of the phagophore, the function of Atg8/ATG8s conjugated to the outer autophagosomal membrane remains elusive.

1.4.2. ATG12–ATG5 complexes

In humans, at least three proteins associate with ATG12–ATG5 to form a multimeric complex, ATG16L1, ATG16L2, and TECPR1. For ATG16L1 and ATG16L2 this complex has a size of ~800 kDa [Mizushima et al. 2003; Ishibashi et al. 2011]. ATG16L1 and AT16L2 are N-terminally homologous to yeast Atg16, including an ATG5 binding domain and a coiled-coil domain, but possess an additional C-terminal domain, which is dispensable for autophagosome formation [Mizushima et al. 2003; Fujita et al. 2008b]. This C-terminal domain contains seven WD-repeats forming a β -propeller structure that provides a platform for protein-protein interactions [Smith et al. 1999]. For example the transmembrane protein TMEM59 interacts with the WD-repeat of ATG16L1 to label endosomes for autophagic degradation upon bacterial infection [Boada-Romero et al. 2013]. Similarly, a coding variant (T300A) in the WD-repeat region causes Crohn disease, possibly due to a disturbed host cell response upon *Salmonella* infection [Hampe et al. 2007; Rioux et al. 2007].

ATG16L1 shows five different theoretical splice isoforms, with experimental evidence for isoform 1 and 2 in humans. Isoform 1 (ATG16L1 beta) represents the canonical form, isoform 2 (ATG16L1 alpha) a truncated version (www.uniprot.org,

[Zheng et al. 2004]). Both human and mouse isoforms of ATG16L1 show tissue-specific expression patterns [Ishibashi et al. 2011; Mizushima et al. 2003].

Comparable to the yeast Atg8-conjugation system, ATG12–ATG5–ATG16L1 acts as an E3-like enzyme for the lipidation of ATG8s [Fujita et al. 2008b]. Ectopic targeting of ATG16L1 to the plasma membrane resulted in recruitment of ATG12–ATG5 and LC3 lipidation at the plasma membrane [Fujita et al. 2008b]. ATG16L1 therefore acts upstream and its recruitment initiates LC3 lipidation. Interestingly, the coiled-coil domain of ATG16L1 is required for LC3 conjugation, since no autophagosome formation could be observed in cells expressing ATG16L1 lacking the coiled-coil domain and mutant mice died during the neonatal starvation period [Saitoh et al. 2008]. This leads to the hypothesis, that dimer formation of ATG12–ATG5–ATG16L1 plays a role for ATG8 lipidation. Additionally, Rab33B, a small GTPase, interacts directly with ATG16L1 at its coiled-coil domain. Inhibition of this binding attenuated autophagy, suggesting that ATG16L1 interaction with Rab33 modulates autophagosome formation [Itoh et al. 2008; Fukuda et al. 2008]. ATG12–ATG5–ATG16L1 is absent from closed autophagosomes, whereas LC3 serves as a marker for phagophores and closed autophagosomes [Mizushima et al. 2001].

ATG16L2, a homologous protein to ATG16L1, interacts with ATG12–ATG5 as well and forms a similar multimeric complex. ATG16L2 is able to form hetero-oligomers with ATG16L1, however it is not localized to phagophores and not involved in starvation-induced autophagosome formation. This functional discrepancy is most likely based on the coiled-coil region of ATG16L2, which shows only 20,7% amino acid identity to ATG16L1 [Ishibashi et al. 2011], further emphasizing the importance of the ATG16L1 coiled-coil domain in autophagosome formation.

The third protein, which can interact with ATG12–ATG5, is tectonin β -propeller repeat containing protein 1 (TECPR1) and was identified during an autophagy screen in humans [Behrends et al. 2010]. ATG12–ATG5 exclusively interacts with either ATG16L or TECPR1. Recently, it could be shown that TECPR1 also binds PI(3)P and seems to act at later stages of autophagosome biogenesis, however the molecular mechanisms of TECPR1 remain unclear [Chen et al. 2012].

1.5. *Atg8/ATG8 specificities*

Initially, ATG8 proteins in mammals were not discovered in the context of autophagy, but as part of other cellular processes. LC3s were co-purified with microtubule-associated proteins (MAPs) A1 and A2 [Kuznetsov et al. 1987; Mann et al. 1994],

GATE-16 was found to be involved in intra-Golgi protein transport [Legesse-Miller et al. 1998], and GABARAP was found to interact with GABA_A receptors [Wang et al. 1999]. However, apart from this initial characterization in these pathways, no further implications for non-autophagic functions of ATG8 proteins exist, implying that their main activity is restricted to autophagy. An involvement in autophagy was first reported for MAP1LC3 [Kabeya et al. 2000].

At least seven ATG8 homologs were identified in humans. These can be divided into two related subfamilies based on their sequence homology: LC3s and GABARAPs. Humans possess four *LC3* genes (encoding for MAP1LC3A, MAP1LC3B, MAP1LC3B2, MAP1LC3C), with *MAP1LC3A* encoding for two splicing isoforms. The GABARAP family comprises two *GABARAP* genes (encoding for GABARAP, GABARAPL1/GEC1), and one *GATE-16* gene (encoding for GABARAPL2/GATE-16) [Shpilka et al. 2011]. The existence of a fourth GABARAP, GABARAPL3, could only be shown on a transcriptional level [Xin et al. 2001]. ATG8s are expressed in all tissues to different extents [Xin et al. 2001; Mizushima et al. 2004]. E. g., GABARAP shows higher expression in endocrine glands compared to other tissues, whereas GABARAPL1 is mainly expressed in the central nervous system [Nemos et al. 2003]. Interestingly, the three human GABARAPs display a higher protein sequence identity with yeast Atg8 (55-56%) compared to the five human LC3s (36-40%) [Szalai et al. 2015].

The hATG8 family is characterized by an ubiquitin-fold domain and an N-terminal domain consisting of two α -helices, which most likely undergo conformational changes upon conjugation of ATG8 proteins to PE, regulating protein-protein interactions [Paz et al. 2000; Coyle et al. 2002]. These α -helices differ in the ATG8 proteins. The LC3 subfamily possesses a basic first α -helix, in contrast to an acidic α -helix in GABARAP and GATE-16 [Sugawara et al. 2004]. The biological relevance of the different homologs is largely unknown, especially during autophagosome biogenesis.

1.5.1. *Atg8/ATG8 in autophagosome formation*

In yeast, the amount of Atg8 molecules at the PAS correlates with the size of autophagosomes [Xie et al. 2008a]. Similar results have been obtained for human ATG8 proteins, however homolog-dependent. LC3B colocalizes with GABARAP and GATE-16 to autophagosomes [Kabeya et al. 2004; Weidberg et al. 2010]. A knockdown of either LC3 or GABARAP subfamily blocks autophagic flux [Weidberg et al. 2010]. Strikingly, the phagophore structures labeled with YFP-ATG5 appeared smaller upon knockdown of LC3s and larger upon knockdown of GABARAPs.

This led to the assumption that the subfamilies act sequentially in autophagosome formation. Specifically, these results suggested that the LC3 family functions in the elongation process of the phagophore, whereas the GABARAP family acts at a later stage, possibly closure of the autophagosome [Weidberg et al. 2010]. Interestingly, it was reported by another study that autophagic sequestration of bulk cytosole depends solely on GABARAPs and not on LC3s [Szalai et al. 2015]. This obvious discrepancy could result from cell-type and organism dependent differences (HeLa cells vs. rat hepatocytes) and have not been resolved yet. Still, the authors of the second study confirmed the futility of LC3s in autophagy in prostate cancer cells [Szalai et al. 2015]. Intriguingly, the homolog for GABARAP in *C. elegans*, LGG-1, is essential for autophagosome formation, whereas the LC3 homolog, LGG-2, is involved in lysosomal recruitment through interaction with the tethering complex HOPS [Manil-Ségalen et al. 2014]. To make the roles of ATG8-homologs even more complex, it was reported that a knockout mouse for GABARAP did not show a specific phenotype [O'Sullivan et al. 2005]. Taking these results together, ATG8 proteins seem to have non-redundant activities during autophagosome formation, but show partial compensation in case of homolog specific knockouts.

1.5.2. Involvement of *Atg8/ATG8* proteins in sealing, tethering and fusion

Atg8 is a key molecule during autophagosome formation, but its function on the outer membrane of the phagophore was unclear. Therefore it was hypothesized that *Atg8* might play a role in sealing of the phagophore, tethering of small vesicles to the phagophore or in fusion of the autophagosome with the vacuole. *Atg8* is deconjugated from autophagosomes by *Atg4* shortly before or after completion, and upon a defect in deconjugation in $\Delta ATG4$ cells, autophagy is reduced [Kirisako et al. 2000]. Similarly, incomplete autophagosomes that are defective in membrane closure were observed with a protease-inactive form of *ATG4B*, suggesting that without deconjugation the autophagosome cannot form [Fujita et al. 2008a]. Recently another study in yeast supported these findings. A protease protection assay demonstrated that the defect in autophagy was caused by a sealing defect, suggesting that autophagosome sealing is impaired if *Atg8* is retained on membranes. This defect in deconjugation further led to mislocalization of *Atg8* to the vacuolar membrane, and missing dissociation of other *Atg* proteins from the autophagosomal membrane [Nair et al. 2012]. These results imply that *Atg8* deconjugation is necessary for efficient autophagosome biogenesis and fusion with the vacuole.

In contrast to the finding that the deconjugation of Atg8 seems to be important for autophagosome biogenesis, several studies try to shed light on the possible membrane tethering and hemifusion activity of Atg8, however with partially contradicting results. It was suggested in an *in vitro* reconstitution system, that Atg8-PE and its human homologs tether and hemifuse vesicles for phagophore expansion [Nakatogawa et al. 2007; Weidberg et al. 2011]. However, so far no *in vivo* evidence was found to support these findings. The suggested hemifusion function could be ruled out, since it requires non-physiological PE concentrations [Nair et al. 2011]. Instead, SNARE proteins are responsible for vesicle fusion in autophagosome maturation in yeast [Nair et al. 2011], as well as mammals [Moreau et al. 2011]. Regarding tethering of small vesicles to the phagophore, it was discovered that the TRAPPIII complex is involved in vesicle tethering at the PAS [Lynch-Day et al. 2010]. Since TRAPP complexes have functions as vesicle tethers in ER-to-Golgi and *trans*-Golgi-endosome trafficking [Barrowman et al. 2010], it is very likely that TRAPPIII, instead of Atg8, is responsible for tethering vesicles at early steps of autophagosome formation.

LC3 is phosphorylated at T50. With respect to possible involvement of Atg8/ATG8 proteins in fusion of the autophagosome with the vacuole/lysosome, it was demonstrated that loss of this phosphorylation impairs the fusion of autophagosomes with lysosomes and thereby blocks autophagy. The phosphorylation could be essential for recruiting other factors to the autophagosome, which are necessary for fusion, such as SNAREs or tethering factors [Wilkinson et al. 2015]. Indeed, an interaction partner of ATG8 proteins was identified recently, which regulates autophagosome-lysosome fusion: PLEKHM1 (Pleckstrin homology domain containing protein 1). PLEKHM1 is thought to bridge autophagosomal and lysosomal membranes by binding to ATG8 proteins and Rab7/HOPS complex and thereby mediating autophagosome-lysosome fusion [McEwan et al. 2015]. The HOPS complex (homotypic fusion and protein sorting) is known as tethering complex on the vacuole [Balderhaar et al. 2013] and Rab7 has already been previously shown to regulate autophagic progression [Gutierrez et al. 2004]. The fusion of the autophagosome with the lysosome is mediated by the SNARE protein Syntaxin17 on autophagosomes in mammals and *Drosophila* [Itakura et al. 2012; Takáts et al. 2013]. Syntaxin17 also interacts with the HOPS complex for autophagosome-lysosome fusion [Jiang et al. 2014; Takáts et al. 2014], but with PLEKHM1 an adaptor protein was characterized that directly binds to LC3s and GABARAPs via its LIR motif [McEwan et al. 2015]. Remarkably, in *C. elegans*, the interaction to the HOPS complex is mediated only by the LC3 homolog LGG-2, not the GABARAP homolog LGG-1 [Manil-Ségalen et al. 2014], indicating a reverse

order of function compared to humans [Weidberg et al. 2010]. In summary, these results indicate that Atg8/ATG8 proteins act as interaction partners for canonical tethering and fusion machines, such as PLEKHM1, SNAREs and HOPS complex, during fusion of autophagosomes with the vacuole/lysosome.

1.5.3. Specificities of Atg8/ATG8-interacting proteins

Besides the role of Atg8 in autophagosome biogenesis, Atg8 and its human homologs are involved as cargo adaptor at the inner autophagosomal membrane. In the Cytoplasm-to-vacuole pathway in yeast, Ape1, a peptidase, is linked to Atg19, which interacts with Atg8 on the inside of phagophores [Chang et al. 2007]. Similarly, Atg34 connects α -mannosidase to Atg8 [Suzuki et al. 2010]. In mammals, Ubiquitin-marked proteins are linked via p62 to ATG8 family members for degradation [Pankiv et al. 2007]. Those protein-protein interactions depend on an **Atg8 Interacting Motif (AIM)** that is present in yeast Atg8-interacting proteins. This motif is also called **LC3 Interacting Region (LIR)** in mammals. The consensus sequence for the AIM and LIR motif is W-X-X-L (X being any amino acid), and it binds to conserved hydrophobic pockets in Atg8 and its mammalian homologs [Noda et al. 2008].

Another protein interacting with Atg8 is Atg1 [Nakatogawa et al. 2012b; Kraft et al. 2012]. Similarly, ATG8 proteins interact with ULK1/2, as well as other members of the ULK1/2 complex. Interestingly, all interacting proteins of the human Atg1 complex had a strong preference for GABARAPs over LC3s, implying that GABARAP family members could act as scaffold proteins for the assembly of the human Atg1 complex [Alemu et al. 2012]. Conversely, the adaptor protein FYCO1, that links autophagosomes to microtubules, prefers LC3 [Pankiv et al. 2010]. Finally, the interaction of NDP52, which exclusively binds to LC3C in *Salmonella* infected cells, accounts for efficient antibacterial autophagy in these cells [von Muhlinen et al. 2012]. A proteomic analysis provided a broader view on ATG8 homolog-interacting proteins, and demonstrated that two-thirds of the interacting proteins are either specific for LC3 or GABARAP, and only one-third is interacting with both [Behrends et al. 2010]. These homolog-specific interactions could partially explain the diversity of ATG8 proteins. For an overview of the different reported roles of human ATG8 homologs see figure 1.3.

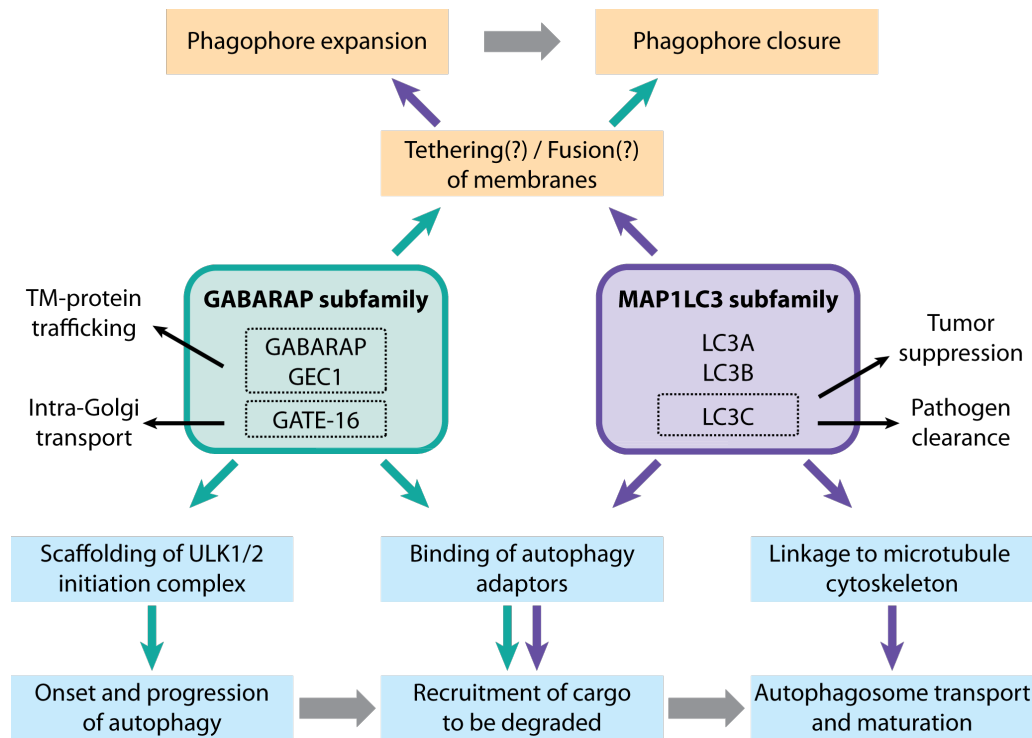


Figure 1.3.: Schematic overview of LC3 and GABARAP family functions, corresponding to the current literature, adapted from Weiergräber et al. [2013]. Light blue boxes represent protein-protein interactions, light orange boxes represent protein-lipid interactions. Strikingly, protein-protein interactions hint towards GABARAPs being involved earlier in autophagosome biogenesis compared to LC3s, whereas protein-lipid interactions suggest that LC3 proteins act earlier.

1.6. Objectives of this study

Autophagy plays crucial roles in cell homeostasis, as well as in development, ageing, and diseases, such as cancer and neurodegeneration. Therefore a complete understanding of the underlying molecular mechanisms is indispensable for identifying new therapeutic targets. Still, a systematic picture of autophagy, specifically autophagosome biogenesis, is lacking [Xie et al. 2008b]. Conjugation of Atg8 to the autophagosomal membrane is a key process in autophagy, but its function on the outer membrane remained elusive, mainly due to the dynamic nature of autophagosome formation *in vivo*. Therefore, studying the interaction of Atg proteins in controlled conditions with each other and with membranes *in vitro*, allows for deeper insights into Atg8 function as well as its interplay with other Atg proteins.

The ubiquitin-like (UBL) systems of autophagy in yeast have been studied in our lab previously. Based on *in vitro* and *in vivo* analyses of Atg8, Atg12–Atg5, and Atg16, the hypothesis emerged that Atg12–Atg5 not only acts as an E3-like

enzyme for Atg8, but has a second structural function in forming a protein scaffold on autophagosomes together with Atg16 and Atg8. The first aim of this study was to verify the hypothesis of this previously unknown protein scaffold on autophagosomal membranes. Due to its capability to image structures with submicrometer resolution and in physiological conditions, it was the aim to utilize Atomic Force Microscopy to provide direct evidence by imaging the proposed scaffold *in vitro*.

The second aim of the thesis was to test whether such a protein scaffold also exists for humans. Comparable to yeast, ATG12–ATG5 enzymatically conjugates human ATG8 proteins to membranes. However, ATG12–ATG5 interacts with three different proteins in the human system. On top of these three ATG12–ATG5 complexes, at least seven different ATG8 proteins were identified in human cells. The biological relevance of these homologs is largely unknown, especially during autophagosome biogenesis. Hence, the goal was to reconstitute the human autophagic UBL systems *in vitro*. Subsequently, possible functional differences of ATG8s should be analyzed. Furthermore, FRAP experiments (Fluorescence Recovery After Photobleaching) should be performed to provide an indication for a protein scaffold by measuring protein and membrane mobility with fluorescently labeled proteins on giant unilamellar vesicles. Thereby, protein combinations can be determined that are able to form the hypothesized scaffold.

2

Materials and Methods

2.1. Reagents

Media and buffers for gels and blotting used in this thesis can be found in table 2.1 and table 2.2, respectively. Buffers for protein purification are listed in table 2.3.

Table 2.1.: Media for bacteria and yeast cultivation.

Medium	Components
LB (lysogeny broth) [Bertani 1951]	1 % tryptone (Bacto) 0.5 % yeast extract (Bacto) 0.75 % NaCl (AnalaR Normapur)
TB (terrific broth) [Tartoff et al. 1987]	1.2 % tryptone 2.4 % yeast extract 0.5 % glycerol (Carl Roth) 17 mM KH ₂ PO ₄ (Carl Roth) 72 mM K ₂ HPO ₄ (Carl Roth)
SOC (super optimal broth with catabolite repression) [Hanahan 1983]	2 % tryptone 0.5 % yeast extract 8.56 mM NaCl 2.5 mM KCl (Carl Roth) 10 mM MgCl ₂ (Merck) 10 mM MgSO ₄ (Carl Roth) 20 mM glucose (Merck)
SD (synthetic defined)	0.67 % Difco YNB (Becton, Dickinson & Company) 2 % Glucose amino acid mix (specific for yeast strain)
SD-N	0.17 % Difco YNB 2 % glucose

Table 2.2.: Buffers for agarose gels, SDS-PAGE and Western Blotting.

Buffer	Components
TAE buffer	40 mM Tris 20 mM acetic acid (Sigma-Aldrich) 1 mM EDTA, pH 8.0 (Carl Roth)
5x Laemmli-SDS loading buffer	225 mM Tris-HCl, pH 6.8 50 % glycerol (Carl Roth) 5 % SDS (Carl Roth) 0.05 % bromphenol blue (Merck) 250 mM DTT (PanReac AppliChem)
SDS Running Buffer	25 mM Tris-HCl 19.21 mM glycine (Sigma-Aldrich) 0.1 % SDS
MES SDS Running Buffer	50 mM MES (PanReac AppliChem) 50 mM Tris-HCl, pH 7.3 0.1 % SDS 1 mM EDTA
Coomassie Staining Solution	0.25 % (w/v) Coomassie R-250 (PanReac AppliChem) 30 % (v/v) ethanol (Sigma-Aldrich) 10 % (v/v) acetic acid
Coomassie Destaining Solution	40 % (v/v) ethanol 10 % acetic acid
Shrinking Solution	50 % (v/v) methanol (Sigma-Aldrich) 3 % (v/v) glycerol
Blotting (Transfer) Buffer	25 mM Tris 192 mM glycine 0.1 % SDS 20 % (v/v) methanol
Tris-buffered saline with Tween 20 (TBS-T) buffer	25 mM Tris-HCl, pH 7.6 150 mM NaCl 0.05 % Tween-20

Table 2.3.: Lipidation buffer and buffers for protein purification.

Medium	Components
Lipidation buffer	12.5 mM Tris-HCl, pH 7.4 (Sigma-Aldrich) 137.5 mM NaCl (AnalaR Normapur)
Lysis Buffer	100 mM Tris-HCl, pH 8.0 300 mM NaCl (500 mM for ATG16L1) 20 mM imidazole, pH 8.0 (Merck) 10 % glycerol 5 mM β -mercaptoethanol (Merck) 0.5 % protease inhibitor cocktail (Sigma)
Washing Buffer (Ni-NTA)	50 mM Tris-HCl, pH 8.0 300 mM NaCl (500 mM for ATG16L1) 5 mM imidazole, pH 8.0 10 % glycerol 5 mM β -mercaptoethanol
Elution Buffer (Ni-NTA)	50 mM Tris-HCl, pH 7.4 300 mM NaCl (500 mM for ATG16L1) 500 mM imidazole 10 % glycerol
Running Buffer (size exclusion chromatography, SEC)	25 mM Tris-HCl, pH 7.4 275 mM NaCl (400 mM for ATG16L1)

2.2. AFM experiments with yeast UBL proteins

2.2.1. Sample preparation

Supported Lipid Bilayer (SLB) preparation All lipids were purchased from Avanti Polar Lipids. Lipid stocks and mixtures were stored at -80°C . The lipid mixture for supported lipid bilayers (SLBs) consisted of Cholesterol (20 mol %), 1-palmitoyl-2-oleoyl-*sn*-glycero-3-phosphocholine (POPC, 39.9 mol %), 1-palmitoyl-2-oleoyl-*sn*-glycero-3-phospho-L-serine (POPS, 20 mol %), 1-palmitoyl-2-oleoyl-*sn*-glycero-3-phosphoethanolamine (POPE, 20 mol %), and lissamine-rhodamine-PE (0.1 mol %) in chloroform (7 mM total lipid concentration). Supported lipid bilayers (SLBs) were prepared by deposition and fusion of small unilamellar vesicles (SUVs, Chiantia et al. [2005]). The first step in production of SUVs are multilamellar vesicles (MLVs). For MLVs, 50 μl of lipid mixture was dried in a glass vial under nitrogen flow while turning the vial constantly for an even distribution of the lipid film. For complete evaporation of chloroform the vials were further dried for 1 h in vacuum. For lipid resuspension 50 μl lipidation buffer (table 2.3) was added to the vial. The mixture was vortexed until the MLV solution was opaque. MLVs could now be aliquoted and stored at -20°C . For SUV preparation, the MLV mix was diluted 10 fold with lipidation buffer and sonicated for 10 minutes until the solution was clear. 180 μl of this SUV suspension was deposited with 4 μl CaCl_2 (0.1 M) and 16 μl lipidation buffer on the support for 20 minutes at room temperature and then rinsed at least 10 times with lipidation buffer to remove unbound vesicles. As support either plasma-cleaned glass coverslips or silanized mica was used. Mica was freshly-cleaved and glued to plasma-cleaned coverslips, before silanization was carried out Heinemann et al. [2011]. The silanization charges the surface positively. Therefore, the negatively charged lipids adhere better to the support.

Atg8 lipidation reconstitution Recombinantly expressed proteins were purified as described in chapter 2.5.2 or provided by V. Beier (Atg8-Alexa488). Atg7, Atg3, Atg8, DTT and ATP were incubated at 30°C for 10 minutes, as well as Atg12–Atg5 together with Atg16. Both incubated mixtures were mixed, pipetted on top of the SLB, and further incubated for 15 minutes. The final concentrations in the AFM chamber were 0.6 μM Atg8, 0.2 μM Atg7, 0.2 μM Atg3, 0.1 μM Atg12–Atg5, 0.1 μM Atg16, 0.5 mM ATP, and 0.1 mM DTT. The membrane was washed again with lipidation buffer to remove unbound proteins.

2.2.2. LSM (Laser Scanning Microscopy)

For SLB experiments a combined atomic force/laser scanning microscopy setup was used with a JPK Instruments Nanowizard III BioAFM mounted on top of a Carl Zeiss laser scanning microscope (LSM) Meta 510 system. For LSM measurements, a 40x NA 1.2 UV-VIS-IR C Apochromat water-immersion objective was used. Alexa488 labeled Atg8 was excited with a 488 nm Argon-ion laser and the Rhodamine-labeled bilayer with a 543 nm Helium-neon laser, respectively. Typical images were acquired with a size of 57.6 x 57.6 μm , 512 x 512 pixel resolution, and 3.2 μs per pixel scanning rate.

For fluorescence recovery after photobleaching (FRAP) experiments, a 28 x 28 μm area at the center of the LSM images was photobleached for 40 seconds with 100% laser power (both lasers), followed by image scanning every 75 seconds for a maximum of 45 minutes.

2.2.3. AFM (Atomic Force Microscopy)

Binnig et al. [1986] developed the first scanning probe microscope suitable for the investigation of biological samples in aqueous solutions - the Atomic Force Microscope (AFM). In Atomic Force Microscopy, different kinds of interactions (e. g. van-der-Waals or electrostatic) between a sharp tip and a sample are measured, usually by scanning the sample with the tip mounted on a flexible cantilever arm. Therefore, an image with AFM is not obtained with light that passes through several lenses (like in a conventional light microscope), but through topological scanning of the sample with the tip and utilizing the deflection of a laser beam from the cantilever (Fig. 2.1). Thus, the microscopic resolution is not restricted to the wavelength of light. Biological samples can be imaged in physiological buffer conditions with very high resolution.

Here, AFM imaging was performed in intermittent-contact (also called ‘tapping’, see Fig. 2.1, C) mode with BioLever Mini BL-AC40TS-C2 cantilevers (Olympus) with typical spring constants of 0.09-0.1 N/m. The scan rate was set to 0.8 Hz, the setpoint close to 0.85 V, resolution to 512 x 512 pixels and cantilever oscillation frequency between 18 and 25 kHz. The force applied on the sample maintained at the lowest possible value by continuously adjusting the setpoint and gains during the imaging. Height, error, deflection and phase-shift signals were collected and images were line-fitted as required with JPK SPM Data Processing Software v4.2.47 (JPK Instruments). Estimations of particle sizes were performed using the analysis software Gwyddion v2.30 (Czech Metrology Institute), demonstrated in Fig. 3.6, p. 54. Height

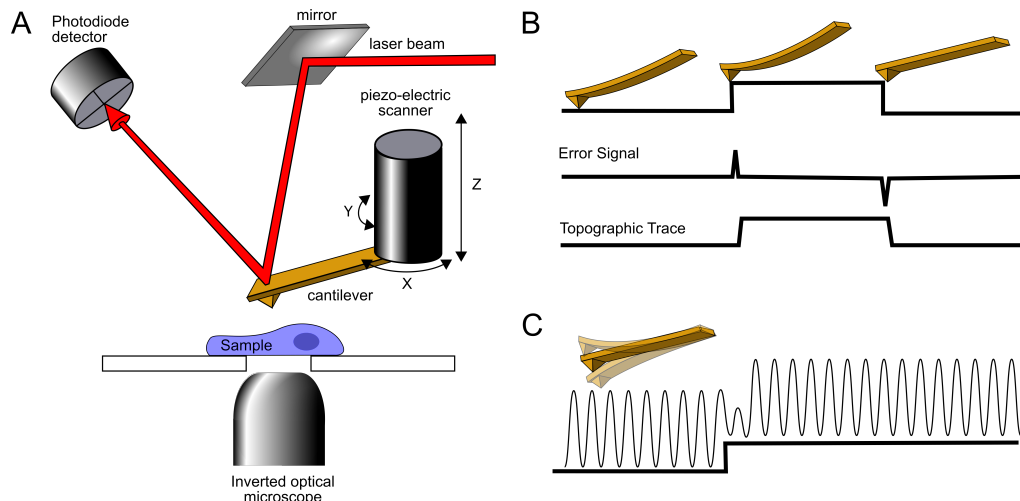


Figure 2.1.: Scheme illustrating the working principle of Atomic Force Microscopy (AFM)¹. **(A)** Representation of an Atomic Force Microscope mounted on an inverted optical microscope, comparable to the setup used in this thesis. An infrared laser beam is deflected from the cantilever tip. Cantilever deflection is measured by a 4-quadrant photodiode. A feedback-loop connects laser detection with the piezo-electric scanner to apply constant force on the sample. **(B)** Imaging is often performed in scanning mode. Deflections of the cantilever correspond to height changes in the sample. By scanning the sample a topological image is acquired. **(C)** Delicate samples can be imaged in tapping mode (depicted here). Here, the cantilever oscillates while scanning the sample. Topological changes are recorded through amplitude changes of the cantilever.

analysis was performed using the histogram representation of at least 8 different $2 \times 2 \mu\text{m}$ bilayer areas on 2-3 distinct bilayer-protein samples. The height-scales for the images shown were adjusted for best visualization of the protein layer on top of the bilayer. Large white spots correspond to height-saturated protein aggregates. Orthogonal 3D height images in Fig. 3.3 were processed from the average of the trace and retrace raw images with posterior 3 pixel-sized mean value fitting.

2.3. Electron Microscopy of yeast cells

S. cerevisiae strains were provided by B. Hofmann and listed in table 2.4. Strains were cultured in SD medium at 30°C and 180 rpm (table 2.1), supplemented with appropriate antibiotics and amino acids (table 2.4). When cells reached an optical density of 0.8 at 600nm (OD_{600}), nitrogen starvation was induced by washing cells twice with SC-N (nitrogen starvation medium, table 2.1), followed by incubation in SC-N medium for 4 hours. 9.5 ml cell suspension with an OD_{600} of 0.8 were

¹<http://www.freesbi.ch/en/illustration/figures>

harvested before and after starvation by centrifugation (3 minutes, 1500 g). Fixation, embedding, and staining were performed according to the PIPES-KMnO₄ protocol for ultrastructural analysis [Wright 2000]. Cells were mixed 1:1 with prefixative solution (table 2.5), incubated for 5 minutes, centrifuged, and incubated in prefixative at 4 °C over night.

Next, samples were washed 3 times with water, postfixed in 2 steps with 2% potassium permanganate (Sigma-Aldrich) for 45 minutes, washed, and stained with 1% uranyl acetate (Serva) for 1 hour. All washing steps were carried out with autoclaved water to reduce carbon content of samples through evaporation of CO₂ during boiling. Subsequently, samples were gradually dehydrated in rising ethanol solutions (25%, 50%, 75%, 95%) by centrifugation (5 minutes,

1500 g) and resuspension. During dehydration steps, Spurr's resin according to the 'standard medium firm' formula was prepared (Spurr Low Viscosity Embedding Kit, Sigma-Aldrich). After 5 incubations in 100% ethanol, samples were resuspended in 2:1 ethanol:resin and incubated for 2 hours. Samples were centrifuged for 5 minutes at 1500 g and resuspended in 1:1 ethanol:resin. To allow ethanol evaporation, samples were incubated rotating over night at room temperature in 2 ml tubes (Eppendorf) sealed with Pleated Dialysis Tubing (Snake Skin, Thermo Scientific). Next, samples were centrifuged and incubated twice in 100% resin for 1 hour, followed by another resin exchange and incubation for 2 hours under vacuum. Samples were then transferred to beam embedding capsules (size 3, Electron Microscopy Sciences) and

Table 2.5.: Prefixative [Wright 2000].

Prefixative
0.2 M PIPES, pH 6.8 (Sigma-Aldrich)
0.2 M sorbitol (Carl Roth)
2 mM MgCl ₂ (Merck)
2 mM CaCl ₂ (Carl Roth)
4% glutaraldehyde (Carl Roth)

Table 2.4.: Yeast strains (all BY4741) used for electron microscopy.

Name	Specifications
WT (Y_BH222)	pep4Δ::clonNat
ΔAtg18 (Y_BH223)	pep4Δ::clonNat, atg18Δ::KanMX6
ΔAtg21 (Y_BH224)	pep4Δ::clonNat, atg21Δ::KanMX6
ΔAtg18, ΔAtg21, Atg21oe (Y_BH225 with pCEN_BH37)	pep4Δ::clonNat, atg18Δ::KanMX6, atg21Δ::hphNT1 pCEN_BH37: pTL58 (Leu2 auxotrophy), pPmaI-Atg21

incubated for 2 hours under vacuum. Capsules were centrifuged for 20 minutes at 2000 g in 2 ml tubes for pelleting the cells to the bottom of the capsule and subjected to vacuum for 1 hour. Finally, samples were hardened at 70°C for 24 hours.

Embedding capsules were cut open, samples were mounted in a sample holder, and 60-100 nm thin sections were prepared using a Ultracut E ultramicrotome (Reichert-Jung). The ultra-thin sections were mounted on copper grids coated with Formvar carbon film (FCF-100-Cu, Electron Microscopy Sciences), post stained for 2 minutes with Reynolds' lead citrate (kindly provided by R. Kutlesa) and washed twice with autoclaved water for 10 minutes.

Imaging was performed on a JEM-1230 (JEOL) transmission electron microscope with a voltage of 80 kV, images were acquired using an Orius SC1000 digital camera (Gatan) and the accompanying software DigitalMicrograph.

2.4. Cloning of human ATG proteins

To express the desired proteins of the human autophagic UBL protein cascades recombinantly, the cDNAs had to be cloned into suitable expression vectors. cDNA clones of human proteins were picked from the ImaGenes cDNA Library at the in-house Biochemistry Core Facility (table 2.6) and 5 ml cultures were grown overnight at 37°C and 180 rpm. Plasmid DNA was isolated using the QIAprep Spin Miniprep Kit (Qiagen) and cDNA was amplified by polymerase chain reaction (PCR), according to primer melting temperature and cDNA length. A general PCR protocol and cycle, as used in this thesis, are described in table 2.7. Successful PCR was monitored by agarose gel electrophoresis, using self-casted 1% agarose gels (Biomol) containing 0.01% Ethidium Bromide solution (Serva) in TAE-buffer (table 2.2).

All cDNAs were sequenced (sequencing primers in table 2.12) and mutations, as well as deletions were reversed using the QuikChange Lightning Site-Directed Mutagenesis Kit (Agilent). All primers were purchased from Metabion and can be found in chapter 2.11, p. 41.

SLIC cloning Cloning of cDNAs into expression vectors provided by the Biochemistry Core Facility (MPIB) was performed via Seamless Ligation Independent Cloning (SLIC, Li et al. [2007]). Expression vectors by the Core Facility are constructed such, that identical PCR cDNA fragments can be fused to different tags or into different host vectors for recombinant protein expression [Scholz et al. 2013]. To reduce vector background, the toxic *ccdB* gene is expressed in non-linearized or non-recombined vectors. Commonly used vectors were pCoofy1 (pETM14 with N-His₆), pCoofy3 (pETM33

Table 2.6.: cDNA clones used in this thesis, with corresponding vector and antibiotic resistance.

Protein	Clone Name	Vector	Resistance
ATG3	IRAU _{p969F0878D}	pOTB7	Chloramphenicol
ATG5	IRAT _{p970D01100D}	pBluescriptR	Ampicillin
ATG7	IRAU _{p969E0513D}	pOTB7	Chloramphenicol
ATG10	IRAT _{p970F0347D}	pCMV-SPORT6	Ampicillin
ATG12	IRAT _{p970G0416D}	pCMV-SPORT6	Ampicillin
ATG16L1	IRAU _{p969E0649D}	pOTB7	Chloramphenicol
TECPR1	IRAT _{p970H0679D}	pCMV-SPORT6	Ampicillin
LC3A	IRAT _{p970E0811D}	pCMV-SPORT6	Ampicillin
LC3B	IRAU _{p969H0456D}	pOTB7	Chloramphenicol
GABARAP	IRCM _{p5012H094D}	pCR-BluntII-TOPO	Kanamycin, Zeocin
GATE-16	IRAU _{p969E1044D}	pDNR-LIB	Chloramphenicol

Table 2.7.: General PCR protocol and cycle using Phusion polymerase (New England Biolabs, NEB). Annealing temperature was adjusted to primer melting temperatures and elongation step to cDNA length, respectively.

PCR protocol		PCR cycle		
10 μ l	5x GC or HF Buffer (NEB)	98°C	30 sec	Denatuaration
4 μ l	dNTP Mix (2.5 mM each, NEB)	98°C	10 sec	Denat.
2.5 μ l	Forward Primer (10 μ M)	45-72°C	30 sec	Anneal. 30 cycles
2.5 μ l	Reverse Primer (10 μ M)	72°C	30 sec/kb	Elong.
1 μ l	template (10-20 ng)	72°C	10 min	Final Extension
ad 49 μ l	H ₂ O (Mol. biol. grade, AppliChem)			
1 μ l	Phusion DNA Polymerase (NEB)			

Table 2.8.: Reaction mixture and PCR cycle for colony PCR using Pfu-Polymerase (provided by the Core Facility). Colonies were first swirled in medium for over night culture before tip was dipped into PCR reaction mixture. Annealing temperature was adjusted to primer melting temperatures(T_m) and elongation step to cDNA length, respectively.

PCR reaction (25 μ l)		PCR cycle		
15 μ l	H ₂ O	95°C	5 min	Cell rupture
2.5 μ l	10x Pfu-buffer	95°C	1 min	Denat.
2 μ l	dNTP Mix (2.5 mM each)	T_m -5°C	30 sec	Anneal. 30 cycles
2.5 μ l	Forward Primer (5 μ M)	72°C	2 min/kb	Elong.
2.5 μ l	Reverse Primer (5 μ M)			
0.25 μ l	Pfu-Pol (5U)	72°C	5 min	Final Extension

with N-His₆-GST), pCoofy4 (pETM44 with N-His₆-MBP), pCoofy16 (pETM66 with N-His₆-NusA), and pCoofy37 (modified by M. Perna, N-MBP, C-His₁₀). These vectors also contain a Precision protease cleavage site to remove the N-terminal tag and pCoofy37 a TEV protease cleavage site to remove the C-terminal His₁₀. Insert amplification was performed with primers that consist of a gene specific sequence and a sequence that is homologous to the linearized vector. For recombination, linearized vector and amplified insert were added, together with Recombinase A (provided by Core Facility), and incubated for 30 minutes at 37°C, according to the protocol [Scholz et al. 2013]. 3-10 μ l of the Plasmid were incubated with chemically competent cells for 30 minutes on ice, 45 seconds at 42°C, 2 minutes on ice and 1 hour in SOC medium (table 2.1) under constant shaking. Cells were then plated on LB-Agar plates with the correct antibiotics and incubated over night at 37°C. Colonies were picked and Colony-PCR (table 2.8) was performed to verify insert ligation into the vector. 5 ml cultures were grown over night at 37°C and 180 rpm. 0.5 ml were used for glycerol stocks (25 % glycerol), which were stored at -80°C, and Plasmid DNA was isolated using the QIAprep Spin Miniprep Kit from the remaining 4.5 ml.

Atg8 homologs Four Atg8 homologs were used in this thesis, namely LC3A, LC3B, GABARAP, and GATE-16. The cDNA of these proteins was amplified from their original vectors (table 2.6) and cloned into pCoofy1, pCoofy3, pCoofy4, and pCoofy16. All cDNAs corresponded to isoform 1, and therefore to the ‘canonical’ form, as specified in Uniprot. Uniprot identifiers are Q9H492-1 for LC3A, Q9GZQ8-1 for LC3B, O95166-1 for GABARAP, and P60520-1 for GATE-16. Primers used for

amplification are listed in table 2.13, p. 42. Primers were designed such, that the last amino acid in the construct corresponds to the C-terminal Glycine of hATG8s, to which PE is conjugated. Therefore, pre-processing by ATG4 is unnecessary for the conjugation reaction. Furthermore, an N-terminal cysteine was introduced for fluorescent labeling using the QuikChange Lightning Site-Directed Mutagenesis Kit. Primers used for site-directed mutagenesis are listed in table 2.13, p. 42.

ATG3 The cDNA for ATG3 corresponded as well to isoform 1 (Uniprot identifier Q9NT62-1) and was cloned into pCoofy1, pCoofy3, pCoofy4, and pCoofy16 with the primers specified in table 2.13, p. 42).

ATG12–ATG5 ATG7 and ATG10 are E1- and E2-like enzymes, respectively, and are therefore part of the enzymatic cascade needed for production of the ATG12–ATG5 conjugate. Sequencing revealed, that the ATG10 cDNA contained a deletion of two nucleotides and two point mutations. These errors were removed by site-directed mutagenesis and the sequence corresponded to the ‘canonical’ sequence of isoform 1 (Uniprot identifier Q9H0Y0-1, mutagenesis primers in table 2.13, p. 42). ATG7 cDNA retrieved from the ImaGenes library corresponded to isoform 2, but was correct apart from that (Uniprot identifier O95352-2). ATG5 cDNA matched the long and therefore canonical isoform (Uniprot identifier Q9H1Y0-1), as well as ATG12 (Uniprot identifier O94817-1).

For the production of ATG12–ATG5 several cloning strategies were tried in parallel. One was to express all proteins involved in the enzymatic cascade individually. Therefore the cDNAs of ATG7, ATG10, ATG12 and ATG5 were cloned from their original vectors (table 2.6) into pCoofy1, pCoofy3, pCoofy4, and pCoofy16 (primers in table 2.13, p. 42). A second cloning strategy was the coexpression of all proteins that are part of the cascade at once. There, the aim was to produce the ATG12–ATG5 conjugate directly and purify it, without having to express and purify four individual proteins. For this strategy, a polycistronic expression vector, pST39, was used [Tan 2001] and cloning was performed with the In-Fusion HD Cloning Kit (Clontech). Additionally, also vectors were produced that contained a fifth protein, either ATG16L1 or TECPR1. These two proteins are known to bind ATG12–ATG5 and it was hypothesized that they could stabilize ATG12–ATG5. For polycistronic expression, a ribosomal-binding site, consisting of a translational enhancer and a Shine-Dalgarno sequence, was inserted between the coding cDNAs. Cloning was performed in two steps, since five proteins are likely too many for a correct insertion in one step. In the first step, pST39 was linearized and cDNAs of ATG7, ATG10,

and ATG12 were ligated into pST39. In a second step, the vector was linearized once again and cDNAs of ATG5 and either ATG16L1 or TECPR1 were ligated. Additionally, an N-terminal His₆-tag was added to ATG5, for subsequent affinity chromatography (primers in table 2.15, p. 43). First test-expressions did not yield the ATG12–ATG5 conjugate, which is why the vector was modified further. The turning point in the production of ATG12–ATG5 was the substitution of ATG7 isoform 2 to isoform 1. Isoform 1 contains 27 additional amino acids, which were added into pST39 by linearization and religation of pST39 via recombination. Further, due to an unstable N-terminus of ATG12, a His₁₀-tag was added to ATG12 instead of the His₆-tag on ATG5, and a Precision Protease cleavage site was introduced to remove the tag later. Temporarily, ATG12 was expressed in this construct as MBP fusion protein, however later it was found that MBP was not necessary for ATG12 stabilization. These modifications were also achieved by recombination (primers in table 2.15, p. 43). Finally, a codon for cysteine was added to the N-terminus of ATG12 for fluorescent labeling of the conjugate by site-directed mutagenesis. Figure 2.2 depicts the final pST39 vector cloned for ATG12–ATG5 production.

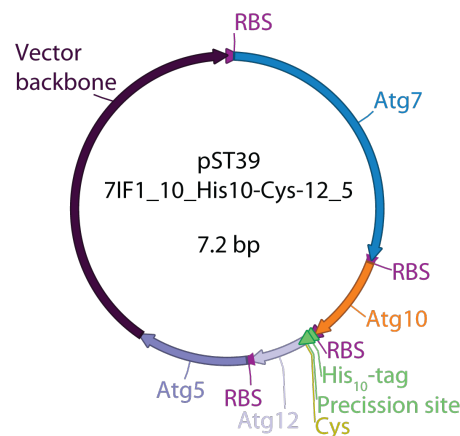


Figure 2.2.: Vector map of final pST39 polycistronic expression vector for ATG12–ATG5. cDNA of all proteins part of the enzymatic cascade for conjugate production (ATG7, ATG10, ATG12, ATG5) were cloned into the vector backbone, separated by ribosomal binding sites (RBS). A His₁₀-tag for affinity purification was cloned at the N-terminus of ATG12, followed by a cleavage site for precision protease to remove the tag after purification. Furthermore, a cysteine codon was added before the methionine start-codon for labeling of the protein.

ATG7 As mentioned in the above paragraph, the cDNA picked from the library for ATG7 translated for isoform 2. As found out for ATG12–ATG5, only isoform 1 is enzymatically active. ATG7 is needed as purified protein as well for conjugating

hATG8 to PE. Therefore isoform 1 linearization and recombination was also performed on pCoofy vectors with the same primers (Atg7_IF1_lin_fw and rv, table 2.15, p. 43). Aside from pCoofy1, 3, 4, and 16, other vectors and strains were tried for expression of ATG7, amongst others pCoofy37 or pGEX-6P-1. However, expression in *E. coli* was not successful, which is why ATG7 was also cloned in vectors suitable for insect cell expression. Due to the modular expression system provided by the Core Facility, the same primers could be used for SLIC of ATG7 (table 2.13) into pCoofy27 (pFastBac, N-terminal His₇), pCoofy28 (pFastBac, N-terminal His₆-GST), and pCoofy29 (pFastBac, N-terminal His₆-MBP).

ATG16L1 The cDNA for ATG16L1 picked from the library contained one deletion of four base pairs and one point mutation. These errors were removed by site-directed mutagenesis (primers in table 2.17). Furthermore, the ATG16L1 cDNA translated for isoform 2. The missing 19 amino acids were cloned into the cDNA by linearization and religation (SLIC, primers in table 2.17, Uniprot identifier Q676U5-1). ATG16L1 cDNA was cloned into pCoofy1, 3, 4, 16, 37, 27, 28, and 29 via SLIC cloning (primers in table 2.17), as well as in pST39 via InFusion cloning (primers in table 2.15). Furthermore, truncated forms of ATG16L1 were cloned, namely ATG16L1^{ΔWD}, missing the WD domain, into pCoofy1, 3, 4, 16, 37, and pST39 (AA 1-319, as in Boada-Romero et al. [2013]), and two forms of ATG16 N-terminus, both containing only the ATG5 binding domain, into pCoofy1, 3, 4, 16, 37, and pST39 (AA 1-43 and AA 11-43, as in Otomo et al. [2013]).

TECPR1 TECPR1 cDNA was picked from the library and corresponded to isoform 1, the canonical form (Uniprot identifier Q7Z6L1-1). The cDNA was cloned into pCoofy1, 3, 4, 16, 27, 28, 29, and pST39 by SLIC (primers in table 2.17 and 2.15).

2.5. Protein expression and purification

2.5.1. Test expressions

To test, whether the desired protein is expressed and if the protein is soluble, test expressions were carried out. Strains usually tested were *E. coli* BL21 (DE3) Rosetta, BL21 (DE3) with pGKJE8 vector (TaKaRa), which encodes for *E. coli* chaperones dnaK-dnaJ-grpE and groES-groEL, and *E. coli* Arctic Express. 50 ml cultures were grown in LB or TB medium (table 2.1) with the appropriate antibiotics at 37°C (Arctic Express at 30°C) and 180 rpm over night. Expression of chaperones was

induced after 1 hour with 0.2% (W/v) arabinose (Carl Roth) and 5 ng/ml tetracycline (PanReac AppliChem). When cells reached an OD_{600} of 0.4, cultures were cooled to 18°C and at $OD_{600} = 0.6$ induced for recombinant protein expression with 0.3 mM IPTG (Carl Roth) and grown over night. Samples of $OD_{600} = 1$ were taken before and after induction ('non-induced' and 'induced'). 25 ml culture was harvested for 10 minutes at 4000 g, resuspended in 1 ml lysis buffer (table 2.3), and lysed by sonication. The lysate was centrifuged for 20 minutes at 17000 g and the pellet was resuspended in 1 ml 6 M Urea (Sigma-Aldrich; 'pellet'). The supernatant was collected ('soluble fraction') and incubated with 30 μ l of washed Ni-NTA agarose (QIAGEN) for 1 hour at 4°C. The His-tag of the recombinant proteins binds to Ni^{2+} and therefore bound proteins are not removed by washing. Ni-NTA was washed twice with lysis buffer by centrifugation and resuspension ('pull-down'). All samples were mixed with SDS loading buffer (table 2.3) and subjected to SDS-gel electrophoresis.

2.5.2. Large scale expression and purification

Final constructs, which were used for protein production are listed in table 2.9. These constructs were chosen based on best test-expression and purification results.

Table 2.9.: Final constructs, strains, and medium used for protein expression of human ATG proteins. ICM Insect cell medium.

Insert	Vector	Expression strain	Medium
Cys-LC3A	pCoofy1	<i>E. coli</i> , Rosetta	LB
Cys-LC3B	pCoofy1	<i>E. coli</i> , Rosetta	LB
Cys-GABARAP	pCoofy1	<i>E. coli</i> , Rosetta	LB
Cys-GATE-16	pCoofy1	<i>E. coli</i> , Rosetta	LB
ATG3	pCoofy1	<i>E. coli</i> , Rosetta	LB
ATG7-ATG10-His ₁₀ -Cys-ATG12-ATG5	pST39	<i>E. coli</i> , Rosetta	LB
ATG7	pCoofy27	Insect cells SF9	ICM, 5% FCS
ATG16L1	pCoofy29	Insect cells H5	ICM
ATG16L1 N-Terminus (11-43)	pCoofy4	<i>E. coli</i> , Rosetta	LB
ATG16L1 Δ WD	pCoofy4	<i>E. coli</i> , Rosetta	LB

Expression ATG3 and ATG8 proteins were produced by setting up 3 liters of culture with appropriate antibiotics, growing the cells at 37°C and 180 rpm to OD_{600} of 0.6, inducing them with 0.3 mM IPTG and growing them for 3 hours at 37°C.

For all other proteins expressed in *E. coli*, as well as yeast proteins used in AFM experiments (cloned constructs provided by V. Beier), 6 liters culture were set up, grown at 37°C and 180 rpm until they reached an OD₆₀₀ of 0.3, cooled to 18°C, induced with 0.3 mM IPTG when an OD₆₀₀ of 0.6 was reached, and grown over night at 18°C and 180 rpm.

For production of ATG7 and ATG16L1, SF9 (ATG7) and H5 (ATG16L1) insect cells were grown to 1x10⁶ cells/ml in EX-CELL 420 serum-free medium (Sigma-Aldrich), supplemented with 5 % Fetal Bovine Serum (FCS, heat inactivated, F4135, Sigma) for SF9 cells. Baculovirus-infected insect cells (BIICs) were provided by the Core Facility and added in a ratio of 1:4000 (ATG7) or 1:1000 (ATG16L1). Cultures were shaken for 72 hours at 25°C and 85 rpm.

Purification *E. coli* cells were harvested by centrifugation at 4500 g for 10 minutes, resuspended in lysis buffer, supplemented with protease inhibitor cocktail (Sigma) and benzonase (Sigma). *E. coli* cells were either lysed by sonication (2x 10 minutes) or with a microfluidizer processor (Microfluidics). Insect cells were harvested by centrifugation at 2000 g for 15 minutes, washed with Dulbecco's phosphate buffered saline (DPBS, Gibco) and resuspended in lysis buffer. ATG7 and ATG8 buffers did not contain β-mercaptoethanol and ATG16L1 (as well as its constructs) lysis buffer contained 500 mM NaCl. Insect cells were lysed using a dounce homogenizer.

After lysis, cell suspensions of *E. coli* and insect cells were treated equally. Cell suspension was centrifuged at 45000 g for 1 hour and the supernatant was incubated with 1-2 ml Ni-NTA agarose for 1 hour at 4°C. Unbound proteins were removed by washing with washing buffer, which contained 5 mM imidazole and competes for binding to Ni²⁺ ions. Recombinant proteins were eluted with elution buffer, containing 500 mM imidazole and therefore removing also His-tagged proteins. Washing and elution buffer for ATG16L1 and its constructs contained 500 mM NaCl. Except for ATG16NT(11-43), where the fusion protein was purified, the affinity tag of the recombinant proteins was removed by incubation of the eluate with PreScission protease for 45 minutes at room temperature in presence of 5 mM DTT (AppliChem) and 1 mM EDTA (Carl Roth). The digested proteins were subjected to size-exclusion chromatography (SEC) with size exclusion buffer (table 2.3) on a HiLoad 16/60 Superdex 75 (Atg16, ATG3, ATG8 proteins) or Superdex 200 column (all others; both columns GE healthcare). ATG16L1 size exclusion buffer contained 400 mM NaCl. Chromatography was performed on an ÄKTAexplorer (GE healthcare).

Mass spectrometry All purified proteins were pooled and concentrated using Vivaspin cellulose centrifugation filters according to the size of the protein (Sartorius stedim). Subsequently, proteins were flash frozen in liquid nitrogen and stored at -80°C . Protein concentrations were determined using a Pierce BCA Protein Assay Kit (Thermo Scientific), according to the manufacturer's protocol. To confirm the identity of the protein, samples were analyzed with Liquid Chromatography-Mass Spectrometry (LC-MS), using an Aeris WIDEPOR C4 column with $3.6\ \mu\text{m}$ particle size and $300\ \text{\AA}$ pore size (Phenomenex) with an acetonitrile gradient from 30% - 80% (v/v) in 15 minutes, coupled to an ESI-MS microTOF (Bruker Daltonik, operated by the Core Facility). Both water (solution A) and acetonitrile (solution B) contained 0.05% trifluoroacetic acid. All mass spectra were calibrated with sodium formate standard and detection ranged from 800 to 3000 Da in positive mode.

2.6. Protein and lipid labeling

Proteins were labeled by maleimide-coupling of fluorescent dyes to cysteine residues. To avoid sterical hindrance of the fluorescent dyes, N-terminal cysteine residues were introduced for hATG8s and ATG12-ATG5 (chapt. 2.4). ATG16L1 possesses 12 native cysteines, therefore an additional N-terminal cysteine was considered not to be necessary. Used dyes were CF405M (Biotium), Alexa Fluor 488 C5 maleimide (Molecular probes), and Atto590 maleimide (ATTO-TEC). Proteins were labeled immediately after size exclusion chromatography to avoid disulphide-bond formation. In the absence of a reducing agent, the fluorescent dye was added in a 1:1 molar ratio (protein : dye) to the protein (GABARAPs, ATG12-ATG5, ATG16L1) and incubated for 1 hour at room temperature. To remove unbound dye, labeled proteins were subjected to desalting, using either two consecutive HiTrap Desalting columns (GE healthcare), or Zeba Spin Desalting Columns (7k MWCO, Thermo scientific, for ATG16L1). LC3A and LC3B were binding to the desalting matrix. Therefore, LC3A and LC3B were labeled with a molar ratio of 1:0.8 and unlabeled dye was not removed, because it was assumed that the dye was completely bound to the proteins. The concentration and degree of labeling was determined spectroscopically according to the manufacturer's protocol.

Phosphatidylethanolamine (PE) was labeled with Atto680 NHS-Ester (ATTO-TEC). For labeling, 0.63 mM Atto-680-NHS (in DMSO) was first mixed with 17.64 mM triethylamine (Alfa Aesar), in a second step mixed with 0.84 mM POPE or DOPE in chloroform, and incubated for 1 hour at room temperature.

2.7. Gel electrophoresis and Western Blotting

Gel electrophoresis SDS-PAGE gels with different concentrations of polyacrylamide were prepared, according to the size of the protein to be analyzed. Concentrations of resolving and stacking gels are stated in table 2.10. 10-15 μ l sample and marker were loaded. For SDS-PAGE and gradient gels (NuPAGE 4-12 % Bis-Tris gels, Novex), BenchMark Protein Ladder (Novex) was used, for Urea-SDS-PAGE and gels that were intended for Western Blotting, Sharp Pre-Stained Protein Standard (Novex) was used. SDS-PAGE and Urea-SDS-PAGE gels were run in SDS running buffer, gradient gels in MES SDS running buffer (table 2.2). Electrophoresis was performed at 40 mA for SDS-PAGE, at 16 mA for Urea-SDS-PAGE gels, and at 200 V for gradient gels. Gels were stained with coomassie staining solution for 1 hour and destained using Destaining solution. To remove water from the gels and therefore avoid rupture during drying, gels were placed into shrinking solution (table 2.2) and dried between two cellophane sheets (Carl Roth).

Western Blotting Western Blotting was performed with SDS-PAGE gels. Gels were equilibrated in blotting buffer for 10 minutes (table 2.2) and PVDF membrane (Bio-Rad) was activated for 1 minute in methanol. Blotting was performed in a semi dry blotting chamber at 15 V for 45 minutes. Membrane was then blocked in 5 % milk (Carl Roth) in TBS-T buffer (w/v, Carl Roth) for 1 hour at room temperature, washed 3 times in TBS-T and incubated with primary antibody at 4°C over night. Membrane was washed 3 times with TBS-T for 10 minutes each, incubated in secondary antibody for 1 hour at room temperature, and washed again 3 times. Specifications of antibody dilutions can be found in table 2.11. Blots were developed using SuperSignal West Femto Substrate kit (Thermo Fisher Scientific) and chemiluminescence was detected with a luminescent Image Analyzer LAS-3000 (Fujifilm).

Table 2.10.: Concentrations for polyacrylamide gel electrophoresis (PAGE) with variable percentage of acrylamide. The same stacking gel mixture was used throughout. Urea-SDS gel was prepared according to Nakatogawa et al. [2012a].

SDS-PAGE (4 gels)	resolving gel				stacking gel
	7.5 %	10 %	12 %	15 %	
H ₂ O (Milli-Q grade)	14.8 ml	12.2 ml	10.2 ml	7.2 ml	6.2 ml
1.5 M Tris-HCl, pH 8.8	7.6 ml	7.6 ml	7.6 ml	7.6 ml	
0.5 M Tris-HCl, pH 6.8					2.5 ml
30 % Acrylamid/Bisacrylamid (37.5:1, Carl Roth)	7.5 ml	10 ml	12 ml	15 ml	1.34 ml
10 % SDS	300 µl	300 µl	300 µl	300 µl	100 µl
TEMED (Serva)	40 µl	40 µl	40 µl	40 µl	10 µl
25 % APS (Serva)	40 µl	40 µl	40 µl	40 µl	20 µl
Urea-SDS-PAGE (1 gel)	13.5 %				
Urea		3.6 g			
30 % Acrylamid/Bisacrylamid		4.5 ml			
1.5 M Tris-HCl, pH 8.8		2.5 ml			
10 % SDS		100 µl			
TEMED		10 µl			
25 % APS		40 µl			

Table 2.11.: Antibodies used in this thesis; BSA Bovine Serum Albumin.

Primary Antibodies	Dilution
Mouse anti-His (No. 05-949, Millipore)	1:2000 in 3 % milk
Rabbit anti-Atg12 (Human specific) (No. 2010, Cell Signaling Technology)	1:1000 in 5 % BSA (VWR)
Rabbit anti-Atg7 (human, mouse & rat) (No. A2856, Sigma-Aldrich)	1:1000 in 5 % BSA
Secondary Antibodies	Dilution
Goat anti-mouse, horseradish peroxidase conjugate (No. AP308P, Merck Millipore)	1:4000 in 3 % milk
Goat anti-rabbit, horseradish peroxidase conjugate (No. 611-1302, Rockland Immunochemicals)	1:4000 in 3 % milk

2.8. Preparation of Liposomes

Large unilamellar vesicles The lipid mixture for large unilamellar vesicles (LUVs) consisted of 20 mol % Cholesterol, 49.9 mol % POPC, 10 mol % POPS, 20 mol % POPE, and 0.1 mol % lissamine-rhodamine-PE in chloroform (7 mM total lipid concentration). 1 mg total lipid was dried under rotation in a small glass vial (8 x 70 mm, Duran) under nitrogen flow and further in vacuum over night. Lipids were resuspended with 1 ml lipidation buffer (table 2.2) by vortexing for 1 minute repeatedly until mixture was opaque, containing multilamellar vesicles (MLVs). LUVs were produced by extruding the MLV mixture using a Mini-Extruder (Avanti) and a 100 nm pore size membrane (no. 800309, Whatman).

Giant unilamellar vesicles The lipid mixture for giant unilamellar vesicles (GUVs) consisted of 20 mol % Cholesterol, 39.9 mol % POPC, 10 mol % POPS, 30 mol % 1,2-dioleoyl-*sn*-glycero-3-phosphoethanolamine (DOPE), and 0.2 mol % Atto680-DOPE in chloroform (provided by L. Dempfle, 7 mM total lipid concentration). GUVs were prepared by electroformation, using custom-made teflon chambers [Betaneli et al. 2012]. 7 μ l of lipid mixture were spread evenly on two platinum wires and dried in vacuum for 30 minutes. The chamber was assembled, containing 600 mM sucrose solution (osmolarity 600 mOsm/l). Electroformation was induced by applying an alternating electric current (2 V, 10 Hz) for 1.5 hours, followed by a reduced frequency of 2 Hz for 30 minutes, to detach vesicles from the electrodes. GUVs were diluted 1:1 with 600 mM sucrose solution.

2.9. *In vitro* lipidation reaction

GUV experiments The hATG8 proteins were preincubated with ATP, DTT, ATG7 and ATG3, for thioester intermediate formation, and ATG12-ATG5 was preincubated with ATG16L1 for complex formation, in SEC running buffer (table 2.3) for 30 minutes at 37°C. Final concentrations were: 0.1 mM DTT, 1 mM ATP/Mg²⁺, 1 μ M ATG7, 1.5 μ M ATG3, 1 μ M ATG7, 6 μ M hATG8, and 0.5 μ M ATG12-ATG5-ATG16L1. hATG8s were used in a 2:1 ratio of unlabeled and labeled protein. After separate preincubation, protein mixtures were combined. During incubation time, 8-well microscopy chambers (Lab-Tek) were coated with BSA (5 mg/ml in 25 mM Tris, pH 7.4) by covering the complete bottom of the chamber, incubating for 10 minutes at room temperature and then washing the chamber with lipidation buffer.

Final samples were prepared by pipetting 100 μ l of GUV suspension in the coated

chambers, together with 100 μ l of combined preincubated proteins and mixing carefully to not disrupt GUVs. Due to this 1:1 dilution, final buffer concentration corresponded to the lipidation buffer, because proteins were preincubated in SEC running buffer (= 2x lipidation buffer, table 2.3). For conjugating hATG8s to GUVs, samples were incubated further for 1 hour at 37°C.

Thioester intermediate detection Proteins were directly mixed in lipidation buffer, but otherwise treated similarly as in GUV experiments, except of conjugating LC3A to LUVs instead of GUVs. The reaction was stopped by adding 3x sample buffer without DTT and heating the protein mixtures for 5 minutes at 42°C, to not disrupt thioester bonds. Samples were subjected to gradient gels for thioester intermediate detection, and Urea-SDS-gels for detecting conjugated LC3A [Nakatogawa et al. 2012a].

2.10. Confocal microscopy

Microscopy experiments with human proteins were conducted on a Zeiss LSM780 confocal laser scanning microscope with a 63x/1.4 NA objective. 405 nm, 488 nm, 594 nm, 561 nm, and 633 nm laser lines were used for excitation of CF405M, Alexa488, Atto590, rhodamine, and Atto680, respectively. For overview images, at least 3 different non-overlapping positions were chosen. Images were acquired using Zeiss ZEN 2011 software and analyzed with FIJI [Schindelin et al. 2012].

FRAP experiments on GUVs For FRAP experiments, ~10 % of one GUV was bleached with 100 % of all lasers used in the respective experiment and 2 iterations. Recovery was observed for 20 cycles over 6-8 minutes. For FRAP analysis with Zeiss ZEN 2011, additional regions of interest (ROIs) were chosen as references for background and non-bleached fluorescence (same GUV). Recovery was fitted with an exponential fit for one mobile species, and immobile fractions (100% -I1) were determined. The following formula was used for fitting:

$$I = IE - I1 * \exp(-t/T1)$$

2.11. Primers

Table 2.12.: Sequencing primers used in this thesis.

Protein	Primer Name	Primer Sequence
general	SP6	athtagtgacactatagaa
	T7_fw	taatacgactcactataggg
	M13-FP	tgtaaacgacggccagt
	M13-RP	caggaaacagctatgacc
	GST-seq	catggaccaatgtgcctg
	MBP_seq_rv	cgggtgtctgcattcatgtgttg
	pCoofy27_seq	ctatagttctagtggtggctacg
ATG3	Atg3_Hs_91_Fw	cagggtgaattaccccagaagag
	Atg3_Hs_696_Fw	gcacatgtatgaagacatcagtc
ATG5	Atg5_Hs_180_fw	gagacaagaagacattagtgag
	Atg5_Hs_796_fw	catattagttatcatcccacagcc
	Atg5_Hs_83_rv	gtatggttctgcttcctttcag
ATG7	Atg7_Hs_426_fw	ccacttctactattggttttgc
	Atg7_Hs_1028_fw	gattggttctacttttagacttgg
	Atg7_Hs_1599_fw	cctcctgggctcatcgctttttgc
	Atg7_Hs_606_rv	cagccatgttctcatcatac
ATG10	Atg10_Hs_225_fw	cgagctacccttgatgattg
	Atg10_seq_rv	cttcagagttaaaggtctcccatc
ATG12	Atg12_188_fw	gagacactcctattatgaaaacaaag
	Atg12_Hs_174_rv	ggagtgtctcccacagccttttagc
ATG16L1	Atg16L1_Hs_135_fw	gtcagatcttcattcagtgttgg
	Atg16L1_Hs_589_fw	gagaaagcccaggaagccaatcg
	Atg16_Hs_931_fw	ccagctactgccttgtgtgtc
	Atg16L1_Hs_1204_fw	gcgcggattgtctcaggaagtc
	Atg16L1_Hs_45_rv	ctcagttgctccgagatgtgg
	Atg16L1_Hs_1204_rv	gacttcctgagacaatccgegc
TECPR1	TECPR1_Hs_236_fw	ccatgggaggccttctgtgag
	TECPR1_Hs_567_fw	ccccttcaacgacctctctgtag
	TECPR1_Hs_1190_fw	gcttcttcggtgatgaggtgaggg
	TECPR1_Hs_1782_fw	ggagaactcagacactacgagc
	TECPR1_Hs_2415_fw	ggccagcagcaccagtaacatc
	TECPR1_Hs_3016_fw	gacggctccgccttctaccg

Table 2.13.: Primers for SLIC cloning of human Atg8 homologs, ATG3, ATG10, ATG12, and ATG5. Gene specific sequences are marked in blue. (**First part**) Primers for SLIC cloning of hATG8s. The C-terminal Glycine is marked in green. (**Second part**) Primers for site-directed mutagenesis for introduction of cysteine (orange) at N-terminus before Start-Codon. (**Third part**) Primers for SLIC cloning of human ATG3. (**Fourth part**) Primers for site-directed mutagenesis of ATG10. Changed bases are marked in green. (**Fifth part**) Primers for SLIC cloning of ATG7, ATG10, ATG12, and ATG5. Gene specific sequences are marked in blue.

Primer Name	Primer Sequence
LC3A_pCoofy1_fw	aagttctgttcaggggccccatgccctcagaccggc
LC3A_pCoofy1_rv	cccagaacatcagggttaatggcgctcagccgaaggtttcctggg
LC3B_pCoofy1_fw	aagttctgttcaggggccccatgccctcggagaagaccttc
LC3B_pCoofy1_rv	cccagaacatcagggttaatggcgcttaccgaacgtctcctggg
GABARAP_pCoofy1_fw	aagttctgttcaggggccccatgaagttcgtgtacaaagaagagcatcc
GABARAP_pCoofy1_rv	cccagaacatcagggttaatggcgctcaccgtagacactttcgtcactgtagg
GATE-16_pCoofy1_fw	aagttctgttcaggggccccatgaagtggatgttcaaggaggacc
GATE-16_pCoofy1_rv	cccagaacatcagggttaatggcgctcagccaaaagtgttctctccgc
LC3A_CysIns_fw	gttcaggggccccatgcatgccctcagaccg
LC3A_CysIns_rv	cggctctgagggcatgcaagggccctggaac
LC3B_CysIns_fw	gttcaggggccccatgcatgccctcggagaag
LC3B_CysIns_rv	cttctccgacggcatgcaagggccctggaac
GABARAP_CysIns_fw	gttcaggggccccatgcatgaagttcgtgtacaaagaag
GABARAP_CysIns_rv	cttctttgtacacgaacttcatgcaagggccctggaac
GATE-16_CysIns_fw	gttcaggggccccatgcatgaagtggatgttcaagg
GATE-16_CysIns_rv	ccttgaacatccacttcatgcaagggccctggaac
Atg3_Hs_pCoofy1_fw	aagttctgttcaggggccccatgcagaatgtgattaatactgtgaaggaaagg
Atg3_Hs_pCoofy1_rv	cccagaacatcagggttaatggcgcttacattgtgaagtgtcttgtgtagtcattctattgttgg
Atg10_ins_ag74/75_fw	agaattcattaaacattcacaacagataggtgatagttgggaatggag
Atg10_ins_ag74/75_rv	ctcattcccaactatcacctatctgttgtgaatgtttaatgaattct
Atg10_mut_t635c_fw	ctgagttatgccaagcaaagcgtctcaggatgaacgaa
Atg10_mut_t635c_rv	ttcgttcacctcagacgttgccttggcataactcag
Atg10_mut_a659c_fw	tctcaggatgaacgaaatgtcccttaacaagattcttctattgag
Atg10_mut_a659c_rv	ctcaatagaagaatcttgttaaaggacatttcgttcacctcagaga
Atg5_Hs_pCoofy1_fw	aagttctgttcaggggccccatgacagatgacaaagatgtgcttcgagatg
Atg5_Hs_pCoofy1_rv	cccagaacatcagggttaatggcgctcaatctgttgctgtgggatgataactaatatg
Atg7_Hs_pCoofy1_fw	aagttctgttcaggggccccatggcggcagctacgg
Atg7_Hs_pCoofy1_rv	cccagaacatcagggttaatggcgctcagatggctcatcatcgctcatg
Atg7_pCTEV_rv	gccctgaaaatacaggttttcgatggctcatcatcgctcatg

Atg10_H_pCoofy1_fw	aagttctgttccaggggccc atggaagaagatgagttcattggagaaaaaacattcc
Atg10_H_pCoofy1_rv	cccagaacatcaggttaatggcg ttaaggacatttcgttcacctgagacg
Atg12_Hs_pCoofy1_fw	aagttctgttccaggggccc atgactagccgggaacaccaag
Atg12_Hs_pCoofy1_rv	cccagaacatcaggttaatggcg tcacccccacgcctgag

Table 2.15.: Primers for In-Fusion cloning of ATG7, ATG10, ATG12 and ATG5 into pST39. (**First part**) Green marks homology sequences to either pST39 or the preceding protein. Blue and violet mark the translational enhancer and the Shine-Dalgarno sequence, respectively. Start and stop codons are marked in red and the His₆ tag in orange. (**Second part**) Primers for further modifications of pST39. Additional sequence of ATG7 isoform 1 marked in violet, cysteine codon for fluorescent labeling of Atg12 marked in orange.

Primer Name	Primer Sequence
pST39_linalize_rv	gaattcactggcgcgctgttttacagg
pST39_linalize_fw	ggtaccagcggataacaatttcacatc
InFus_At7_fw	acggccagtgaattc aataat ttgtttaactttaagaaggag atatacat atggcggcagctacgggg
InFus_At7_rv	tcagatggtctcatcatcgctcatgtc
InFus_At10_fw	gatgagaccatctga aataat ttgtttaactttaagaaggag atatacat atggaagaagatgagttcattggag
InFus_At10_rv	ttaaggacatttcgttcacctg
InFus_At12_fw	cgaaatgtcccttaa aataat ttgtttaactttaagaaggag atatacat atgactagccgggaacaccaag
InFus_At12_rv	ttatccgctggtacctc atccccacgcctgagac
pST39_linalize2_rv	tcacccccacgcctgagac
InFus_At5_His_fw	caggcgtgggatga aataat ttgtttaactttaagaaggag atatacat atgggcagcagccatcaccatcaccatcacggcagcatg acagatgacaaagatgtgcttc
InFus_At5_rv	tcaatctgttgctgtggg
InFus_At16L1_fw	cagccaacagattga aataat ttgtttaactttaagaaggag atatacat atgtcgtcgggctccgc
InFus_At16L1_rv	ttatccgctggtacctc agtactgtgcccacagcacagct
InFus_TECPR1_fw	cagccaacagattga aataat ttgtttaactttaagaaggag atatacat atgcccaactcagtgtgtggg
InFus_TECPR1_rv	ttatccgctggtacctc agcagcagacggggcc
Atg7_IF1_lin_fw	ggcatttgacaaatgtacagcttgttcttccaaa gttcttgatcaatatgaacgagaaggatttaacttc
Atg7_IF1_lin_rv	ctgtacatttgtcaaatgccaggctgacgggaagg acattatcaaaccgtgaaagaaatccccggatctggtgaggcacaagcccaag
pST_At10_lin_rv	aattgttatccgctggtaccttaaggacatttcgttcacctg

pST_At5_lin_Rv	acatctttgtcatctgtcatatgtatatctccttcttaaagttaaa caaaattatttcatccccacgcc
pST_At5_lin_Fw	atgacagatgacaaagatgtgcttcg
pST_At12_lin_Rv	tggtgatggtgatgtttcatatgtatatctccttcttaaagttaaaca aaattattttaaggacatttcg
pST_At12_VL_lin_Fw	aagttctgttccaggggcccattggcggaggagccgcagtc
His-MBP-Fw	atgaaacatcaccatcaccatcacccc
pST_His10_lin_rv	acccgcggagtgatggtgatggtgatggtgatggtgatgtttcatatg
pST_His10_lin_fw	catcaccatcactccgcgggtctggaagttctgttccagggg
ATG12_CysIns_fw	gttccaggggccc tg catggcggaggagc
ATG12_CysIns_rv	gctcctccgcat g cagggccctggaac

Table 2.17.: Primers for ATG16L1 and TECPR cloning. **(First part)** Primers for site-directed mutagenesis of ATG16. Changed bases and additional sequence for ATG16L1 isoform are marked in green. **(Second part)** Primers for SLIC cloning of ATG16. Gene specific sequences are marked in blue. **(Third part)** Primers for truncated versions of ATG16L1. Stop codons introduced by site-directed mutagenesis marked in red. **(Fourth part)** Primers for TECPR1 cloning.

Primer Name	Primer Sequence
Atg16_ins_ttag316_fw	acaagaaacgtggggag ttag ctcaactggtgattgac
Atg16_ins_ttag316_rv	gtcaatcaccagttgag cta actccccacgtttcttgt
Atg16L1_Mut_g840a_fw	ccccaggacaatgtggat act catcctgttctggtaaag
Atg16L1_Mut_g840a_rv	ctttaccagaaccagatgat t atccacattgtcctggggg
Atg16L1_IF1_fw	gccatcagcagagcagccact taagc actct cg cagcct gct ggaggcct tctggattctatacta aatatctttgggagacgctctgtctcttctccc
Atg16L1_IF1_rv	gggaaggaagagacagagcgtctcc aa agatattagtgatagaatccag aaggcctccagcaggetgcg agag tcgct ttagtggetgctctgctgatggc
Atg16L1_pCoofy1_fw	aagttctgttccaggggccc atg tc g tcgggcctcc
Atg16L1_pCoofy1_rv	cccagaacatcaggttaatggc g tcag t actgtgccacagc
Atg16L1_pCTEV_rv	gccctgaaaatacaggtttt g act g tc g ccacagcagc
ATG16_pC1_DltWD_fw	tgacgccattaacctgatgttctgg
ATG16_pC1_DltWD_rv	gaacatcaggttaatggcgtcaatcgaagacacacaaggcagtagctgg
ATG16_pC37_DltWD_rv	ccctgaaaatacaggttttcatcgaagacacacaaggcagtagctgg
ATG16_DltWD_Stop_fw	gccttgtgtgtcttcgat ga catgatggggaagtcaac
ATG16_DltWD_Stop_rv	gttgacttccccatcat g caatcgaagacacacaaggc
ATG16_1-43_Stop_fw	ctgcagtataacaaattgct g ta aa agtcagatcttcattcagtg
ATG16_1-43_Stop_rv	cactgaatgaagatctgact tt acagcaatttgttatactgcag
16.2-10_Del_pST39_fw	ctttaagaaggagatatacatatgccccgctggaagcggccac

16.2-10_Del_pST39_rv	gtggcgcttccagcggggcatatgtatatctccttcttaaag
16.1-10_Del_pC_fw	gaagttctgttccagggcccccgctggaagcgccac
16.1-10_Del_pC_rv	gtggcgcttccagcgggggggccctggaacagaacttc

TECPR1_pCoofy1_fw	aagttctgttccagggccccatgccaactcagtgtgtg
TECPR1_pCoofy1_rv	cccagaacatcaggtaatggcgtcagcagcagacgggg

3

Results

3.1. Characterization of the yeast Atg8-scaffold by AFM

The decoration of autophagosomal membranes with Atg8 conjugated to phosphatidylethanolamine (PE) is the hallmark of macroautophagy. Atg8 serves as cargo adaptor on the inner membrane of the growing phagophore, but so far its purpose on the outer membrane remained elusive. Previous studies in our lab led to the hypothesis that Atg8 and Atg12–Atg5–Atg16, the two Ubiquitin like (UBL) systems in yeast, are part of a new protein scaffold that forms on emerging autophagosomes. This hypothesis was based on *in vitro* experiments, in which the lipidation reaction of Atg8 to PE has been reconstituted on giant unilamellar vesicles (GUVs) with fluorescently labeled proteins. However, a direct visualization of the proposed scaffold was needed to validate this hypothesis. Due to technical difficulties of imaging a protein scaffold on liposomes with electron microscopy, Atomic force microscopy (AFM) was considered suitable owing to its high resolution in combination with imaging under physiological conditions.

Since only flat membranes can be imaged with AFM, the first aim was to reconstitute the lipidation reaction of Atg8 on flat model membranes, namely supported lipid bilayers (SLBs). A frequently used sample support for Atomic Force Microscopy is the mineral mica, since this sheet silicate is extremely flat and clean when freshly cleaved. SLBs could be reconstituted on mica, however, the conjugation reaction of Atg8 to PE destroyed the membrane (Fig. 3.1). Therefore, different supports were tested: first, by chemically cross-linking silane to the mica surface, the lipidation was reconstituted without destruction of the membrane. This approach preserved the flatness of the support, but was technically challenging due to a long preparation and low reproducibility of the lipidation reaction. Another support used was plasma-cleaned glass. Glass is rougher compared to mica, but the preparation was faster and the lipidation reaction did not destroy the membrane. Thus, the lipidation of Atg8 could

be successfully reconstituted on SLBs using two types of support: glass and silanized mica. For a successful reconstitution of this reaction, all participating proteins had to be incubated together with SLBs, to conjugate Atg8 to PE in the membrane. The final protein ratios used were 6:2:2:1:1 for Atg8:Atg7:Atg3:Atg12–Atg5:Atg16, together with ATP (for concentrations see chapter 2.2, p. 24).

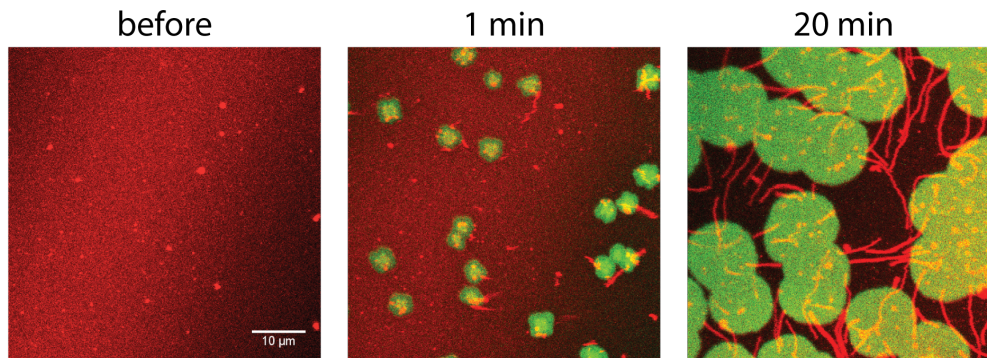


Figure 3.1.: Confocal microscopy image of supported lipid bilayer deposited on freshly-cleaved mica, labeled with Lissamine-Rhodamine in red. The bilayer is intact before the addition of proteins (**left**) but is destroyed upon addition of the yeast UBL proteins (displayed after 1 minute (**middle**) and 20 minutes (**right**), Atg8 labeled with Alexa488 in green). Atg8 binds directly to mica and displaces the bilayer from the support.

Combining AFM with confocal microscopy was an essential prerequisite for successful experiments. First, the lipidation reaction was monitored by confocal microscopy, and only if the membrane was lipidated with fluorescent Atg8 molecules, further experiments were performed with AFM. To control for a successful reaction after incubation of the proteins, the membrane was washed thoroughly to remove any soluble or unbound proteins from the membrane. Previous Fluorescence Recovery After Photobleaching (FRAP) experiments on GUVs demonstrated, that Atg8 is mobile when conjugated to the membrane with Atg12–Atg5, but immobile with Atg12–Atg5–Atg16. Therefore, similar FRAP experiments were carried out on SLBs to test whether the mobility of Atg8 can be reproduced on SLBs. In the absence of Atg16, Atg8–PE slowly recovers, indicating lateral mobility of Atg8–PE on the membrane (Fig. 3.2). The very slow recovery on SLBs compared to free-standing membranes has been reported before [Sonnleitner et al. 1999]. In the presence of Atg16, no recovery is visible even after 45 minutes of imaging. This is in agreement with previous results obtained on GUVs, where no fluorescent recovery of Atg8 or Atg12–Atg5–Atg16 was detectable. These experiments demonstrated that the lipidation reaction was successfully reconstituted on SLBs and similar results compared to

GUVs can be obtained on flat model membranes.

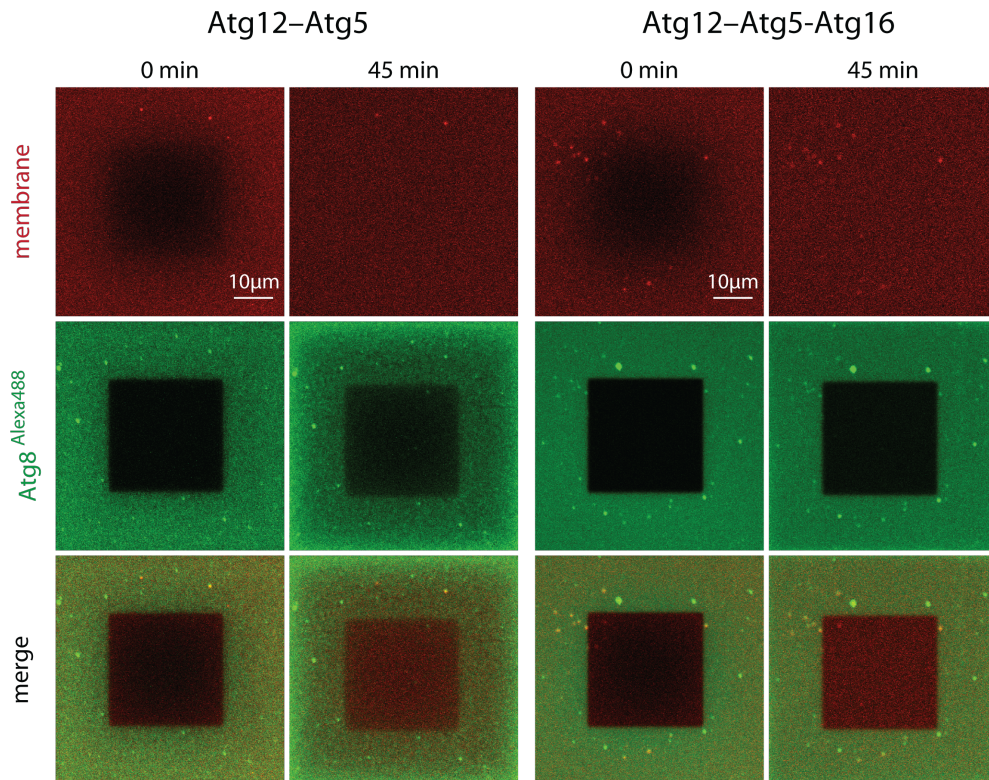


Figure 3.2.: Lipidation reaction of Atg8 (labeled with Alexa488 in green) on supported lipid bilayers (SLBs, containing Lissamine-Rhodamine-PE in red) on glass. A quadratic area was bleached on the SLB (dark square). These FRAP experiments reveal that Atg8-PE fluorescence recovers in the absence of Atg16 (left side), whereas in the presence of Atg16 no recovery is visible, even after 45 minutes (right side).

After the verification that experiments on SLBs yielded comparable results to GUVs, AFM was performed on Atg8-lipidated membranes. Fluorescence microscopy showed that the proteins of the UBL systems, namely Atg8 and Atg12-Atg5-Atg16, formed an immobile protein structure on membranes. Yet, how the proteins were structurally organized on a nanoscopic scale needed to be investigated. This was analyzed by AFM imaging of Atg8-lipidated SLBs with Atg12-Atg5 or Atg12-Atg5-Atg16.

The Atomic Force Microscope can be operated in different modes. Two major operation forms exist for imaging the topology of samples. In scanning mode, the cantilever is in constant contact to the sample and scans its surface with steady force that is controlled by a feedback loop according to the topology. This mode is well suited for hard and stable samples, because it allows for high resolution and

rapid image acquisition without deforming the sample. In tapping mode, the second mode of operation, the tip scans the sample while oscillating with a preset frequency, which is also controlled by a feedback loop. Thus, the tip is not constantly in contact with the sample and therefore minimizes deformation of the sample, but imaging acquisition is slower compared to scanning mode and oscillation frequency needs to be adjusted regularly. Here, the Atomic Force Microscope was operated in tapping mode, because proteins on top of a bilayer in physiological conditions constitute a very soft and fragile sample. Imaging these samples in scanning mode would cause distortions and disruption of delicate protein connections.

Bigger protein aggregates were detected in all samples (~ 100 nm in diameter and >20 nm in height, bright spots in Fig. 3.3). In the absence of Atg16, only small particles with no obvious structure were detectable (Fig. 3.3, A). These particles represent most likely Atg8 proteins or Atg8-PE/Atg12-Atg5 complexes, which are linked to PE but freely mobile within the membrane. They were hardly imageable due to their lateral mobility. The stripy appearance in the image stems from particles, which were stuck to the tip and dragged along by the cantilever during the horizontal scan (Fig. 3.3, A, right).

The appearance changed drastically, when also Atg16 was present in addition to Atg12-Atg5. No individual particles could be detected, rather a continuous protein layer formed on top of the SLB (Fig. 3.3, B, left). This protein layer was organized in a meshwork-like structure, which becomes even more pronounced when the topological data was averaged and filtered (Fig. 3.3, B, right). Therefore, Atg16 immobilizes and organizes Atg8-PE/Atg12-Atg5 complexes into a two-dimensional protein layer.

By using plasma-cleaned glass instead of silanized mica as support, it was possible to reduce the movement of the Atg8 particles in the absence of Atg16 considerably (Fig. 3.4). Here, regular protein aggregates were forming, consisting of Atg8 and Atg12-Atg5. Presumably the higher surface roughness of glass compared to mica hampered the diffusion of the protein aggregates and enabled a closer examination. Measuring and cross-sectioning of obtained images yielded a diameter of these particles of 50 ± 10 nm and a height of 6 ± 1 nm (Fig. 3.5, upper part). However, the diameter of Atg8 and Atg12-Atg5 is only ~ 3 nm and $\sim 6 \times 4$ nm², respectively, according to PDB entries 3VXW and 3W1S. Therefore the particles are too big to represent individual Atg8-PE conjugates or one Atg8-PE/Atg12-Atg5 complex. Taking the lateral dimensions of the cantilever into account, as well as Brownian motion of the particles, the size of the particles corresponds to two but not more than four Atg8-PE/Atg12-Atg5 complexes. Interestingly, the particles show a

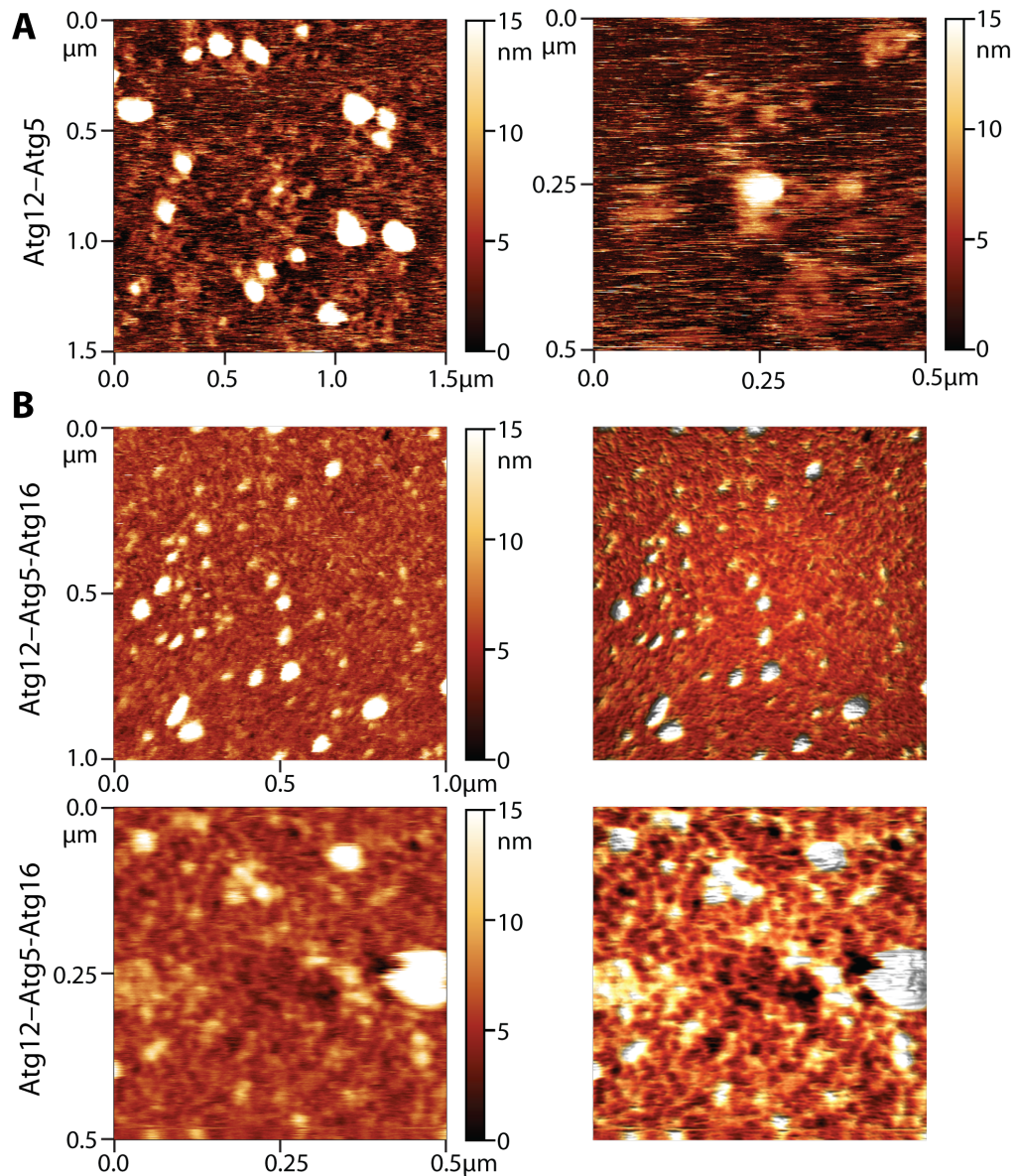


Figure 3.3.: Conjugated Atg8 to SLBs deposited on silanized mica and imaged with atomic force microscopy, in the absence or presence of Atg16. **(A)** Control reaction with Atg12-Atg5, shown in different scales, line-fitted but otherwise unmodified. White spots represent protein aggregates >15 nm in height. **(B)** In the presence of Atg16, the autophagic membrane scaffold forms, shown here in an area of $1 \mu\text{m}^2$ (upper panel) and $0,25 \mu\text{m}^2$ (lower panel). On the left side line-fitted but otherwise unmodified images are displayed, on the right side the corresponding data was averaged, filtered, and displayed in 3D projection for better visualization. A lateral meshwork-like structure of the scaffold becomes apparent.

very homogeneous size distribution, which demonstrates that Atg8-PE/Atg12-Atg5 associates into well-defined oligomeric complexes on SLBs.

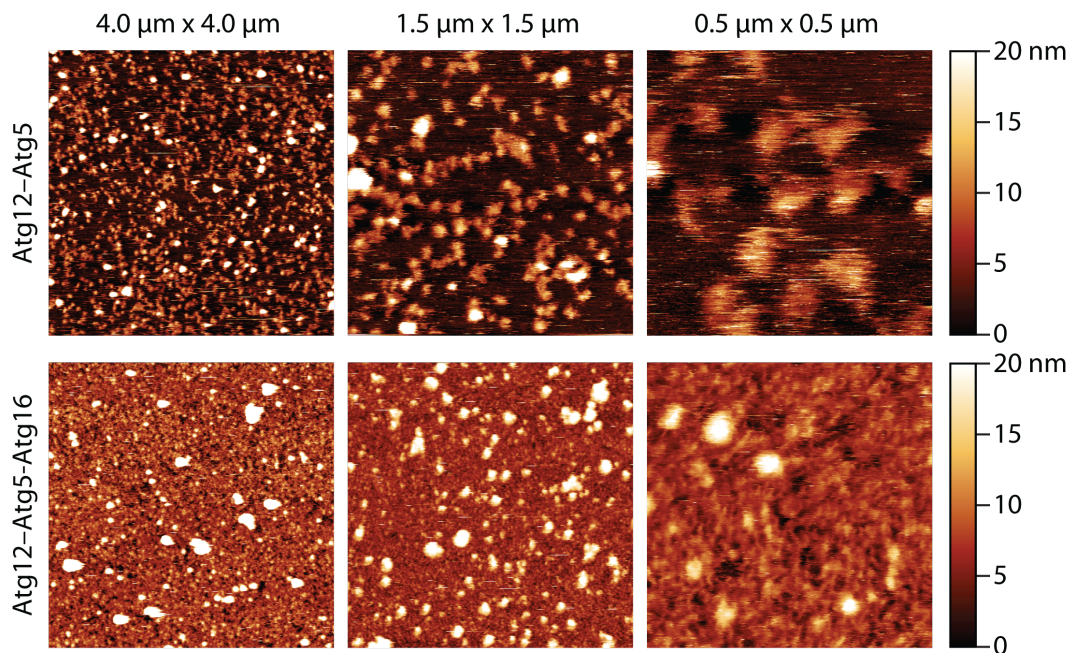


Figure 3.4.: Conjugated Atg8 to SLBs deposited on glass, in the absence (**upper part**) or presence of Atg16 (**lower part**), imaged with atomic force microscopy. Images are line fitted but otherwise unmodified. Atg8-PE/Atg12-Atg5 complexes are less mobile on SLBs with plasma-cleaned glass as support compared to mica. They form homogeneous aggregates, shown at different magnifications (top part). A similar continuous protein layer is observed on plasma-cleaned glass compared to mica, which forms from nano- to microscopic scale (bottom part).

Atg8 conjugation and scaffold formation occur sequentially and diffusion of Atg8-PE might facilitate assembly into more regular scaffolds. Therefore, presumably due to the restricted mobility of Atg8-PE on glass, the protein scaffold did not form as regularly as compared to the one on mica (compare Fig 3.4 with Fig. 3.3). Nevertheless, the scaffold could form across a wide size range, from $0.5 \mu\text{m} \times 0.5 \mu\text{m}$ to $4.0 \mu\text{m} \times 4.0 \mu\text{m}$ (Fig. 3.4, lower part), demonstrating that the immobility observed in FRAP experiments on GUVs or SLBs indeed stems from a protein layer formed at the nanoscopic scale. It could be observed that the scaffold covered almost the whole SLB, yet sometimes membrane areas could be detected which were devoid of any protein (Fig. 3.5, height image lower part). These ‘holes’ in the scaffold made it possible to determine the height of this protein layer (Fig. 3.5, cross section and height distribution). The observed height of the scaffold was $8 \pm 2 \text{ nm}$, compared to $6 \pm 1 \text{ nm}$ for Atg8-PE/Atg12-Atg5 complexes. The crystal structure of Atg16

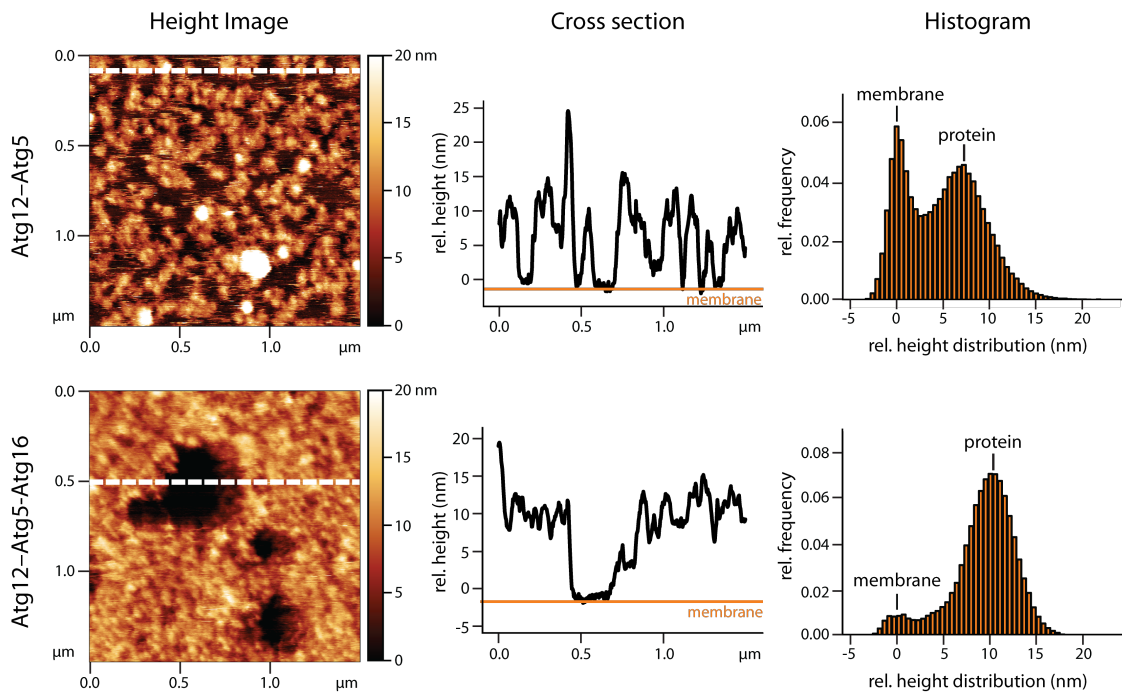


Figure 3.5.: Height quantification of similar images as in Fig. 3.4, on glass as support. Membrane parts are shown in black. The white dashed line in the height images indicates the cross section shown in the middle panels. The histograms in the right panels visualize the relative height distribution of the whole height image (membrane height was set to 0, bin size = 0,5 nm).

revealed, that the coiled-coil domain of Atg16 has a length of 11 nm [Fujioka et al. 2010]. Therefore, the height difference of only 2 nm for the scaffold measured by AFM compared to Atg8-PE/Atg12-Atg5 complexes is in agreement with a model, that Atg16 intercalates in between Atg8-PE/Atg12-Atg5 complexes horizontally on the membrane and structures them into a protein layer with meshwork-like architecture. The crystal structure also revealed a stretch of exposed hydrophobic residues in Atg16, which stabilized a crystal contact between two antiparallel Atg16 dimers [Fujioka et al. 2010]. Therefore, the hypothesis was developed that Atg16 forms antiparallel tetramers to cross-link Atg8-PE/Atg12-Atg5 complexes. This hypothesis could be fortified by determining the edge length of the scaffold to be 17 ± 4 nm (Fig 3.6), which corresponds to the current estimate of the length of an Atg16 coiled-coil tetramer. In conclusion, AFM imaging proved, that Atg8 together with Atg12-Atg5-Atg16 forms a so far undescribed protein scaffold on membranes *in vitro*.

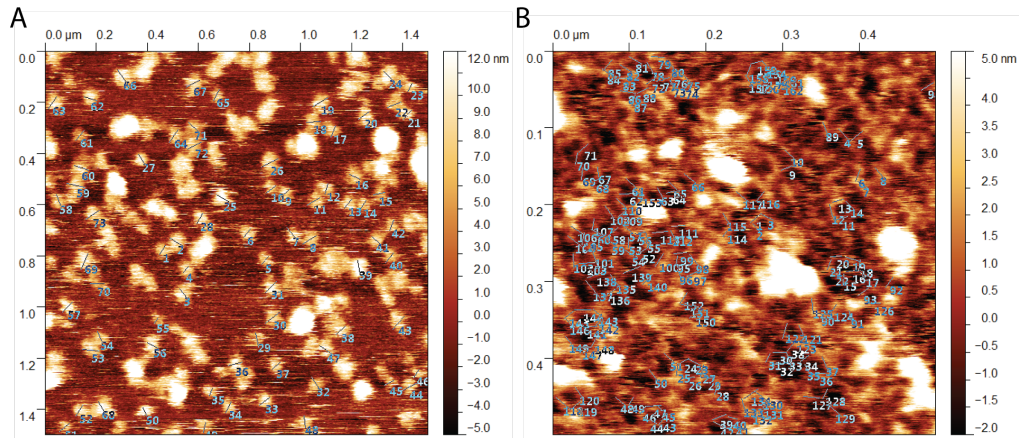


Figure 3.6.: Size measurements determined by manual estimation of reconstituted lipidation experiments, based on line-fitted but otherwise unmodified AFM images. **(A)** Diameter estimation of Atg12-Atg5/Atg8-PE oligomers on SLB on glass. No Atg16 was used for the lipidation reconstitution. **(B)** Edge length estimation of autophagic membrane scaffold on SLB on silanized mica. Here, Atg16 was added to the protein mixture.

3.2. Electron microscopy of yeast cells

In yeast, it is still unclear how the lipidation machinery is recruited to the autophagosomal membrane. In mammals, WIPI2b (WD-repeat PtdIns(3)P effector protein 2b) acts upstream of LC3 conjugation by directly binding ATG16L1 and therefore recruiting ATG12–ATG5–ATG16L1 to the autophagosomal membrane [Dooley et al. 2014]. However, if the yeast homolog of WIPI2, Atg18, has a similar upstream function in Atg8 lipidation remains a matter of debate [Suzuki et al. 2007]. Furthermore, it was recently demonstrated that Atg21, a closely related protein to Atg18, directly interacts with Atg16 and therefore defines the conjugation site of Atg8 in vegetative conditions [Juris et al. 2015]. To decipher the individual roles of Atg18 and Atg21 during starvation induced autophagy, the two genes were knocked out and transmission electron microscopy was performed of whole yeast cells under non-starvation conditions (Fig. A.8, p.98) and after four hours of nitrogen starvation (Fig. 3.7). This set of experiments was performed to support the research of B. Hofmann, who provided the yeast strains. To investigate the impact of the knocked out protein directly on autophagosome formation, the cells were carrying another knockout, the gene for peptidase Pep4. Thereby autophagosomes are not degraded, but stay in the vacuole as autophagic bodies and their size and number can be investigated.

In starved ‘wildtype’ cells, which only carried the pep4 knockout, the accumulation of autophagic bodies is clearly visible (white arrows in Fig. 3.7, WT). Similarly, also autophagic bodies can be observed for Atg21 knockout, however, they are smaller and fewer compared to WT autophagic bodies (white arrow in Fig. 3.7, Δ Atg21). This result is in line with the finding, that Atg21 recruits Atg12–Atg5–Atg16 to the autophagosomal membrane and therefore enhances Atg8 conjugation [Juris et al. 2015]. In Atg18 knockout cells, occasionally granular vacuoles were observed, but no autophagic bodies could be detected (arrow head and arrow in Fig. 3.7, Δ Atg18). Therefore, Atg18 is essential for autophagosome formation, but since the phenotype differs compared to Atg21, the two proteins seem to have diverging functions. To test whether high levels of Atg21 can compensate for the loss of Atg18, cells with a double knockout of Atg18 and Atg21 were imaged, which carry an additional vector for overexpression of Atg21. Here again, no autophagic bodies could be observed. Therefore even an overexpression of Atg21 cannot compensate for the loss of Atg18. This result further demonstrates, that Atg18 and Atg21 act differently in autophagosome formation. Notably, the vacuoles showed a pronounced granular phenotype. These light structures, that do not contain electron dense material, are either lipid droplets, or correspond to intra-luminal vesicles of multi-vesicular

pathways (Fig. 3.7, Δ Atg18, Δ Atg21, Atg21oe).

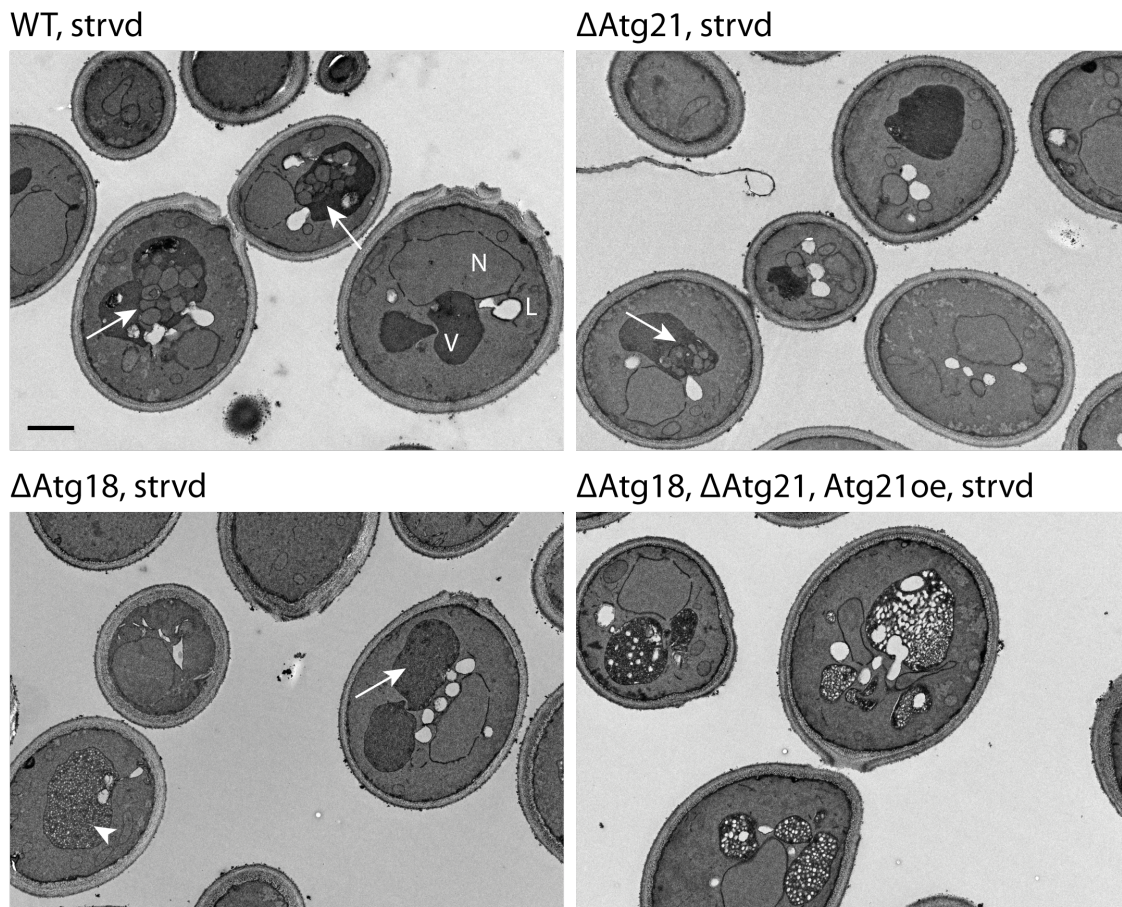


Figure 3.7.: Transmission electron microscopy images of whole yeast cells with pep4 deletion after 4 hour starvation. Pep4 deletion leads to accumulation of autophagic bodies in the vacuole. (**WT**) Wildtype cells, carrying only the pep4 deletion, show a strong accumulation of autophagic bodies in the vacuole (white arrows). (**Δ Atg21**) In vacuoles of cells with an Atg21 knockout smaller and fewer autophagic bodies accumulate in the vacuole (white arrow). (**Δ Atg18**) Cells knocked out for Atg18 do not show any autophagic bodies (arrow). Occasionally, the vacuole has a granular appearance (arrow head). (**Δ Atg18, Δ Atg21, Atg21oe**) Cells with an overexpression of Atg21 cannot compensate for loss of Atg18, since no autophagic bodies accumulate in the vacuoles. The granular phenotype of the vacuole corresponds to either lipid droplets that were taken up and partially degraded, or intra-luminal vesicles of multi-vesicular bodies. **V** vacuole, **N** nucleus, **L** lipid droplet, scale bar 1 μ m.

3.3. The human UBL protein toolbox

3.3.1. Expression and purification of human ATG8 proteins

The two interconnected Ub-like conjugation systems, which coordinate lipidation of Atg8 in yeast, are highly conserved in humans. However, the human UBL systems are more complex, with at least seven Atg8 homologs (hATG8s) and different ATG12–ATG5 interaction partners. Interestingly, most of the homologs are expressed in all tissues, arguing that evolution-driven diversification and specialization occurred in response to a change from single cell to multicellular organisms. This implies, that hATG8s demonstrate varying functions during autophagosome formation. Therefore, the identification of a new protein scaffold, that might be present on autophagosomes in yeast, raised two questions: (1) Is a similar scaffold existent in humans? And (2) if so, which of the human ATG proteins is involved as building block? To answer these questions and also to elucidate the possible different functions of hATG8s, it was necessary to purify the “toolbox” of human UBL proteins, namely different Atg8 homologs, but also ATG7, ATG3, ATG12–ATG5, and ATG16L1. Four hATG8 proteins were chosen, that are LC3A, LC3B, GABARAP, and GATE-16. These four hATG8s represent the two subfamilies of Atg8 homologs: LC3A and LC3B for the subfamily LC3, and GABARAP and GATE-16 for the subfamily GABARAP.

All cDNA clones for human ATG proteins were picked from the in-house Imagenes cDNA Library. For a successful *in vitro* reconstitution of the lipidation reaction, hATG8 cDNAs were cloned without the C-terminal amino acid(s), which are cleaved off *in vivo* by the protease ATG4. Also, a cysteine was inserted at the N-terminus of each hATG8 for labeling with fluorescent dyes (see chapter 2.4, p. 30). These modified proteins are referred to their original names for simplicity. ATG proteins were cloned in expression vectors with different purification tags, provided by the Biochemistry Core Facility (MPIB, Martinsried). hATG8s were successfully expressed in *E. coli* from the vector pCoofy1, in which a His₆-tag is fused to the N-terminus of the recombinant protein. Expression over night at 18°C or for three hours at 37°C was equally successful (Fig. 3.8). hATG8s were subjected to a two-step purification scheme, first a Ni-NTA affinity chromatography in batch, and second a size exclusion chromatography to remove further impurities and rebuffer them. After affinity chromatography, the proteins were digested by GST-PreScission protease for one hour at room temperature. Correct mass was verified by mass spectrometry (Fig. 3.9). GST-PreScission protease was chosen over His-PreScission due to its larger size and therefore to avoid a co-purification during size-exclusion chromatography

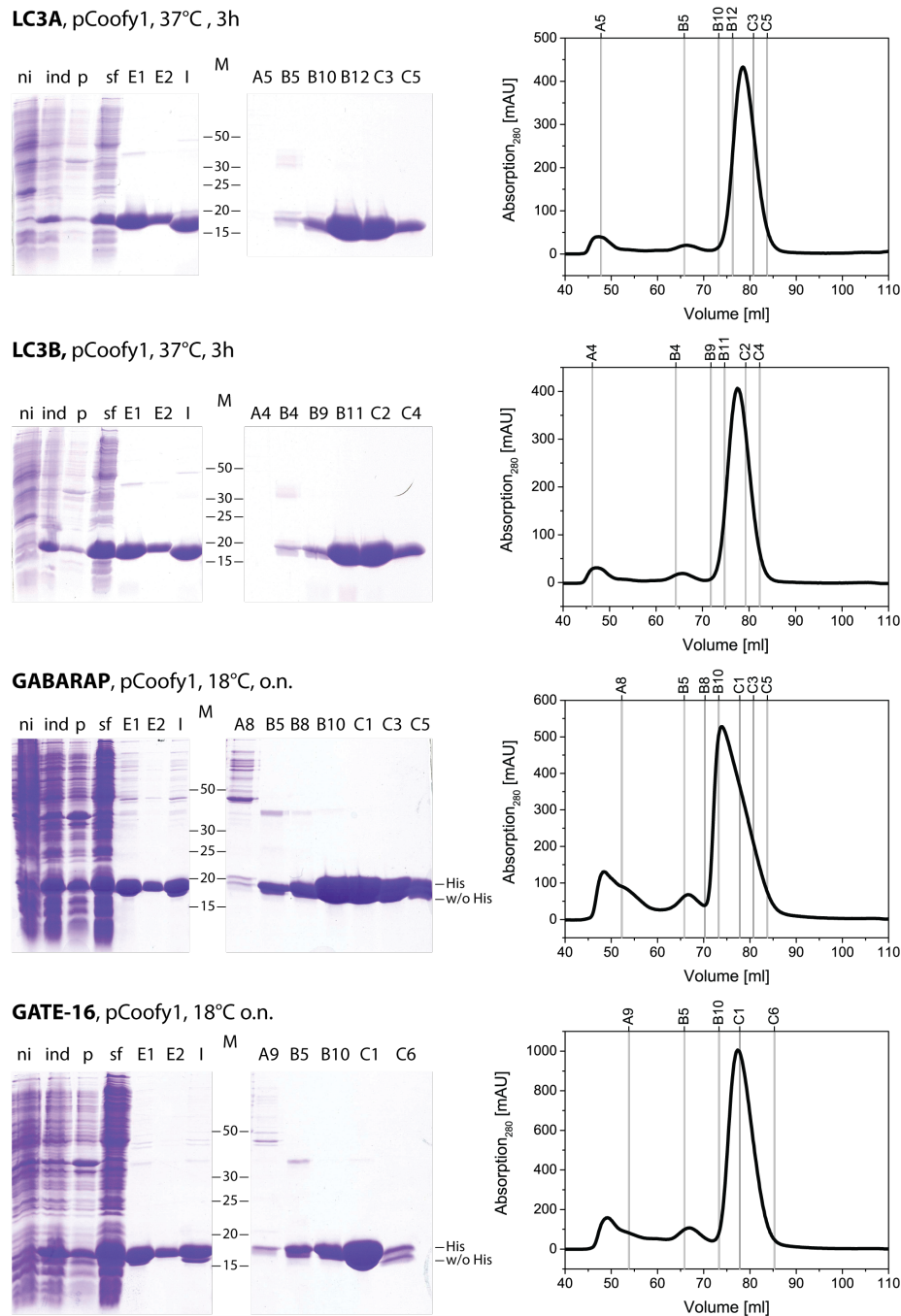


Figure 3.8.: Expression and purification of human ATG8 proteins with used expression vector and expression conditions. From top to bottom: **LC3A** (14.4 kDa), **LC3B** (14.4 Da), **GABARAP** (14.1 kDa), **GATE-16** (13.8 kDa). (**Left panel**) Samples from expression and purification steps were run on 15% SDS-PAGE gels. Left from the protein marker different steps of affinity chromatography are displayed, on the right fractions from size exclusion chromatography (SEC). The double band for GABARAP and GATE-16 indicates partial cleavage of the His₆-tag. (**Right panel**) SEC profile from a Superdex75 column. ni - not induced sample; ind - induced sample; p - pellet (insoluble fraction); sf - soluble fraction; E1, E2 - elution fractions of Ni-batch purification; I - input (for SEC); M - protein marker in kDa; A4-C6 - SEC fractions, as indicated in the respective profile on the right.

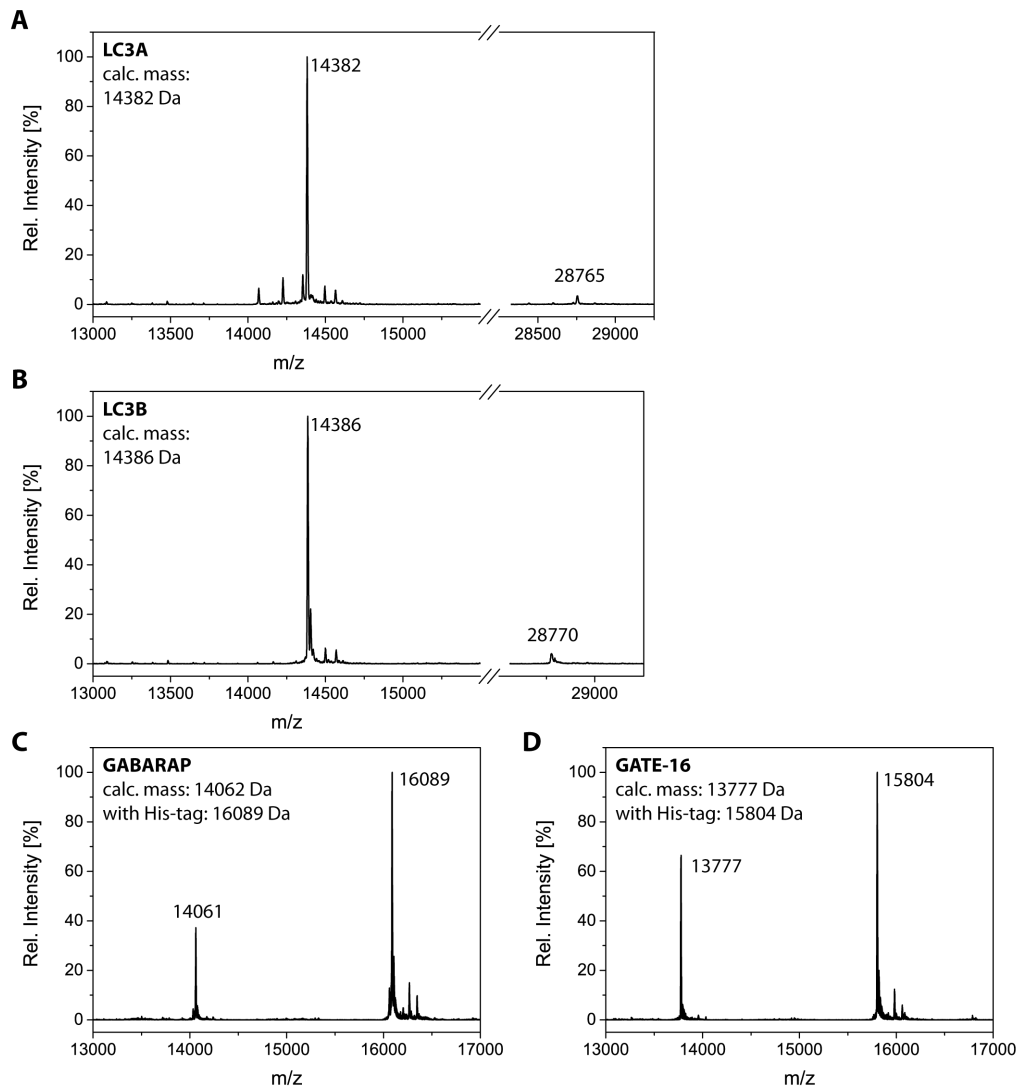


Figure 3.9.: Mass spectra of purified hATG8s, corresponding to the proteins in Fig. 3.8. (A-D) The calculated masses of LC3A (14382 Da), LC3B (14386 Da), GABARAP (14061 Da), and GATE-16 (13777 Da) could be detected. In case of LC3A and LC3B, a small portion of the purified protein was existent as dimer (small peak on the right in A and B). GABARAP and GATE-16 mass profiles show a large portion of uncleaved protein (peak with higher mass in C and D).

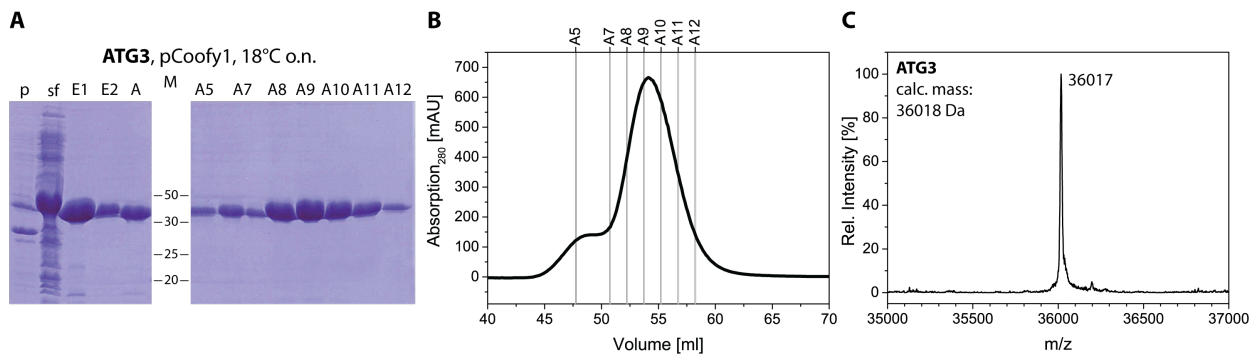


Figure 3.10.: Expression, purification, and mass spectrometry of human ATG3 (36.0 kDa) from pCoofy1, at 18°C over night. **(A)** Samples from expression and purification steps in 15% SDS-PAGE gels. Left from the protein marker different steps of affinity chromatography are displayed, on the right fractions from size exclusion chromatography (SEC). **(B)** SEC profile from a Superdex 75 column. **(C)** Mass spectrometry yielded the correct size of 36017 Da for human ATG3. ni - not induced sample; ind - induced sample; p - pellet (insoluble fraction); sf - soluble fraction; E1, E2 - elution fractions of Ni-batch purification; A - after PreScission digest; M - protein marker in kDa; A5-A12 - SEC fractions, as indicated in the respective profile in B.

(His-PreScission: 21.7 kDa, GST-PreScission: 46.3 kDa). When only partial cleavage of the His₆-tag was observed (GABARAP and GATE-16 in Fig. 3.8, Fig. 3.9, C and D), the proteins were cleaved again and their successful digestion was monitored by SDS-PAGE. The yield of purified hATG8s ranged from 3.7 to 5 mg protein per liter bacterial cell culture.

3.3.2. Expression and purification of ATG3

Before hATG8 is conjugated to PE, it is activated by ATG7 and then transferred to ATG3. ATG3 was cloned in the vector pCoofy1, containing an N-terminal His₆-tag, and successfully expressed in *E. coli* at 18°C over night (Fig. 3.10). After affinity chromatography with Ni-NTA, the recombinant protein was subjected to PreScission protease digestion at room temperature for 45 minutes. To remove further impurities and rebuffer the protein, size exclusion chromatography with a Superdex 75 column was performed. The correct mass of ATG3 was verified by mass spectrometry (Fig. 3.10, C). The yield of purified protein was 2.4 mg per liter bacterial cell culture.

3.3.3. Expression and purification of ATG12–ATG5

Atg12–Atg5 catalyzes the conjugation of Atg8 to PE as the E3-like enzyme. In yeast, Atg16 is not required for the lipidation reaction per se, only for the formation of

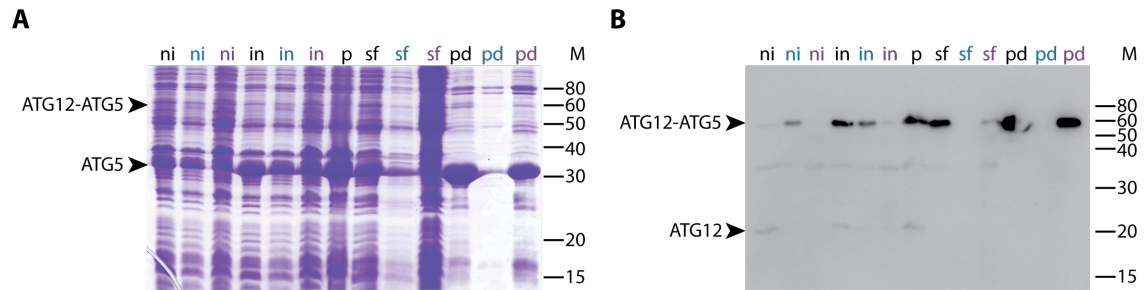


Figure 3.11.: Test expression samples of human ATG12–ATG5 (47.8 kDa) from pST39 in *E. coli* over night at 18°C with ATG7 isoform 1 and His₆-tagged ATG5. Samples marked in black are from a vector containing ATG7, ATG10, ATG12, and ATG5, and either ATG16 (blue) or TECPR1 (violet). **(A)** 12 % SDS-PAGE gel, with majority of pulled down protein being ATG5. **(B)** Western Blot with ATG12 antibody of the same samples as in A. Faint bands can be detected for ATG12 alone, but majority exists in conjugate form. Due to its conjugate nature, ATG12–ATG5 runs at a higher position than is expected from its calculated weight. ni - not induced sample; in - induced sample; p - pellet (insoluble fraction); sf - soluble fraction; pd - pull down.

the autophagic scaffold. Therefore, the recombinant expression of ATG12–ATG5 was essential to achieve successful lipidation of hATG8s *in vitro*. The challenge for the recombinant production of ATG12–ATG5 was the reconstitution of the whole enzymatic cascade required to covalently link ATG12, an UBL protein, to its sole target ATG5 (see Fig. 1.2). Two main strategies were followed in parallel to accomplish production of ATG12–ATG5: (1) purification of the individual components, ATG7, ATG10, ATG12, and ATG5 to achieve conjugation of ATG12 to ATG5 *in vitro*, and (2), production of all components *in situ* in *E. coli*, so that the completed ATG12–ATG5 conjugate can be purified from bacterial cell lysate.

Following the first strategy, expression of the individual components, major difficulties were encountered. ATG12 possesses an N-terminal disordered region that comprises roughly one third of the protein (based on a prediction for protein crystallizability with XtalPred¹) and ATG12 expression, even as fusion protein for stabilization, remained unsuccessful due to degradation (Fig. A.1, A, p. 93). Additionally, the expression of ATG7 in *E. coli* did not yield the desired protein (chapter 3.3.4, Fig. A.1, B, p. 93).

It was shown previously in our lab that the second strategy proved successful for yeast Atg12–Atg5, which is why a similar cloning strategy for human ATG12–ATG5 was pursued. To achieve a simultaneous expression of ATG7, ATG10, ATG12, and ATG5, the corresponding cDNAs were cloned into a vector suitable for polycistronic

¹<http://ffas.burnham.org/XtalPred-cgi/xtal.pl>

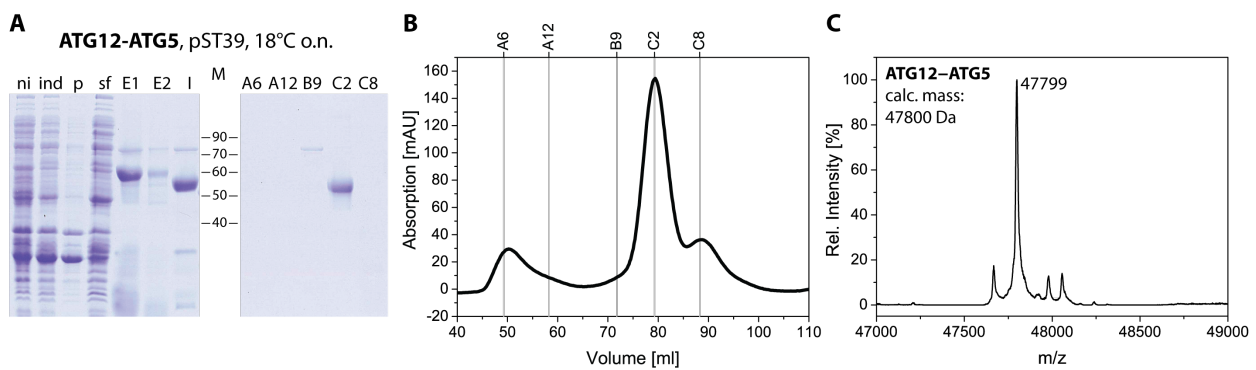


Figure 3.12.: Expression and purification of human ATG12–ATG5 (47.8 kDa) from pST39 in *E. coli* over night at 18°C with His₁₀-tagged ATG12. **(A)** 10% SDS-PAGE gel with samples from affinity (left from marker) and size exclusion chromatography (right from marker) purification steps. **(B)** SEC profile of ATG12–ATG5 from a Superdex 200 column. **(C)** Mass spectrometry confirmed that ATG12–ATG5 (47800 Da) was successfully formed and purified. p - pellet (insoluble fraction); sf - soluble fraction; E1, E2 - elution fractions of Ni-batch purification; I - input for SEC; M - protein marker in kDa; A6-C8 - SEC fractions, as indicated in the respective profile on the right.

expression, namely pST39 [Tan 2001], and ATG5 was tagged with a His₆-tag to purify the conjugate. Further, the cDNAs of ATG16 or TECPR1 were cloned into the vector to possibly stabilize the conjugate.

Two isoforms of ATG7 exist in humans. First, isoform 2 was tested, which corresponded to the cDNA provided by the cDNA library for ATG7. However, no ATG12–ATG5 production could be detected, instead ATG5 was stably expressed and purified (Fig. A.1, C, p. 93). When the cDNA of ATG7 isoform 2 was exchanged for the cDNA of isoform 1 by mutagenesis, the ATG12–ATG5 conjugate could be detected by Western Blotting (Fig 3.11, B). Test expressions however showed, that more unconjugated ATG5 was purified compared to ATG12–ATG5, possibly due to the instability of ATG12 (Fig 3.11, A).

In order to stabilize ATG12 and to purify mainly the conjugate and not unconjugated ATG5, the N-terminal affinity His₆-tag was exchanged from ATG5 to an N-terminal His₁₀-tag on ATG12, and Maltose-binding protein (MBP) was cloned in between His₁₀-tag and ATG12 to improve solubility. This strategy allowed for the purification of ATG12–ATG5, but in these samples MBP was co-purified due to insufficient separation on the SEC column. To improve purity, the coding sequence of MBP was removed from the vector and His₁₀-ATG12 was co-expressed with ATG5, ATG10, and ATG7, which generated the recombinant conjugate in high purity. The average yield was 0.5 mg protein per liter bacterial cell culture (Fig. 3.12, A and B).

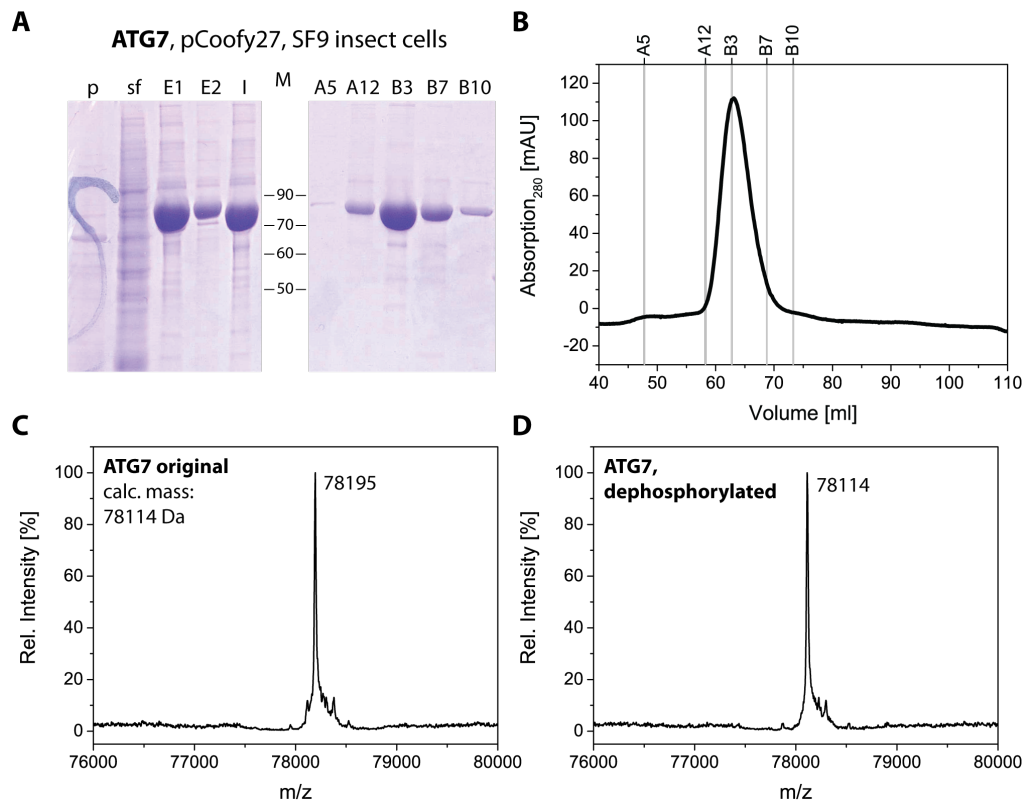


Figure 3.13.: Expression, purification and mass spectrometry of recombinantly expressed human ATG7 (78.1 kDa) from pCoofy27 in SF9 insect cells. **(A)** 10% SDS-PAGE gel with samples from affinity (left from marker) and size exclusion chromatography (right from marker) purification steps. **(B)** SEC profile of ATG7 from a Superdex 200 column. **(C)** The detected mass of 78195 Da corresponds to an increase of 81 Da compared to the theoretical mass of 78114 Da, and represents a posttranslational phosphorylation. **(D)** After treating hATG7 with phosphatase (CIP), the calculated mass of 78114 Da is detected. p - pellet (insoluble fraction); sf - soluble fraction; E1, E2 - elution fractions of Ni-batch purification; I - input for SEC; M - protein marker in kDa; A5-B10 - SEC fractions, as indicated in the respective profile in B.

For labeling, an N-terminal cysteine was added to ATG12 (final vector in Fig. 2.2, p. 32). The final purification scheme consisted of two steps, first affinity chromatography with Ni-NTA resin, after which the His₁₀-tag was cleaved off by PreScission protease, and second SEC on a Superdex 200 column. Mass spectrometry analysis detected the exact theoretical weight of ATG12-ATG5 (47.8 kDa, Fig. 3.12, C).

3.3.4. Expression and purification of ATG7

ATG7 is the E1-like enzyme in the activation of ATG12 and hATG8s, and the first protein of the enzymatic cascade for lipidation of hATG8. Therefore its expression

and purification was indispensable for a successful reconstitution of the human lipidation machinery. Test expressions of ATG12–ATG5 demonstrated, that only isoform 1, the canonical form of ATG7, is enzymatically active for conjugating ATG12 to ATG5 (Fig. 3.11). Therefore, all expressions and purifications were executed with ATG7 isoform 1. Even though test expressions with different tags for purification yielded promising results in *E.coli*, large scale expression in bacteria remained unsuccessful (one example is displayed in Fig. A.1, B, p. 93). Consequently, the cDNA was cloned into insect cell expression vectors, that contained different affinity tags. Test expressions with SF9 and H5 insect cells, as well as different concentrations of Baculovirus-infected insect cells (BIICs) were carried out by the Biochemistry Core Facility (MPIB). Best expression was achieved from either pCoofy27, a vector adding an N-terminal His₇-tag to the recombinant protein, or from pCoofy28, a vector adding an N-terminal Glutathione S-transferase (GST). Both samples were obtained from SF9 cells with BIICs used in the concentration of 1:4000 (Fig. A.2, p. 94). These expression conditions were used again in a mid-scale expression and a pull-down experiment was performed with the samples. Here, the yield of recombinant ATG7 was much higher in pCoofy27 compared to pCoofy28 (Fig. A.3, p. 95).

After determining the best expression conditions, large scale expression and purification of ATG7 was performed in SF9 insect cells. A two-step purification scheme was executed, first affinity chromatography with Ni-NTA resin, after which the His₆-tag was cleaved off by PreScission protease, and second SEC on a Superdex 200 column. Expressions yielded up to 2.5 mg protein per liter insect cell culture (Fig. 3.13, A and B). Mass spectrometry confirmed that ATG7 was successfully expressed and purified. Still, the theoretical mass of 78114 Da could not be detected, instead a mass of 78195 Da was measured, which corresponds to a change of +81 Da. ATG7 was therefore most likely posttranslationally modified, since this mass change corresponds to a phosphorylation of ATG7 (expected mass gain of 81 Da, Fig. 3.13, C). To test whether ATG7 was indeed phosphorylated, a sample was incubated with Calf-intestinal alkaline phosphatase (CIP) and subjected again to mass spectrometry. The second measurement yielded the calculated mass of 78114 Da, confirming the phosphorylation of ATG7 (Fig. 3.13, D).

3.3.5. Detection of thioester intermediates

In yeast, Atg8–PE production depends on Atg7 and Atg3, as well as Atg12–Atg5–Atg16. Previous studies in our lab showed, that *in vitro*, yeast Atg8 can be conjugated to large unilamellar vesicles (LUVs) without Atg12–Atg5. However, the lipidation

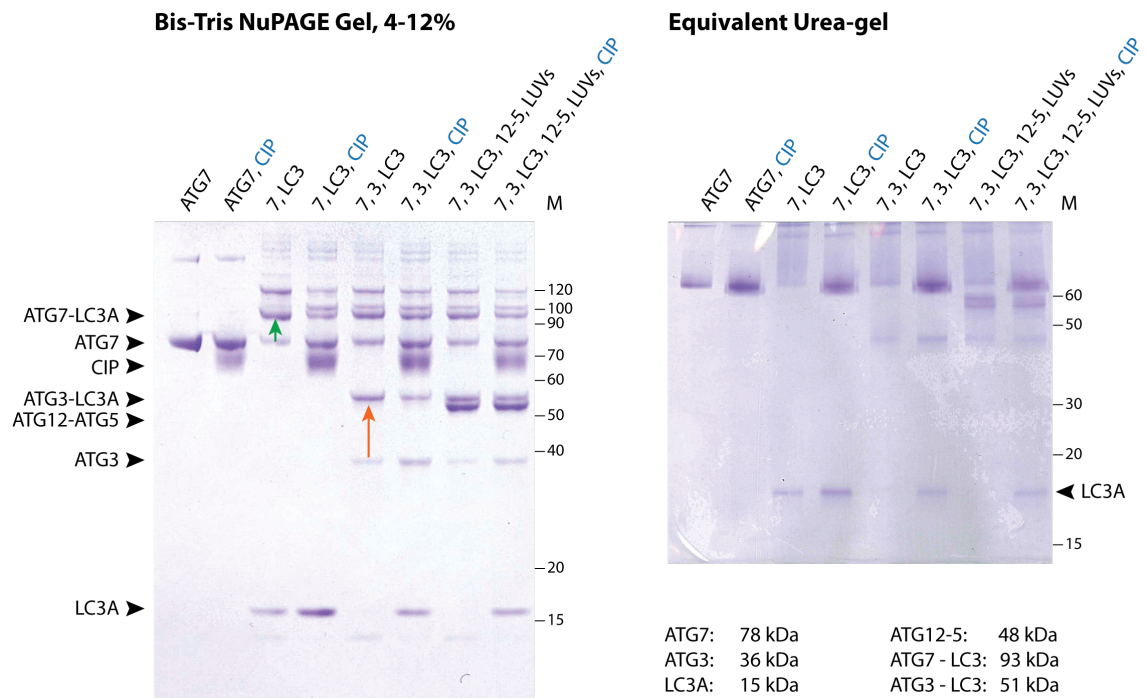


Figure 3.14.: Detection of thioester intermediates and possible formation of the LC3A–PE conjugate. **(Left)** SDS-PAGE gradient gel for the detection of thioester intermediates. The proteins of the lipidation reaction were added consecutively to each other. ATG7–LC3A can be observed from lane 3 on (green arrow) and ATG3–LC3A from lane 5 on (orange arrow). Phosphatase (CIP) was added to every other reaction mixture to test if phosphorylation of ATG7 had an effect on intermediate formation. **(Right)** Same samples from the left panel were subjected to gel electrophoresis in an urea gel for detection of LC3A–PE. No LC3A–PE could be detected in the lanes with added lipids, which should be visible as LC3A double band in urea gels (large unilamellar vesicles (LUVs) in the last two lanes). Therefore, the last step of the lipidation reaction was compromised.

of Atg8 to giant unilamellar vesicles (GUVs) requires Atg12–Atg5, presumably related to the lower membrane curvature, but Atg16 is dispensable. For the human system, conflicting data existed [Otomo et al. 2013; Nath et al. 2014]. Therefore, the requirement for different conditions was systematically investigated by setting up the steps of the lipidation reaction sequentially *in vitro*. A gradient gel allowed the detection of thioester intermediates, which form during the enzymatic cascade. Also, lipidated Atg8 can be detected using Urea-gels [Nakatogawa et al. 2012a]. To see if the proteins are functional, they were added consecutively in their way of action to each other. Indeed, all thioester intermediates could be detected (ATG7–LC3A and ATG3–LC3A, see Fig. 3.14, left panel).

To test if the phosphorylation of ATG7 has an influence on the enzymatic properties

of ATG7, samples with Calf-intestinal alkaline phosphatase (CIP) were also prepared. Interestingly, the reaction efficiency with phosphorylated ATG7 was higher compared to unphosphorylated ATG7, since in samples without CIP no unconjugated LC3A could be detected, and bands corresponding to LC3A-intermediates were more intense in samples with phosphorylated ATG7. Therefore, the phosphorylation of ATG7 might be required for full ATG7 activity *in vitro* and might serve as a regulatory mechanism *in vivo*.

No LC3A-PE could be detected (no LC3A double band in urea gel in Fig. 3.14, right panel). This experiment demonstrated, that the initial steps of the lipidation reaction work (thioester intermediate formation), but not the last step, the conjugation of LC3A to PE. A possible explanation for missing lipidation was that ATG16L1 is required for ATG12-ATG5 to be active, since this was the only component of the system that was missing.

3.3.6. Expression and purification of ATG16L1 full-length and truncated forms

Full-length ATG16L1

Efficient conjugation of LC3 to membranes might require ATG16L1, although a high DOPE-content has been reported to be sufficient for conjugation in the absence of ATG16L1 [Nath et al. 2014]. Therefore, also the expression of ATG16L1 was indispensable. After the cloning of ATG16L1 into different expression vectors for *E. coli*, test expression results looked promising for expression in bacteria. However, comparable to ATG7, larger culture volumes did not improve protein yield. Thus, ATG16L1 was expressed in insect cells. ATG16L1 was cloned into three vectors with different affinity tags suitable for expression in insect cells. Test expressions with SF9 and H5 insect cells, as well as different concentrations of Baculovirus-infected insect cells (BIICs) was carried out by the Biochemistry Core Facility (MPIB). Best expression was achieved from either pCoofy27, or pCoofy29, which allowed expression of ATG16L1 as N-terminal His₇- or His₆-MBP-tagged proteins. Both samples were obtained from H5 cells with BIICs used in the concentration of 1:1000 (Fig. A.4, p. 95). These expression conditions were used again in a mid-scale expression and a pull-down experiment was performed with the samples. Here, the yield of recombinant MBP-ATG16L1 fusion protein was higher compared to His₇-ATG16L1 (Fig. A.5, p. 96).

Therefore, large scale expression and purification of ATG16L1 was performed in

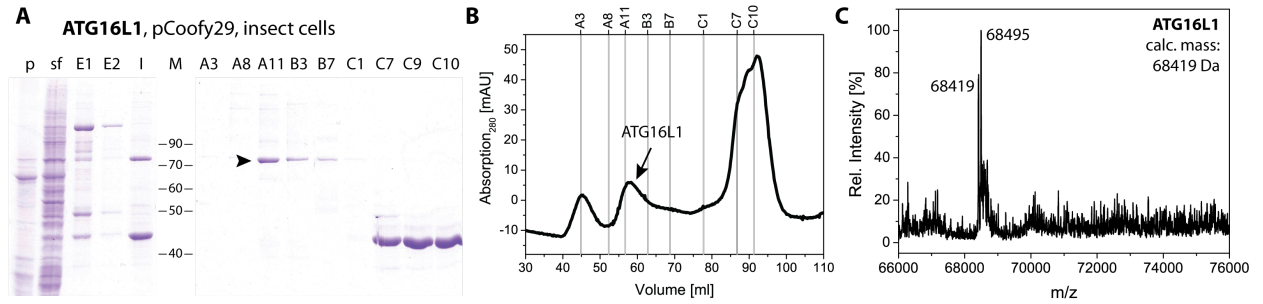


Figure 3.15.: Expression, purification and mass spectrometry of full-length ATG16L1 (68.4 kDa) from pCoofy29 in H5 insect cells. **(A)** 10% SDS-PAGE gel with samples from affinity (left from marker) and size exclusion chromatography (right from marker) purification steps. The arrow head points to ATG16L1 band, the lower band in lanes C7-C10 corresponds to MBP. **(B)** SEC profile of ATG16L1 from a Superdex 200 column. The high peak on the right corresponds to MBP. **(C)** Mass spectrometry profile of purified full-length ATG16L1. Two masses could be detected: 68419 Da corresponds to the exact theoretical mass of the protein, and 68495 Da, which corresponds to a mass increase of 76 Da. This mass increase is equivalent to a β -mercaptoethanol adduct, a remnant from protein purification that could not be removed. p - pellet (insoluble fraction); sf - soluble fraction; E1, E2 - elution fractions of Ni-batch purification; I - input for SEC; M - protein marker in kDa; A3-C10 - SEC fractions, as indicated in the respective profile on the right.

H5 insect cells from the vector pCoofy29 and a two-step purification protocol was applied. First affinity chromatography with Ni-NTA resin was performed, after which the His₇-tag was cleaved off by PreScission protease digestion, followed by SEC on a Superdex 200 column (Fig. 3.15). A typical SEC elution profile is displayed in Fig. 3.15, B. Free MBP could be separated after PreScission protease digest from ATG16L1 by SEC (big peak on the right, Fig. 3.15). Protein identity could be confirmed by mass spectrometry (Fig. 3.15, C), even though ATG16L1 could not always be detected by ESI-MS, probably due to insufficient ionization of the protein. Expression and purification yielded ~0.25 mg of ATG16L1 per liter insect cell culture.

ATG16 Δ WD

Yeast Atg16 does not possess a C-terminal WD-domain and it was demonstrated before that the coiled-coil domain of ATG16L1 is sufficient for autophagy [Mizushima et al. 2003]. Therefore it was hypothesized that the WD-domain, which targets ATG16L1 to non-autophagic membranes by binding specific ATG16L1-receptors [Travassos et al. 2010; Boada-Romero et al. 2013], is also dispensable in the human UBL-system for the formation of the autophagic scaffold. To test this hypothesis, a truncated form of ATG16L1, hereafter referred to as ATG16 Δ WD, with a missing

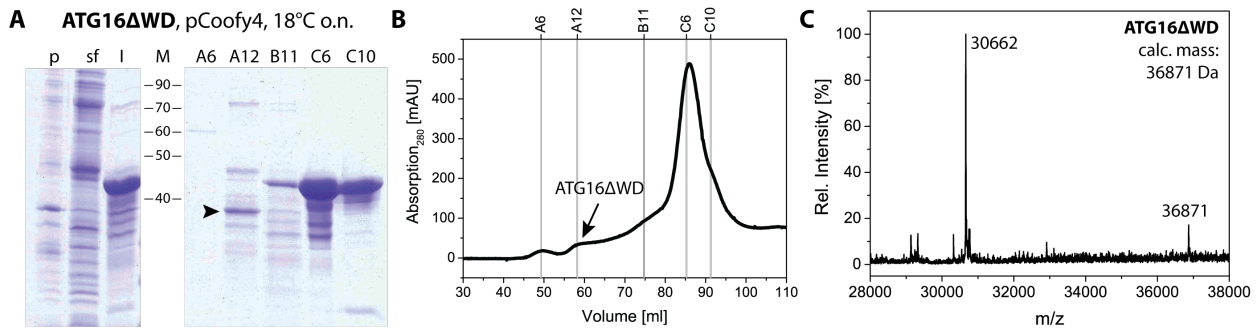


Figure 3.16.: Expression, purification, and mass spectrometry of ATG16 Δ WD (36.9 kDa) from pCoofy4 in *E. coli* at 18°C over night. (A) 10% SDS-PAGE gel with samples from affinity (left from marker) and size exclusion chromatography (right from marker) purification steps. The arrow head points to the ATG16 Δ WD band, the higher band in lanes C6-C10 corresponds to MBP. (B) SEC profile of ATG16L1 from a Superdex 200 column. The high peak on the right corresponds to MBP. (C) Mass spectrometry profile of purified ATG16 Δ WD. Mainly two masses could be detected: 36871 Da corresponds to the theoretical mass of ATG16 Δ WD. A higher intensity was detected for a protein with a mass of 30662 Da. It is not clear, if this protein is an impurity or a degradation product of ATG16 Δ WD. Also, insufficient ionization, which were already observed for full-length ATG16L1, could account for the low intensity measured for ATG16 Δ WD. p - pellet (insoluble fraction); sf - soluble fraction; I - input for SEC; M - protein marker in kDa; A6-C10 - SEC fractions, as indicated in the respective profile on the right.

WD-domain, was produced. ATG16 Δ WD was cloned in different expression vectors for *E. coli* and test expression results yielded the most promising expression conditions with pCoofy4 (MBP as affinity-tag) at 18°C over night. In large scale expression, ATG16 Δ WD was produced and purified (Fig. 3.16, arrow head in A). Even though the purification did not yield a very pure product (lane A12, Fig. 3.16, A), a corresponding mass of 36871 Da was detectable (Fig. 3.16, C). However, a second mass of 30662 Da was more abundant. This mass corresponds to a degradation product of ATG16 Δ WD, lacking the last 59 amino acids from ATG16 Δ WD. Insufficient ionization, which was already observed for full-length ATG16L1, could account for the low amount of non-degraded ATG16 Δ WD detected in mass spectrometry, since only a band corresponding to a mass of ~37 kDa was visible in ATG16 Δ WD containing fractions (Fig. 3.16, A).

ATG16NT

The coiled-coil domain of ATG16L1 might, in analogy to the yeast system, be required for scaffold formation. However, without ATG16L1, no lipidation of LC3A has been

observed (Fig. 3.14). To activate ATG12–ATG5, but prevent formation of scaffolds, another truncated form of ATG16L1 was produced, lacking both WD and coiled-coil domains (ATG16NT, residues 11-43). This 43 amino acid long peptide was shown to bind to ATG5 in the ATG12–ATG5 complex. Additionally, when used together with ATG12–ATG5, it was sufficient to conjugate LC3 to PE *in vitro* [Otomo et al. 2013], probably due to a conformational change in ATG12–ATG5. In order to compare ATG8s on membranes in the presence and absence of ATG16L1, as it has been done for the yeast proteins, ATG12–ATG5 also needs to be activated without autophagic scaffold formation. The peptide should conform to this requirement, since it lacks the coiled-coil domain necessary for scaffold formation in yeast.

A first strategy for peptide production was co-expression of ATG16NT(1-43) together with ATG12–ATG5 in the polycistronal expression vector pST39 (see chapter 3.3.3). The idea was to purify the peptide directly together with ATG12–ATG5. However, the purified peptide was degraded since its theoretical mass could not be detected (data not shown). Also, expression as fusion protein with affinity-tags did not yield a purified product. Otomo et al. [2013] did not use the full length peptide, but amino acids 11-43 of ATG16L1. Thus, ATG16NT(11-43) was expressed and purified as a fusion protein together with MBP in pCoofy4 by affinity and size exclusion chromatography (Fig. 3.17, A). To remove MBP, the fusion protein was subjected to PreScission protease digestion in the presence of ATG12–ATG5 at room temperature for 45 minutes and subsequently subjected to size exclusion chromatography again for removal of MBP and protease (Fig. 3.17, B). The peak of ATG12–ATG5–ATG16NT showed a slight shift to the left compared to ATG12–ATG5, corresponding to an increase in hydrodynamic radius due to peptide binding to ATG12–ATG5 ((Fig. 3.17, B, SEC profile). Mass spectrometry validated that the peptide ATG16NT(11-43) was successfully expressed and co-purified with ATG12–ATG5 (Fig. 3.17, C).

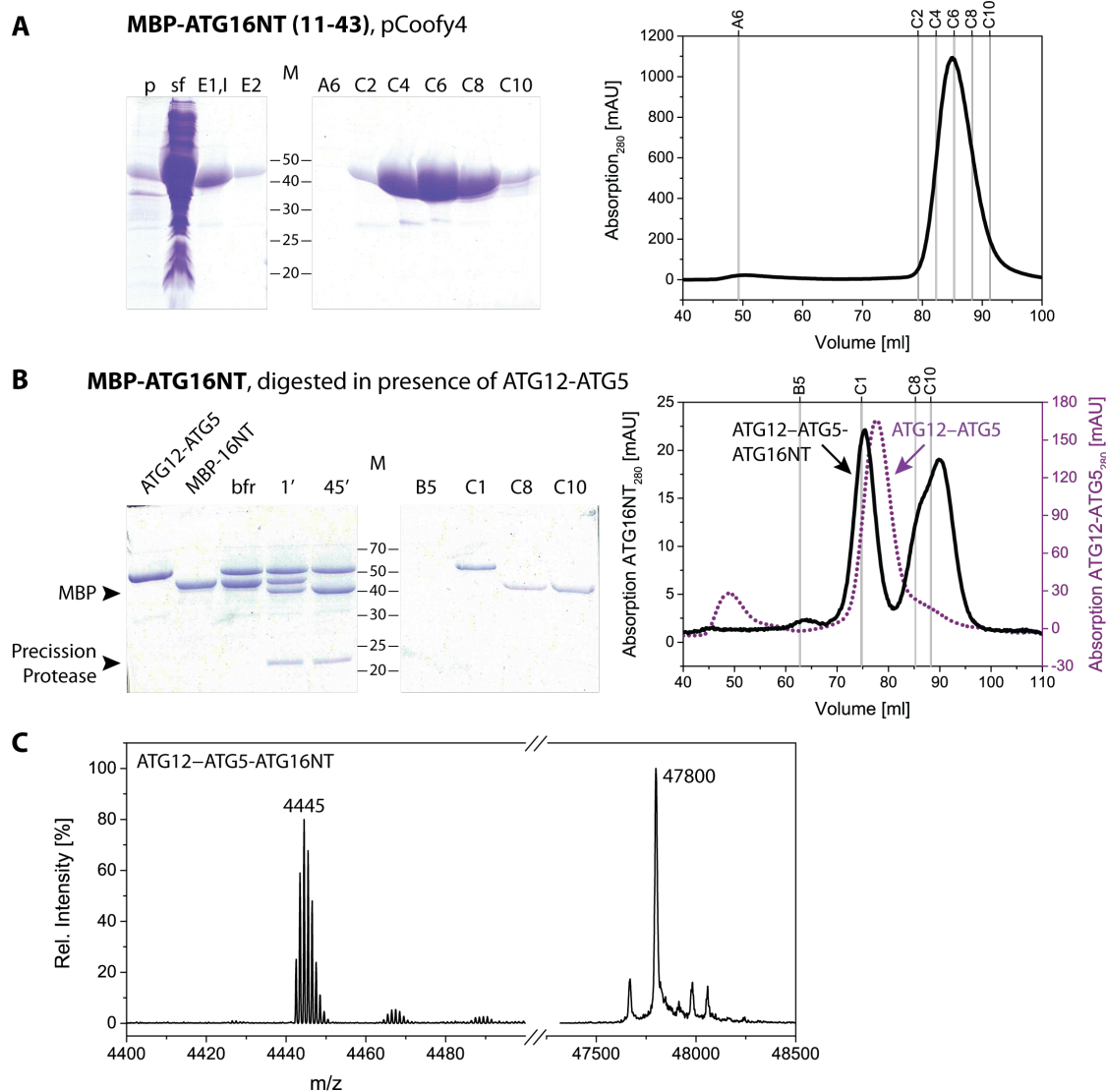


Figure 3.17.: Expression, purification, and mass spectrometry of ATG16NT(11-43) (4.4 kDa). **(A)** 15% SDS-PAGE gel displaying the first step for ATG16NT peptide production: expression and purification of the fusion protein MBP-ATG16NT in *E. coli* at 37°C for 3 hours; The protein was not cleaved by PreScission protease, therefore the first elution fraction (E1) was directly subjected to SEC (corresponding profile on the right). **(B)** 15% SDS-PAGE gel displaying the second step of peptide production: PreScission protease digestion of the fusion protein from (A) in the presence of ATG12-ATG5. The size shift of MBP (compare lane 'bfr' with '45') corresponds to the cleavage process. The peptide binds to ATG12-ATG5 and can be co-purified in SEC (right panel). The binding leads to a small shift of the ATG12-ATG5 peak (compare purple peak for ATG12-ATG5 alone). Both SEC runs were performed on a Superdex 200 column. The peak on the right corresponds to MBP. **(C)** Mass spectrometry profile of co-purified ATG16NT(11-43) with ATG12-ATG5. The detected masses are identical with the theoretical ones, 4445 Da for ATG16NT and 47800 Da for ATG12-ATG5. The peaks corresponding to the peptide mass display the isotopic distribution of ATG16NT. p - pellet (insoluble fraction); sf - soluble fraction; I - input for SEC; E1, E2 - elution fractions of Ni-batch purification; M - protein marker in kDa; A6-C10 - SEC fractions, as indicated in the respective profile on the right.

3.4. Conjugation of hATG8s to Giant Unilamellar Vesicles (GUVs)

3.4.1. ATG16L1 is necessary for hATG8 lipidation

All full-length proteins of the human ubiquitin like (UBL) systems of autophagy were expressed and purified successfully. Thus, the UBL ‘toolbox’ was complete and the reconstitution of the human lipidation reactions *in vitro* was now feasible. Especially a characterization of potential differences of the two ATG8 families, LC3s and GABARAPs, was in the focus of the following reconstitution experiments.

Conjugation reactions of hATG8s were established using giant unilamellar vesicles (GUVs). GUVs are the only free-standing model membrane system that can be investigated with fluorescence microscopy. They therefore allow for rapid accession of lipidation efficiencies, protein visibility, as well as protein-membrane interactions (co-localization). In the following experiments, fluorescently labeled membranes (Phosphatidylethanolamine (PE) labeled with Atto680) were incubated with fluorescently labeled proteins and their colocalization could be observed using confocal microscopy. For the reconstitution of the lipidation reaction, two protein mixtures were prepared: (1) ATG7, ATG3 and one of the human Atg8 homologs were pre-incubated at 37°C with ATP for thioester intermediate formation, as well as (2) ATG12–ATG5 with ATG16L1. Subsequently, GUVs were mixed with the two protein compositions and after further incubation visualized by confocal microscopy.

As already indicated in an initial lipidation experiment using LUVs (chapter 3.3.5), ATG16L1 might be necessary for a successful reconstitution of the hATG8 lipidation. First conjugation reactions were therefore performed to compare lipidation in presence or absence of ATG16L1. Consistent with the results on LUVs, no conjugation of LC3B was detected with the UBL-system excluding ATG16L1 (Fig. 3.18, A and B). Thus, ATG16L1 is necessary for conjugation of LC3B to PE in GUVs, which is in contrast to the UBL system in yeast. When no ATG16L1 is added to the reaction mix, LC3B is not conjugated to the membrane and it stays in the buffer surrounding the GUVs, as well as ATG12–ATG5 (Fig. 3.18, A). In contrast, when ATG16L1 is added to the conjugation mixture, LC3B is conjugated to PE and localizes to the membrane (Fig. 3.18, B). Therefore, colocalization of hATG8 and membrane is equivalent to a successful conjugation, which could be verified by mass spectrometry (L. Dempfle, master thesis). Comparable to the yeast UBL protein system, also ATG12–ATG5 colocalizes with LC3B at the membrane. For its enzymatic activity,

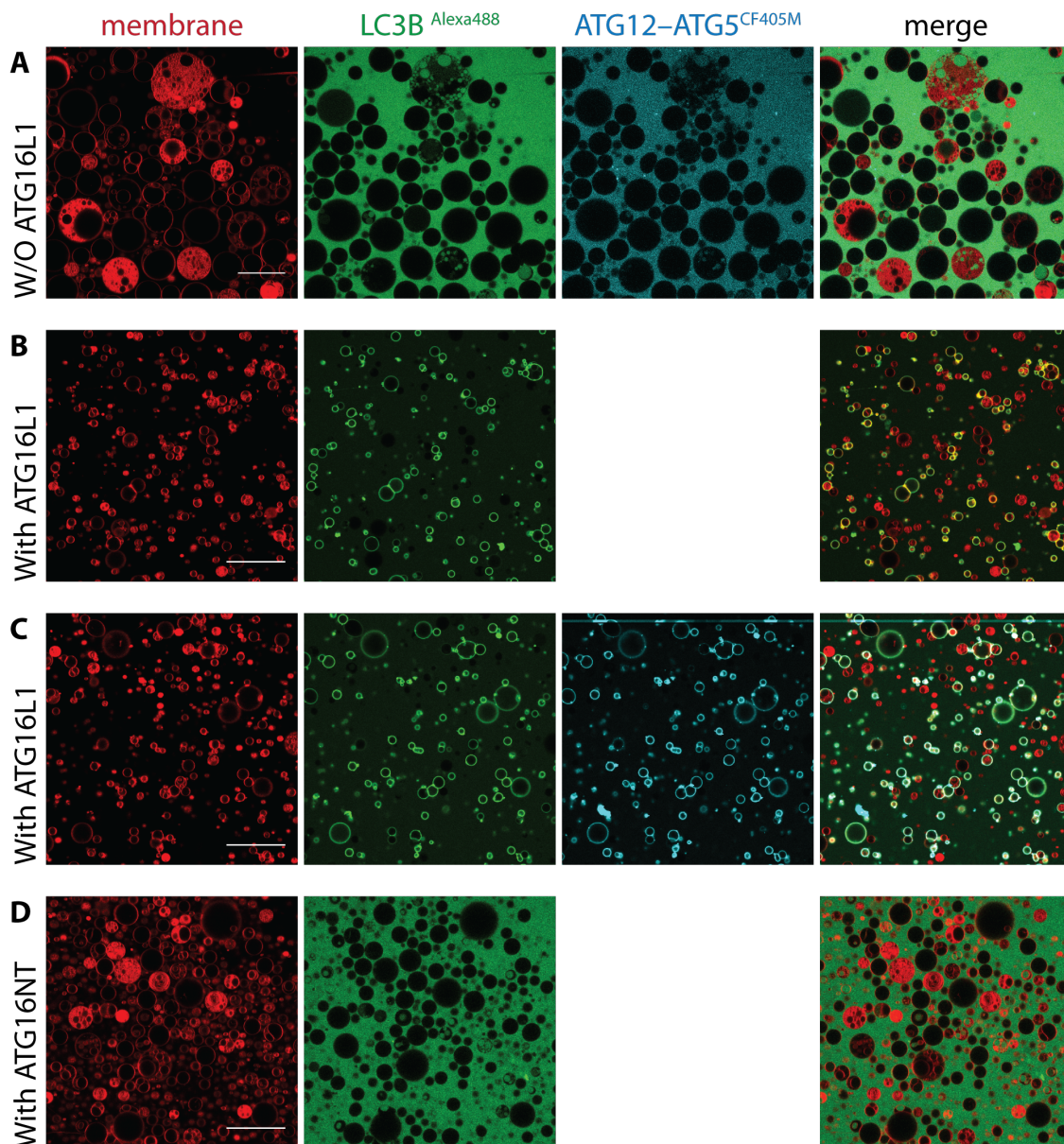


Figure 3.18.: ATG16L1 is necessary for LC3B lipidation. (A) No lipidation of LC3B can be observed in the absence of ATG16L1. (B) Addition of ATG16L1 to the reaction mix leads to successful lipidation of LC3B to PE (colocalization of membrane (red) and LC3B (green) on surface of GUVs). (C) Fluorescent labeling of ATG12-ATG5 with CF405M does not alter lipidation reaction. (D) The peptide ATG16NT(11-43) cannot compensate for full-length ATG16L1. Membrane labeled with Atto680, LC3B labeled with Alexa488, ATG12-ATG5 labeled with CF405M. Scale bar 50 μm .

ATG12–ATG5 recognizes ATG3 in ATG3–ATG8, not ATG8 directly. Therefore, this initial experiment indicated that ATG12–ATG5–ATG16L1 might bind LC3B actively, since ATG12–ATG5–ATG16L1 only associated with lipidated GUV membranes. The labeling of ATG12–ATG5 does not seem to impair lipidation efficiency, since approximately the same number of GUVs is lipidated (compare Fig. 3.18, B with C).

Next, the enzymatic activity of the ATG12–ATG5–ATG16NT(11-43) complex was investigated. It has been demonstrated before that ATG12–ATG5 together with ATG16NT(11-43) was sufficient to conjugate LC3 to PE *in vitro* [Otomo et al. 2013], probably due to a conformational change in ATG12–ATG5. Here, no conjugated GUVs could be detected (Fig. 3.18, D). Also, in a lipidation experiment with large unilamellar vesicles (LUVs) no ATG8-PE could be observed for lipidation with ATG16NT (Fig. A.6, p. 96). These results demonstrate that, contrary to yeast Atg12–Atg5, ATG12–ATG5 is not able to act as an E3-like enzyme alone. Rather, the binding of ATG16L1 is likely to induce a conformational change for the efficient conjugation of LC3B to PE. The ATG5 binding peptide ATG16NT was not able to compensate for full-length ATG16L1 in these experiments.

3.4.2. Lipidation efficiency depends on labeling and Atg8 homolog

Knowing that ATG16L1 full-length was necessary for a successful lipidation of LC3B, similar conditions were applied to conjugate the other human ATG8 proteins to GUVs. The lipidation reaction could be stably reproduced for all four hATG8s (Fig. 3.19). To investigate the influence of protein labeling on conjugation efficiency, several labeling conditions were tested. Because labeling of ATG16L1 with Atto590 impaired lipidation efficiency (Fig. A.7), Alexa488 was used for labeling of ATG16L1.

Strikingly, a reproducible difference in lipidation efficiency for ATG8s was observed. This characteristic was exhibited in all experiments (Fig. 3.19). A quantification of lipidated GUVs yielded the result that LC3A and GATE-16 were not as efficiently conjugated compared to LC3B and GABARAP, with GABARAP being the ATG8 protein that shows the highest lipidation efficiency (Fig. 3.20). Activity of ATG16L1 was variable, resulting in an almost saturated lipidation efficiency in some experiments (Exp3, Fig. 3.20).

In summary, the reconstitution of the human autophagic UBL machinery yielded new results regarding possible diverging functions of hATG8s in autophagosome formation. Lipidation efficiency varied strongly between Atg8 homologs, independent of their subfamily. Interestingly, even in case of apparent optimal lipidation conditions,

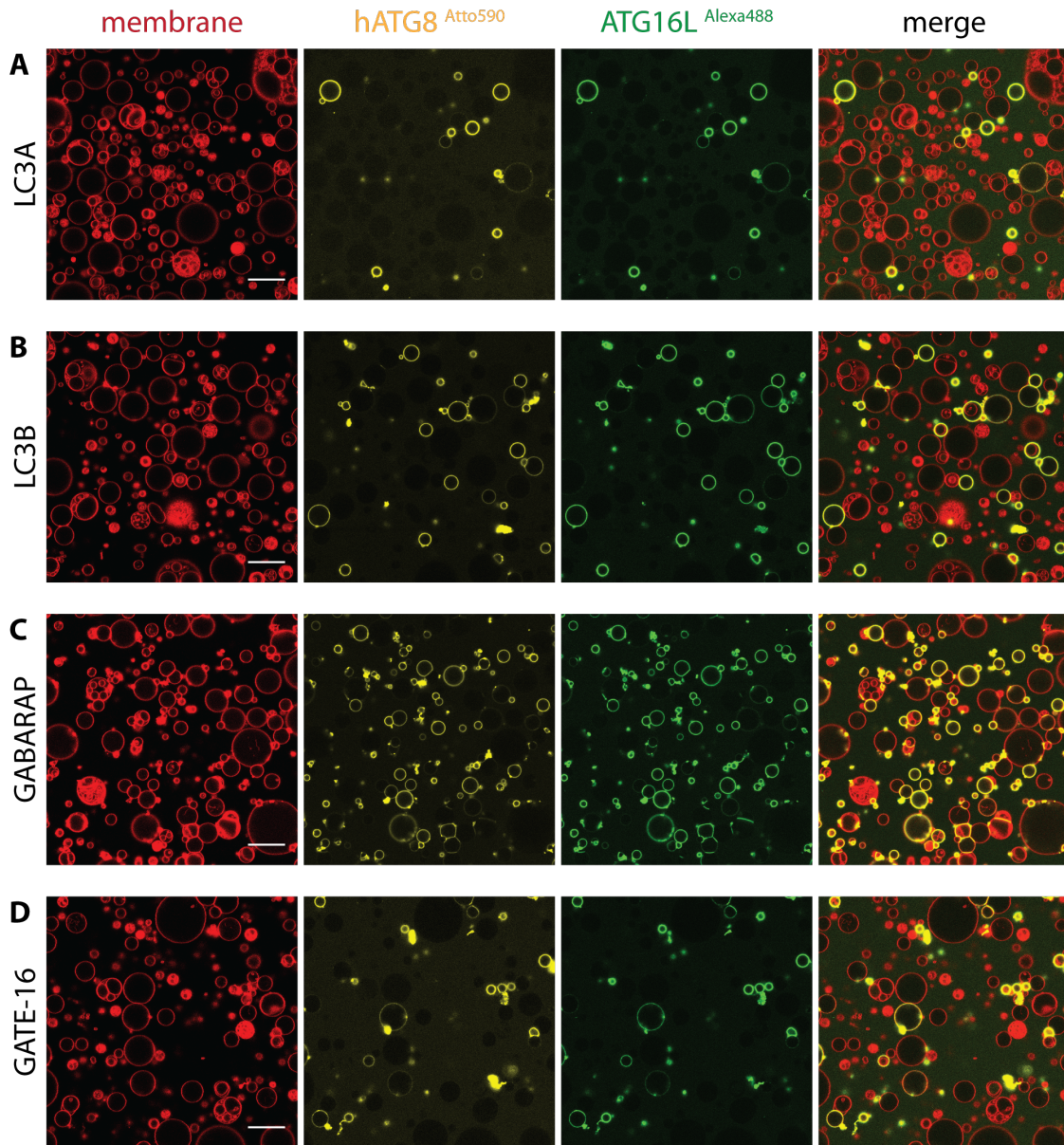


Figure 3.19.: The lipidation reaction with hATG8s labeled with Atto590 and ATG16L1 with Alexa488. HATG8s show different conjugation efficiencies, dependent on the protein used. (A) LC3A, (B) LC3B, (C) GABARAP, (D) GATE-16. Scale bar 50 μm .

lipidation efficiency of GATE-16 remained below 40 %, indicating a deviant function of GATE-16 compared to the other hATG8s.

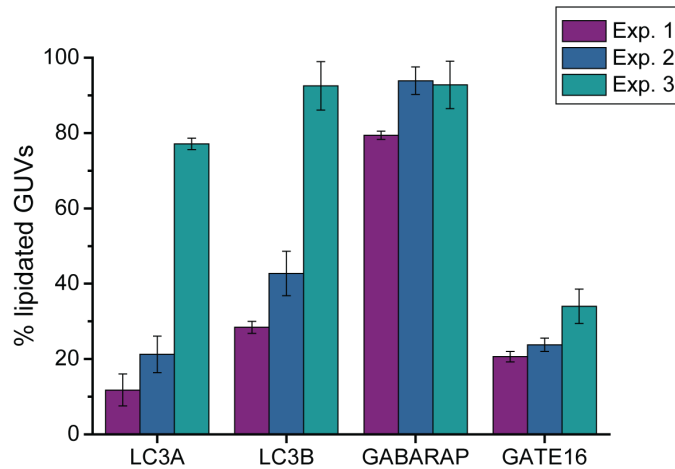


Figure 3.20.: Quantification of lipidated GUVs for three different experiments, $n > 100$ GUVs counted for each experiment.

3.5. FRAP experiments on GUVs

The observation, that ATG12–ATG5–ATG16L1 is retained only on membranes conjugated with ATG8 suggests that a scaffold, similar to the one in yeast, is formed. First evidence of the autophagic membrane scaffold in yeast came from fluorescence recovery after photobleaching (FRAP) experiments. In FRAP experiments, part of the sample is bleached with very strong laser power and the recovery of the fluorescence is monitored. This experiment sheds light on the mobility of the labeled components in the sample. If fluorescence does not recover at all or only to a very limited extent, the majority of fluorescently labeled components is immobile. Such results indicate that the labeled components form large scale macromolecular assemblies, which diffuse slowly. Therefore, these experiments are well suited as first indications, whether a scaffold is being formed with the human UBL system.

FRAP experiments were conducted on GUVs which were successfully lipidated with hATG8 proteins. Part of the GUV was bleached and recovery was monitored for the labeled components in the reaction: the membrane, the ATG8 protein, and ATG16L1. To compare mobility of different Atg8 homologs, similar experimental conditions were applied (Fig. 3.22). Strikingly, the immobile fraction of ATG16L1 is close to 100 % in all four ATG8 homologs tested. Similarly, the immobile fraction of the human

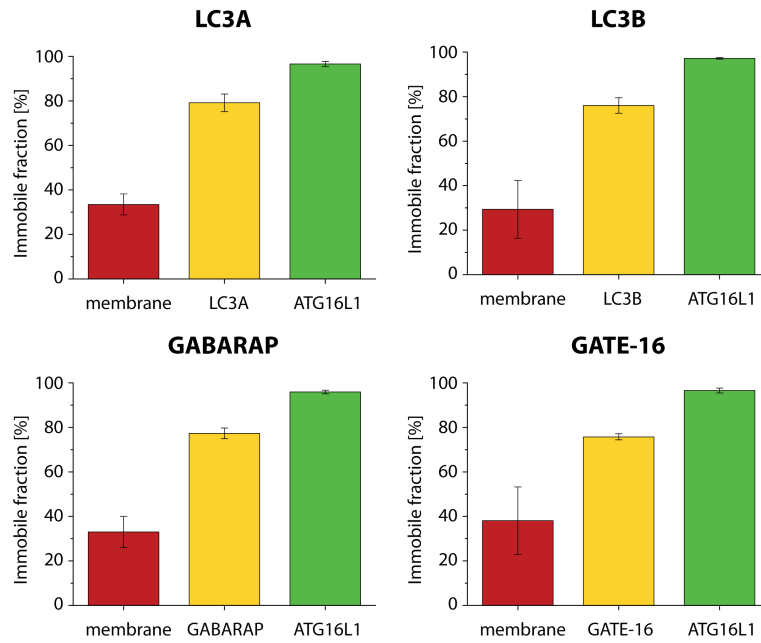


Figure 3.21.: Quantified immobile fraction of the labeled components in the experiment, membrane, ATG16L1, and corresponding ATG8 protein; $n=3$ independent experiments, at least 4 GUVs each.

ATG8 homologs is very high, close to 80%. Membrane lipids, however, display unlimited diffusion and most of the fluorescence signal recovered, corresponding to an immobile fraction of 30-40% (Fig. 3.21). This unexpected immobile fraction of the lipids is due to experimental conditions. Extensive irradiation, that was required for efficient bleaching, lowered fluorescence in non-bleached areas as well, since lipids diffuse rapidly in the membrane. Therefore the GUV as a whole became bleached and could not recover full fluorescence (e.g. Fig. 3.22, A). Additionally, the imaging process after the bleaching event is too slow to catch the bleached area in the membrane directly after the bleaching, again due to rapid lipid diffusion. Therefore, membrane fluorescence is already recovered partially in the bleached area (e.g. Fig. 3.22, D). Both facts contribute to a systematic error in the calculation of the immobile membrane fraction.

Nevertheless, the remarkable effect was the little recovery of ATG16L1 and the human ATG8 proteins. These results hint very strongly to the assumption that indeed also human UBL proteins are part of an autophagosomal membrane scaffold. Noteworthy, all ATG8 proteins tested, namely LC3A, LC3B, GABARAP, and GATE-16, demonstrate comparable immobility of ~80% (Fig. 3.21). These findings give rise to the idea that *in vitro*, all hATG8s have the potential to form a protein scaffold.

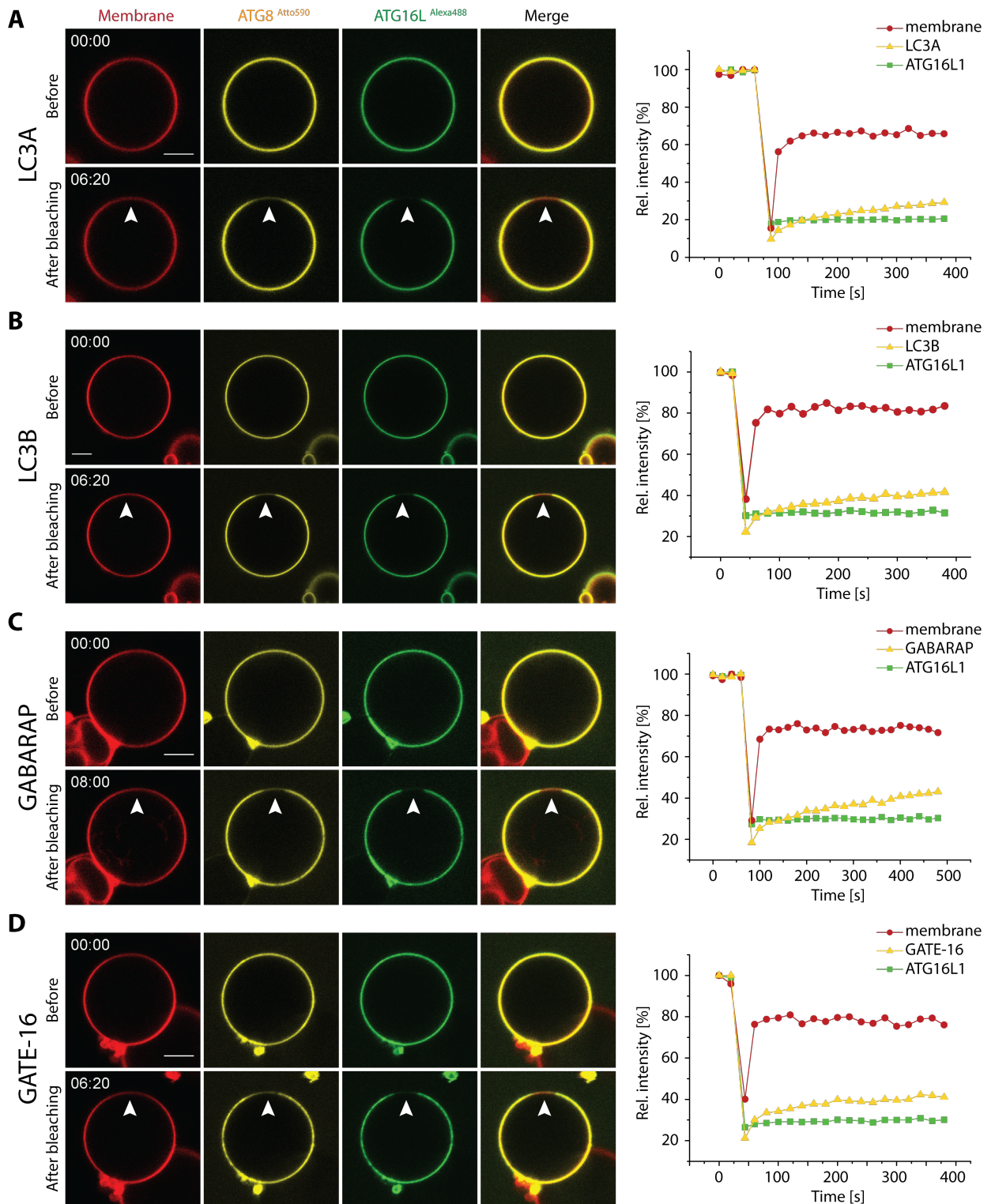


Figure 3.22.: Individual FRAP experiments on lipidated GUVs with ATG8s. Arrowheads point to bleached area. On the right the corresponding relative fluorescence intensity of the experiment is displayed. Fluorescence was set to 100 % for all channels before bleach. The strong decline corresponds to the bleaching timepoint and fluorescence recovery was monitored for at least 5 minutes. (A) LC3A, (B) LC3B, (C) GABARAP, (D) GATE-16. Scale bar 5 μ m.

4

Discussion

4.1. The autophagic scaffold in yeast

Despite the important role for autophagy in development, ageing, and a wide range of diseases such as cancer, neurodegeneration, or infections, mechanistic insights into the formation of autophagosomes are still limited. The interplay of Atg proteins and protein complexes, which orchestrate the formation of this double membrane structure is up to now a matter of debate. Regarding the maturation of the phagophore, it is still unknown how membrane extension is regulated and which mechanism defines the size of autophagosomes. In specific autophagy, cargo determines the size, because the autophagosomal membrane wraps tightly around the cargo, e.g. damaged mitochondria [Xu et al. 2015]. For unspecific autophagy, typical autophagosomal diameters range from 300 to 900 nm in yeast and 0.5 to 1.5 μm in mammalian cells [Shibutani et al. 2014]. But how is this size controlled? Interestingly, the amount of Atg8, an Ubiquitin like protein conjugated to Phosphatidylethanolamine (PE) on the autophagosomal membrane, determines the size of autophagosomes [Xie et al. 2008a]. The conjugation of Atg8, also referred to its ‘lipidation’, is catalyzed by the protein complex Atg12–Atg5–Atg16, with Atg12 being the second Ubiquitin-like protein in autophagy. *In vitro*, Atg12–Atg5 is sufficient to conjugate Atg8 to membranes [Hanada et al. 2007]. *In vivo*, however, Atg12–Atg5 always associates with Atg16 and remains associated with the phagophore [Kuma et al. 2002; Suzuki et al. 2007]. These findings raised further questions: First, why is Atg12–Atg5 retained on the autophagosomal membrane during the expansion of the phagophore, when its sole function is the conjugation of Atg8 to Phosphatidylethanolamine (PE)? Also, the fact that Atg16 binds to Atg12–Atg5 when it is not necessary for the enzymatic reaction *in vitro* was obscure, especially with regard to the somewhat extraordinary elongated structure of Atg16, and its dimer formation. And secondly, what is the purpose of Atg8 decorating the outer membrane of the phagophore, which constitutes the main characteristic of phagophores and autophagosomes? It is well established

that Atg8 acts as cargo adapter on the inner membrane, yet the function of Atg8 binding to the outer membrane remained unexplained.

Previous work in the lab has revealed, that Atg8 is immobilized on liposomes by Atg12–Atg5–Atg16, but not by Atg12–Atg5. These findings confirmed the enzymatic activity for Atg12–Atg5, but implicated a structural function for Atg16. Based on these experiments, the hypothesis was developed, that Atg8 together with Atg12–Atg5–Atg16 is forming a so far undescribed protein scaffold on the phagophore membrane. To verify this hypothesis and unravel the structural organization of the scaffold on the membrane, high-resolution imaging was essential. However, electron microscopy on liposomes would have been technically very challenging, because giant unilamellar vesicles (GUVs) are unstable and previous experiments showed that large unilamellar vesicles are too small for scaffold formation. Therefore, Atomic Force Microscopy (AFM) was the method of choice to confirm and investigate the hypothesized autophagic scaffold.

For imaging the autophagic scaffold with AFM, the lipidation reaction had to be reconstituted on supported lipid bilayers (SLBs). After optimizing the support and adjusting protein concentrations, Atg8 was successfully conjugated to PE on SLBs. Interestingly, regular sized particles with a diameter of 50 ± 10 nm could be observed, consisting of Atg8 and Atg12–Atg5 (Fig. 3.4). Atg8 has an estimated diameter of 3 nm (PDB no. 3VXW) and Atg12–Atg5 dimensions of 6 nm x 4 nm (PDB no. 3W1S). Therefore, these particles were too large for single Atg8 molecules or one Atg8–PE/Atg12–Atg5 complex. Taking into account that the horizontal resolution of the AFM is limited by the width of the cantilever and the lateral mobility of the particles, these complexes consisted of at least two, but not more than four Atg8–PE/Atg12–Atg5. Previous studies showed that Atg8 has the ability to multimerize in response to conjugation with PE [Nakatogawa et al. 2007]. Hence it can be concluded, that Atg8 is at the core of these complexes, forming dimers, trimers, or tetramers, and Atg12–Atg5 is binding to Atg8, thereby extending the dimension of the complexes.

When Atg16 was added to the reaction mixture, the appearance of the proteins changed drastically. A flat protein layer could be observed, which exhibited a meshwork-like architecture (Fig. 3.3). The crystal structure of Atg16 revealed a stretch of exposed hydrophobic residues in Atg16, which stabilized a crystal contact between two antiparallel Atg16 dimers [Fujioka et al. 2010]. This finding indicated, that Atg16 forms antiparallel tetramers, which was supported by the observation that the edge length of the meshwork was 17 ± 4 nm, comparable to the length of an

Atg16 tetramer (Fig 3.6). Taken together, these findings are in agreement with the hypothesis, that indeed the autophagic UBL systems, Atg8 and Atg12–Atg5–Atg16, assemble into a protein scaffold *in vitro*. The scaffold consists of two building blocks, Atg8–PE/Atg12–Atg5 complexes and Atg16 antiparallel tetramers, which link Atg8–PE/Atg12–Atg5 complexes and therefore organize them into a continuous protein layer that is linked to the membrane via Atg8–PE (Fig. 4.1).

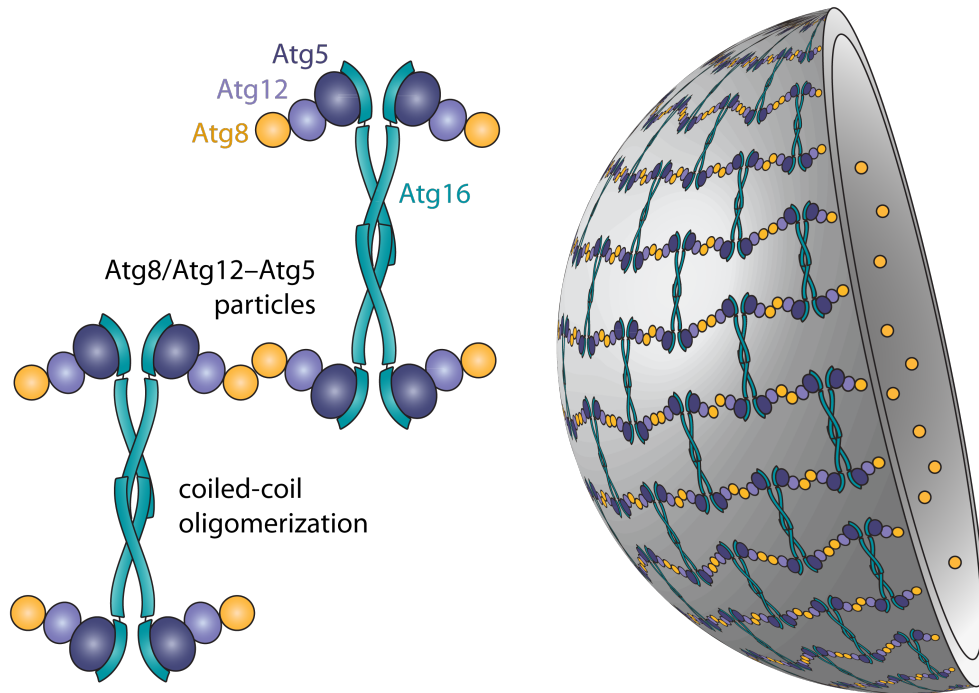


Figure 4.1.: Cartoon representing the possible mode of interaction of yeast autophagic UBL proteins involved in autophagic scaffold formation. **(Left)** Atg8 interacts with itself and therefore clusters Atg8–PE/Atg12–Atg5 complexes in oligomers, consisting of two to four subunits (here interaction of two subunits is drawn). Atg16 cross-links these oligomers via antiparallel coiled-coil formation. **(Right)** The autophagic scaffold forms on the convex side of the phagophore, whereas Atg8 serves as cargo adaptor molecule on the concave side.

4.1.1. The autophagic scaffold in comparison to canonical membrane coats

AFM revealed intriguing similarities of the autophagic membrane scaffold in comparison to canonical membrane coats (clathrin, COPI, and COPII). The 8 nm thick autophagic scaffold resembles the height of COPII (10nm), clathrin (12nm), and COPI (14nm, Faini et al. [2012]) protein layers. Furthermore, the edges of the

autophagic membrane scaffold are built by antiparallel coiled-coil domains of Atg16. These rod-shaped building blocks are comparable to the rod-shaped coat components of canonical coats, which form cage-like structures. Strikingly, even the dimensions of these lattices are comparable. The edge-length of 17 nm measured by AFM for the autophagic membrane scaffold lies in the same range as the edge length of other membrane coats: 18 nm in clathrin coats [Kirchhausen et al. 1984], 13 nm in COPII and 14 nm in COPI [Faini et al. 2013]. Therefore, with respect to building block dimensions, the autophagic scaffold appears structurally analogous to canonical membrane coats.

The meshwork-like architecture of the autophagic membrane scaffold, unveiled by AFM, proved to be flexible, since it could form from nano- to macroscopic scale on flat membranes and round liposomes (Fig. 3.4). Therefore the scaffold meets its biological requirements, since it exhibits flexibility in size and shape, which is required for forming autophagosomes ranging from 300 to 900 nm [Shibutani et al. 2014].

Interestingly, AFM demonstrated, that the structure of the autophagic scaffold exhibits a lower degree of structural organization, compared to clathrin and COPII. Similarly, also COPI coated vesicles display a high amount of structural flexibility [Faini et al. 2013], since cargo of different sizes is transported and the structure of the COPI coat varies in response to membrane curvature [Beck et al. 2008]. In COPI, the structural flexibility is realized via its triangularly shaped repeated unit, which can interact in four different patterns [Faini et al. 2013]. However, transport vesicles enclosed by COPI range in size from 50 to 100 nm and are therefore one magnitude smaller than autophagosomes. Structural flexibility of the building blocks allows therefore assembly of COPI coats on vesicles with different sizes, shapes and curvature, providing diverse cargo to be sequestered and transported [Faini et al. 2013]. With respect to the autophagic scaffold, particle analysis revealed that Atg8-PE/Atg12-Atg5 complexes are homogeneous in size (Fig. 3.4). This finding indicated that only one type of oligomer, either two, three, or four Atg8-PE/Atg12-Atg5 complexes, are assembled into the scaffold. Since autophagosomes are one magnitude larger compared to other transport vesicles, it is not necessary to change the geometry of building block assembly to meet a broad size range. Rather, flexibility is provided by conformational freedom of the building blocks relative to each other and the scaffold can be viewed as a supporting meshwork for phagophores.

The observed lower structural organization could be derived from the unregulated way of assembly, since *in vitro*, Atg8 is conjugated at several sites on SLBs, and

assembly is driven by diffusion, with no active force involved. Since it was shown before that the autophagic proteins act in a hierarchical manner [Suzuki et al. 2007], it can be assumed that *in vivo*, scaffold assembly is regulated by upstream factors, allowing for a more homogeneous structural organization.

Despite its structural similarities, a difference to canonical coats is the spatial and functional separation between scaffold formation on the convex side of the phagophore and cargo-binding via Atg8-PE on the concave side of the phagophore (Fig. 4.1, right). Both tasks are spatiotemporally coordinated in canonical membrane coats, due to direct interactions of cargo-adapters and coat components via transmembrane domains of participating proteins. This spatiotemporal coordination is not possible due to the double-membrane nature of the autophagosome and Atg8 attached to the both convex and concave face. Additional experiments in the lab revealed, that cargo receptor molecules compete for Atg8-PE binding with Atg12-Atg5-Atg16 and are able to disrupt the scaffold. This competitive binding to Atg8 might allow tethering of cargo to the inner membrane for engulfment. Additionally, it remains to be investigated whether the scaffold forms in specific autophagy, since in specific autophagy, the form of the autophagosome is defined and an additional structural support for the membrane might not be necessary.

In addition to its similarities and differences to canonical membrane coats, the autophagic membrane scaffold exhibits some unique features. It is so far the only described membrane scaffold that is covalently linked to lipids. For other canonical coats transmembrane domains of participating proteins provide the connection to the membrane.

Furthermore, it is the only scaffold in which an enzyme catalyzes a primary reaction for coat formation and in a second step participates in coat formation. For the autophagic scaffold, Atg12-Atg5-Atg16 first catalyzes the conjugation reaction of Atg8 to PE and is then in a second step integrated into the scaffold by interacting with conjugated Atg8.

Finally, COPII and clathrin are able to self-associate without cargo or membrane into regular sphere-like structures [Stagg et al. 2006; Fotin et al. 2004]. This is not the case for the autophagic scaffold. Atg8 is only able to multimerize when it is conjugated to PE [Nakatogawa et al. 2007], indicating a conformational change upon conjugation [Ichimura et al. 2004]. In line with this finding, a conformational change of an ‘open’ and ‘closed’ conformation could be demonstrated for GABARAP, a human homolog of Atg8 [Coyle et al. 2002]. Therefore, the conjugation reaction is a prerequisite for scaffold formation, and the autophagic scaffold can only form with

lipidated Atg8 in ‘open’ conformation.

In summary, the building blocks of the autophagic membrane scaffold exhibit similar dimensions compared to the building blocks of canonical vesicle coats. The flexibility of the scaffold meets biological requirements since it can form on liposomes and flat membranes from micro- to nanoscopic scale. The observed organizational irregularity could be related to the experimental *in vitro* system, since particle analysis revealed homogeneous building blocks. Furthermore, upstream factors regulate assembly *in vivo*, but were not included in the reconstitution. The covalent linkage to lipids, the dual function of Atg12–Atg5–Atg16 as conjugating enzyme and coat component, as well as spatial separation of scaffold formation and cargo selection constitute unique characteristics of the autophagic membrane scaffold.

4.1.2. Previous discussions about a possible autophagosomal membrane scaffold

Interestingly, it has been suggested before that Atg12–Atg5–Atg16 might be involved in the formation of a coat on autophagosomes, due to its oligomerization and its localization to the elongating phagophore. Yet, direct evidence was missing [Kuma et al. 2002]. Conversely, a quantitative study on yeast Atg proteins came to the conclusion, that the number of Atg16 proteins on the phagophore is not enough to cover it completely and therefore scaffold formation is unlikely [Geng et al. 2008]. In the latter study, Atg proteins were tagged with fluorescent proteins. The estimated number of Atg8 molecules at the phagophore was determined to be a magnitude higher compared to Atg16 amounts and the authors stated that Atg5- or Atg12-tagged proteins were hardly detectable. Since fluorescent fusion proteins presumably hinder interaction and therefore coat formation, protein numbers of Atg12–Atg5–Atg16 were most likely underestimated. Additionally, the diverging number between Atg16 and Atg8 could be explained if the scaffold would not form on the complete curvature of the phagophore, but only partly to stabilize the growing membrane structure. Experimental evidence suggests that this might be true for phagophores in plants, where ATG5 defines a ring-like domain on the expanding phagophore [Le Bars et al. 2014].

Finally, the maintenance of curvature and structural stabilization of the entire phagophore represents an energetic challenge. This is especially the case for bulk autophagy, where no substrate, e.g. a damaged mitochondrion, stabilizes the membrane structure [Hurley et al. 2014]. Hence, the autophagic membrane scaffold described

here might serve to stabilize the phagophore membrane. This assumption is in line with previous experiments in the lab, which demonstrated that lipidated GUVs were able to withstand larger osmotic pressure compared to uncoated GUVs.

4.2. Varying roles for Atg18 and Atg21 in autophagosome formation

The finding of a so far undescribed membrane scaffold on the phagophore raises the question, how scaffold formation is triggered at the beginning of phagophore expansion. The answer to this question could lie in the proteins acting upstream of the Atg8 conjugation machinery. Two candidates, which could be involved in recruiting Atg12–Atg5–Atg16 to the phagophore, are Atg18, forming a complex with Atg2 [Suzuki et al. 2007], and Atg21. It could be verified recently, that indeed Atg21 is able to recruit Atg12–Atg5–Atg16 to the autophagosomal membrane through direct interaction with Atg16 [Juris et al. 2015]. Furthermore, WIPI2b (WD-repeat PtdIns(3)P effector protein 2b), the mammalian homolog of Atg18, directly binds ATG16L1 and therefore recruits ATG12–ATG5–ATG16L1 to the autophagosomal membrane [Dooley et al. 2014]. However, upon knockout of Atg18 or Atg2, the localization of Atg12–Atg5–Atg16 or Atg8 was not affected, hinting either towards another role of the Atg2–Atg18 complex during autophagosome formation or to a compensatory effect of Atg21 [Suzuki et al. 2007].

To decipher the individual roles of Atg18 and Atg21, transmission electron microscopy (TEM) was performed on knock out strains of these two proteins. Additionally, cells were deficient for the vacuolar protease Pep4, leaving vacuolar cargo undegraded. TEM imaging revealed, that smaller and fewer autophagic bodies are forming in Δ Atg21 cells. This result is in line with the finding that Atg21 recruits Atg12–Atg5–Atg16 to the phagophore [Juris et al. 2015]. Upon knock out of Atg21, Atg12–Atg5–Atg16 cannot be recruited to the autophagic membrane as efficiently any more. Therefore, Atg8 is lipidated to a lesser extend to the growing phagophore, which corresponds to smaller autophagosomes [Xie et al. 2008a]. Conversely, no autophagic bodies could be detected in Atg18 knock out cells. Furthermore, it was not possible to rescue this phenotype by an overexpression of Atg21, leading to following conclusions: Atg18 function diverges from Atg21 function due to its distinct phenotype upon knock out. Additionally, since Atg21 cannot compensate for the loss of Atg18, a functional redundancy during starvation can be excluded. Interestingly, fine-mapping of Atg proteins revealed that Atg18 localizes to the edge of the growing

phagophore [Suzuki et al. 2013], indicating a role in autophagosomal closure. In summary, despite the similarity of Atg18 to Atg21 or WIPI2, Atg18 could play a role during phagophore closure and not necessarily in recruiting Atg12–Atg5–Atg16.

4.3. The autophagic scaffold in humans

Yeast has been the model organism for many ground-breaking discoveries in autophagy. Because Atg proteins are well conserved across species and phyla, findings in yeast often apply to mammals as well. Therefore, the discovery of an undescribed membrane scaffold on phagophores directly implied the question, whether such a scaffold is forming with the homologous proteins in humans. Such a verification would add important information to the understanding of autophagy in humans. Furthermore, underlying protein-protein interactions could be new targets for treating autophagy related diseases.

For the confirmation that a similar scaffold exists in humans, both human autophagic UBL systems had to be reconstituted *in vitro*. In this thesis, this complete reconstitution was achieved in its entirety for the first time. The purification of the human UBL components was more difficult compared to the yeast UBL systems. First, different isoforms of the proteins exist, which complicated the search for the right protein combinations, especially in the case of ATG7. Second, the human proteins possess a more complex architecture, e.g. the WD-domain of Atg16L1, whose folding is enhanced by eucaryotic chaperones [Miyata et al. 2014]. Therefore, earlier studies never contained the entire set of proteins that are involved in the two conjugation reactions of hATG8s and ATG12. Especially full-length ATG16L1, an indispensable part of the yeast autophagic scaffold, has not been purified before.

Moreover, with the ‘toolbox’ of the human autophagic UBL proteins in hand, it was now feasible to shed some light on potential differences between ATG8 proteins. Here, yeast cannot provide an answer, since Atg8 follows the premise ‘one for all’, meaning Atg8 alone fulfills all tasks that might be split in higher eucaryotes, due to the division of ATG8 proteins in its subfamilies LC3s and GABARAPs.

In this thesis, two major findings were made with the reconstituted human UBL systems: (1) A difference in lipidation efficiency between ATG8s could be observed. ATG8s tested were LC3A and LC3B, belonging to the LC3 family, and GABARAP and GATE-16, representing the GABARAP family. Unexpectedly greater differences were detected within subfamilies, with GABARAP showing the highest lipidation efficiency to GUVs, followed by LC3B. LC3A and GATE-16 showed very low lipidation

efficiency. (2) *In vitro* FRAP (fluorescence recovery after photobleaching) experiments strongly implied the formation of a human autophagic membrane scaffold, notably with all ATG8s purified here.

4.3.1. Reconstituted lipidation reaction with hATG8s

It was unclear, whether the human system behaves similarly in GUV experiments compared to the yeast system. Specifically, contradictory results have been published regarding the requirement of ATG16L1 in *in vitro* lipidation experiments. On the one hand, successful lipidation of LC3 to PE has been achieved on LUVs with the ATG5 binding region of ATG16L1, ATG16NT(11-43) [Otomo et al. 2013]. On the other hand, a high DOPE content was sufficient for a successful lipidation without presence of neither ATG12–ATG5 nor ATG16L1 [Nath et al. 2014].

Observations in this thesis on GUVs demonstrated that ATG12–ATG5–ATG16L1 is required for lipidation of hATG8s (Fig. 3.18, L. Dempfle master thesis). The ATG5 binding region of ATG16L1 (ATG16NT¹¹⁻⁴³) was, however, not sufficient for lipidation of hATG8s to GUVs. This finding is in contrast to the yeast system, where Atg12–Atg5 was sufficient for Atg8 lipidation. Interestingly, no LC3 is conjugated to autophagosomal membranes upon deletion of only the coiled-coil domain of ATG16L1 *in vivo* [Saitoh et al. 2008]. This confirms the finding from this thesis, that ATG16L1 is needed for the lipidation of hATG8s *in vitro*. Presumably, ATG16L1 causes a conformational change in ATG12–ATG5, which activates the enzymatic activity of ATG12–ATG5. This finding also implies that the coiled-coil region, and thus dimer formation, is required for the lipidation of hATG8s. The observation, that lipidation can be achieved *in vitro* by ATG16NT on small vesicles with high DOPE-content Otomo et al. [2013] suggests, that highly stressed and instable membranes counteract the requirement of ATG16L1. However, such systems do not represent the situation *in vivo*, where phagophores are flat membrane sacs with PE-contents below 20-30 %.

The main question to be answered with the *in vitro* reconstituted lipidation reaction was, if hATG8s have distinct roles during autophagosome formation, and if they therefore behave differently in GUV experiments. Surprisingly, hATG8s demonstrated varying lipidation efficiencies, with biggest discrepancies within hATG8 families. LC3A and GATE-16 showed a similar low efficiency compared to LC3B and GABARAP with a high lipidation efficiency.

The study by Weidberg et al. [2010] implied that LC3s act before GABARAPs in autophagosome formation. There, knockdowns of hATG8s in HeLa cells were performed targeting whole subfamilies. These knockdowns were rescued by over-

expression of either LC3B or GATE-16. Based on these experiments, the authors drew conclusions for the whole subfamily, so for LC3s and GABARAPs, respectively. In line with the results published by Weidberg et al. [2010], experiments in this thesis revealed different lipidation efficiencies for LC3B and GATE-16. Lipidation efficiency of LC3B was relatively high, whereas GATE-16 showed the lowest lipidation efficiency in all experiments. Assuming that a high lipidation efficiency is necessary for phagophore expansion, it is possible that LC3B acts during phagophore growth and GATE-16 acts at later stages of autophagosome formation, possibly closure.

However, and this is in contrast to the conclusions drawn by Weidberg et al. [2010], GABARAP demonstrated the highest lipidation efficiency in GUUV experiments. Hence, not GABARAPs as a whole subfamily but possibly GATE-16 alone acts at later stages of autophagosome formation. Similarly, the lipidation efficiency of LC3A lied in the same range as GATE-16. Therefore, assuming that LC3s as a whole subfamily are necessary for phagophore expansion and GABARAPs for later stages of autophagosome formation might not be true *in vivo*. Assuming again that a high lipidation efficiency is needed for phagophore growth, GABARAP could act before GATE-16. Interestingly, this assumption would support the study by Szalai et al. [2015], where the authors find LC3s completely dispensable for autophagosome formation in rat hepatocytes, implying that GABARAP can compensate at least partially for loss of LC3B.

In conclusion, the growth of the phagophore could be dependent on hATG8s with high lipidation efficiencies, namely LC3B or GABARAP, and GATE-16 could act at a later stage of autophagosome formation. Which of the proteins is responsible for phagophore growth might be susceptible to cell type. Nevertheless, functional redundancy of hATG8s to a certain extent during autophagosome expansion should be considered as well. All hATG8s reveal a variety of non-identical binding partners and different cargo-specificities. Therefore, not every hATG8 protein comes necessarily with a different role in autophagosome maturation.

4.3.2. Possible scaffold formation with human UBL autophagic proteins

The homology of the UBL protein systems between yeast and mammals implied, that a comparable autophagic membrane scaffold could form in mammals, as was observed with yeast proteins. *In vitro* FRAP experiments revealed, that the human UBL proteins show comparable immobile behavior on GUUVs to the yeast proteins, implying scaffold formation. Moreover, similar immobile behavior was observed for all

hATG8s tested, namely LC3A, LC3B, GABARAP and GATE-16. Although diverging lipidation efficiencies were observed for hATG8s, all hATG8s on lipidated GUVs showed similar immobility. Likewise, ATG16L1 appeared to be almost completely immobile on all GUVs tested, unrelated of the hATG8 used. These results imply that *in vitro*, possibly both LC3s and GABARAPs possess the ability to form a scaffold-like structure on membranes.

Human ATG16L1 also possesses, like Atg16, an ATG5 binding domain and a coiled-coil region for dimer formation. The assumption for the human scaffold was that, according to Atg16, dimers form antiparallel tetramers through interactions within the coiled-coil domain of ATG16L1. Interestingly another homolog of Atg16, ATG16L2, was recently described, which is not involved in autophagy albeit forming an ATG12–ATG5–ATG16L2 complex with dimer formation of ATG16L2 [Ishibashi et al. 2011]. ATG16L2 shows high sequence homology to ATG16L1 in its N-terminal (ATG5 binding) and WD-repeat region, but only little homology (20,7% amino acid identity) in its coiled-coil region. The authors assume that this functional discrepancy might stem from a key factor, possibly Rab33B, that can bind to ATG16L1 but only very weakly to ATG16L2, and therefore induces autophagy. However, assuming that ATG12–ATG5–ATG16L1 assembles the same way as Atg12–Atg5–Atg16, it is plausible that ATG16L2 is not able to form the tetramer needed for scaffold formation due to its non-homologous coiled-coil region.

The binding of Rab33B GTPase to the coiled-coil domain of ATG16L1 has been reported before [Itoh et al. 2008]. Rab33B binding possibly modulates autophagy by regulating the availability of ATG16L1 in the cytoplasm. Fukuda et al. [2008] suggest that upon induction of autophagy, another protein X binds to the coiled-coil domain of ATG16L1. This Protein X could likely be ATG16L1 itself, forming a tetramer during phagophore growth, as part of the autophagic membrane scaffold. In summary, it was shown before that the coiled-coil domain of ATG16L1 is important for autophagosome formation, however the reasons were not completely understood. Results from this thesis indicate that, comparable to yeast Atg16, ATG16L1 dimers form antiparallel tetramers in the coiled-coil region, which leads to similar immobility of the autophagic UBL proteins on GUVs as was the case for yeast in *in vitro* experiments.

The second building block besides Atg16 tetramers in the yeast autophagic membrane scaffold are Atg8–PE/Atg12–Atg5 complexes, where Atg8 oligomerizes with itself. Atg8 undergoes a conformational change upon binding to PE [Ichimura et al. 2004]. This ‘open’ conformation of Atg8–PE induces oligomerization of Atg8–

PE/Atg12–Atg5. Similarly, an ‘open’ and ‘closed’ conformation was described for GABARAP and it was proposed that GABARAP can self interact in open conformation [Coyle et al. 2002]. However, no experimental evidence was found for this interaction so far. Yet, NMR spectroscopy confirmed that GABARAP is able to adopt at least two conformations [Weiergräber et al. 2013]. Assuming a similar mode of self-interaction between hATG8s as compared to Atg8, immobility of the human UBL proteins in FRAP experiments implies self-interaction for all hATG8s. It needs to be elucidated if this self-interaction depends in all cases on a conformational change.

In summary, FRAP experiments demonstrated immobility of hATG8s and ATG12–ATG5–ATG16L1 on GUVs *in vitro*, comparable to similar experiments with yeast autophagic proteins. Remarkably, all hATG8 proteins displayed akin immobility. Further experiments are needed to confirm, if the observed immobility indeed involves scaffold formation. In case this hypothesis holds true, a new perspective might arise on autophagosome formation in humans.

5

Outlook

The finding that Atg8 and Atg12–Atg5–Atg16 are part of a new membrane scaffold could answer many questions in the autophagy field regarding these proteins. Nevertheless, the AFM studies presented here can only be a start for further investigations of the autophagic membrane scaffold. Particularly its structural organization should be of future interest. With high resolution techniques, such as Cryo-electron microscopy, it could be analyzed in more detail if Atg8–PE/Atg12–Atg5 complexes consist of two, three, or four Atg8–PE/Atg12–Atg5 particles. Other promising approaches could be electron microscopy after chemical fixation of the scaffold on supported lipid bilayers with glutaraldehyde, or super resolution fluorescence microscopy methods, such as PALM (photoactivated localization microscopy) or STORM (stochastic optical reconstruction microscopy).

Also, it remains elusive whether the autophagic scaffold forms on the complete growing phagophore or if it only stabilizes parts of the phagophore. Stabilization of the phagophore rim seems to be the case in plant autophagy, where ATG5 could be detected at the rim of growing phagophores by three-dimensional TIRF (total internal reflection fluorescence) microscopy [Le Bars et al. 2014]. However, fine-mapping of Atg proteins in yeast on giant cargo revealed an even distribution of Atg16 on the phagophore [Suzuki et al. 2013]. Nevertheless, a similar approach should yield new information on the *in vivo* formation of the autophagic membrane scaffold, specifically with respect to regulated recruitment of the scaffold building blocks. Here, nucleation experiments with upstream factors, e.g. Atg21, could provide a new view on autophagic scaffold assembly, by recruiting these factors to the plasma membrane followed by TIRF imaging. A similar approach *in vitro* with ultra-fast AFM on supported lipid bilayers could complement these experiments.

With respect to the human autophagic scaffold, a direct proof is needed for verification of scaffold formation, comparable to AFM studies. It will be interesting to observe, if the scaffold shows a similar structural organization compared to yeast. Also, possible structural differences between hATG8 proteins should be

investigated. Using mixtures of hATG8s on GUVs for FRAP experiments and lipidation efficiencies should yield further insights into possible separate roles of ATG8s during autophagosome formation. E. g. ATG8s possibly show diverging mobility in FRAP experiments when used in mixtures, hinting towards a different integration ability into the scaffold.

In vitro time-lapse experiments using the yeast UBL proteins revealed an hierarchical binding of Atg12–Atg5. In a first step Atg12–Atg5 binds Atg3–Atg8 and thereby catalyzes the binding of Atg8 to the membrane. In a second step, Atg12–Atg5 is recruited to the membrane by conjugated Atg8 via a noncanonical Atg8 interacting motif in Atg12. Time-lapse experiments of human UBL proteins could reveal if protein interactions follow a similar sequence compared to yeast UBL proteins. Additional GUV experiments should comprise binding assays with ATG4 and cargo adaptors to examine if the scaffold can be resolved by competitive binding.

Last but not least the *in vitro* results obtained so far should be complemented by *in vivo* autophagy assays using living cells. Especially knock-down experiments of single ATG8s, e. g. only GABARAP or GATE-16, should demonstrate, if the hypothesized functions of single ATG8s can be verified *in vivo*. Furthermore, super resolution fluorescence microscopy could reveal whether ATG8 proteins demonstrate distinct localization and function during phagophore expansion.

A

Appendix

A.1. ATG12–ATG5 production attempts

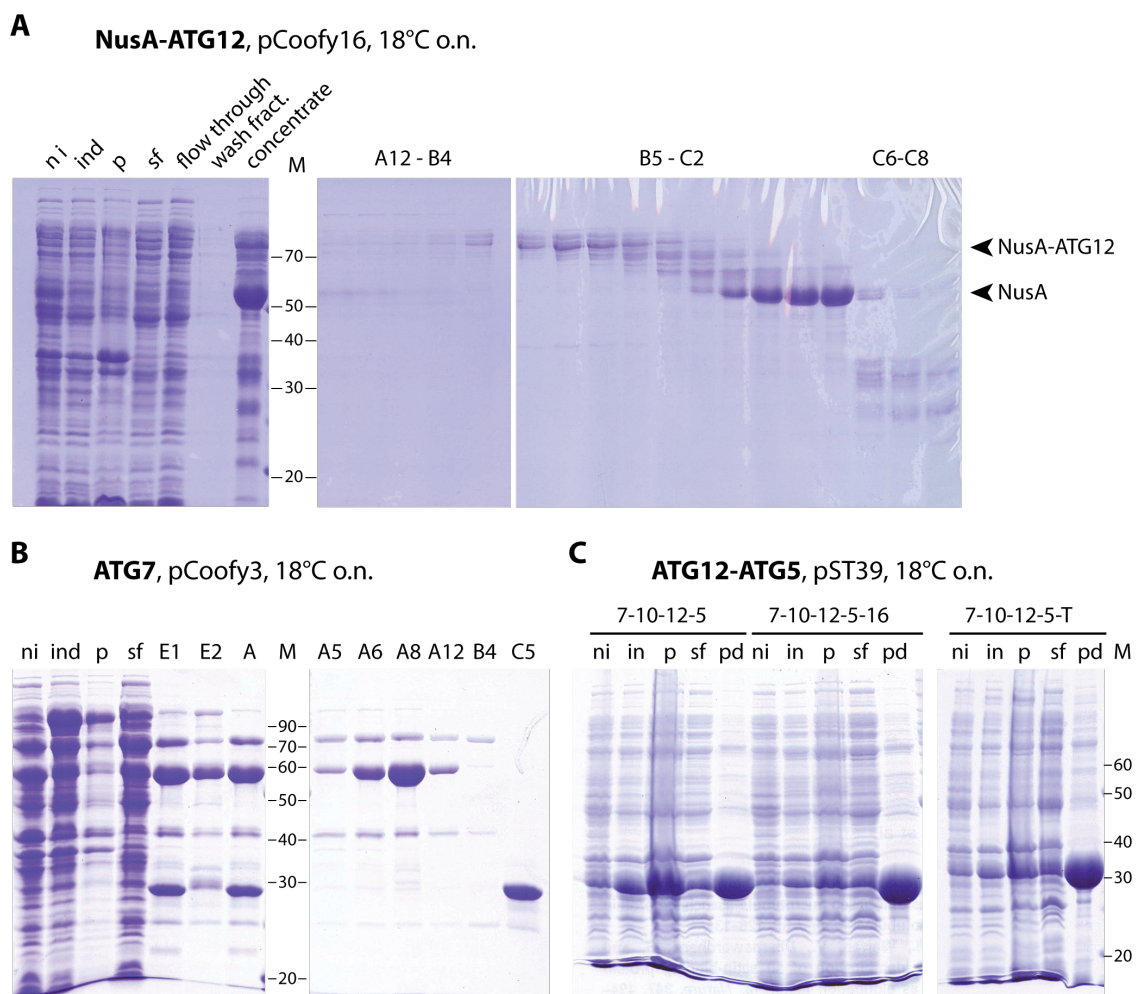


Figure A.1.: Attempts to express proteins for the production of ATG12–ATG5. (**A**) 12 % SDS-PAGE gel of NusA-ATG12 purification steps expressed in *E. coli* BL21. Left from the protein marker different steps of affinity chromatography are displayed, on the right fractions from size exclusion chromatography (SEC). Even though the fusion protein was not cleaved before subjection to SEC, degradation can be detected (compare band of NusA at 59 kDa to band of fusion protein at 74 kDa).

(Continued from previous page) **(B)** 12 % SDS-PAGE gel of ATG7 (isoform 1) purification steps expressed in *E. coli* BL21, with additional chaperone expression (vector pG-KJE8, Takara). Left from the protein marker different steps of affinity chromatography are displayed, on the right fractions from SEC. ATG7 (78 kDa) could not be detected in mass spectrometry, instead all proteins purified during SEC corresponded to chaperones. **(C)** Test expression samples on 12 % SDS-PAGE gel of different polycistronic vectors for Atg12-Atg5 production, expressed in *E. coli* Tuner pLac. The vectors contained cDNA for ATG7 (isoform 2), ATG10, ATG12, ATG5, and ATG16 or TECPR, as indicated. No band corresponding to the Atg12-Atg5 conjugate can be detected in the pull down (47 kDa), instead the band at 30 kDa most probably corresponds to ATG5. ni - not induced sample; ind - induced sample; p - pellet (insoluble fraction); sf - soluble fraction; E1, E2 - elution fractions of Ni-batch purification; I - input (for SEC); M - protein marker in kDa; A5-C8 - SEC fractions.

A.2. Testexpression of ATG7 in insect cells

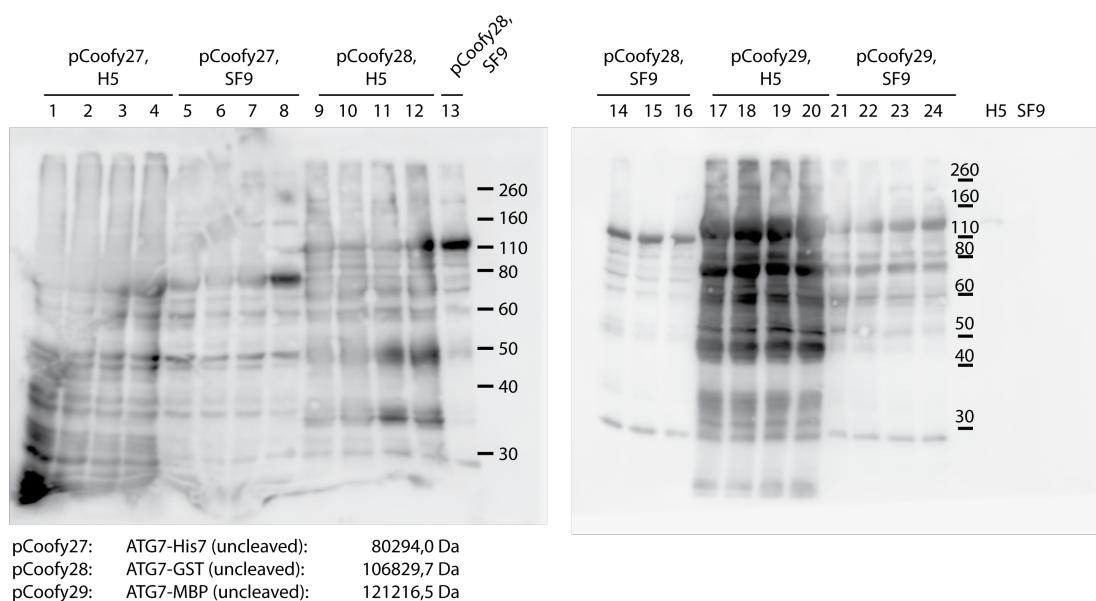


Figure A.2.: Immunoblot of ATG7 test expression results with Anti-ATG7 antibody, samples provided by the Biochemistry Core Facility. ATG7 was cloned into three vectors containing different affinity tags, suitable for insect cell expression: pCoofy27 (His-tag), pCoofy28 (GST-tag), and pCoofy29 (MBP-tag). SF9 and H5 represent different insect cell lines for recombinant protein expression. Ascending numbers indicate used BIIC dilutions: 1:500, 1:1000, 1:2000, 1:4000 (1-4, 5-8, . . .). Here, best results were obtained in SF9 cells, either from pCoofy27 (lane8) or from pCoofy28 (lane16).

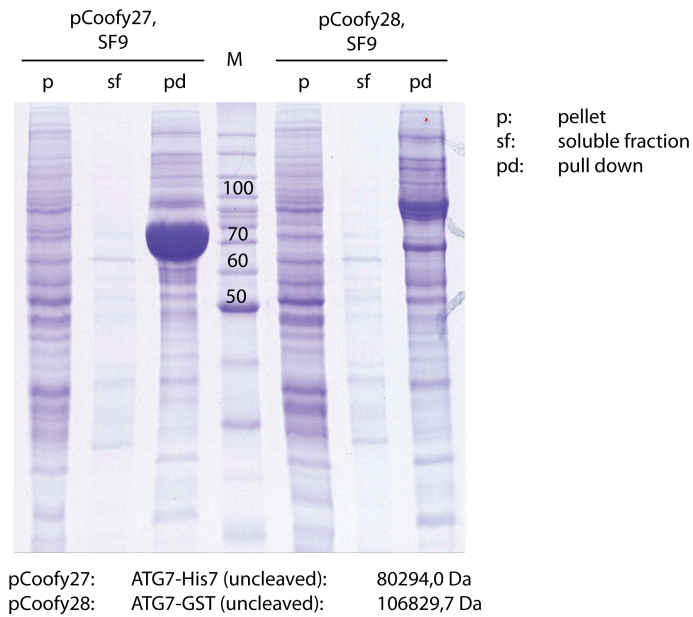


Figure A.3.: 10% SDS-PAGE gel of ATG7 medium scale test expression and pull-down from samples 8 and 16 in figure A.2. Protein amount was higher from pCoofy27 expression compared to pCoofy28 (large protein band between 70 and 80 kDa).

A.3. Testexpression of ATG16L1 in insect cells

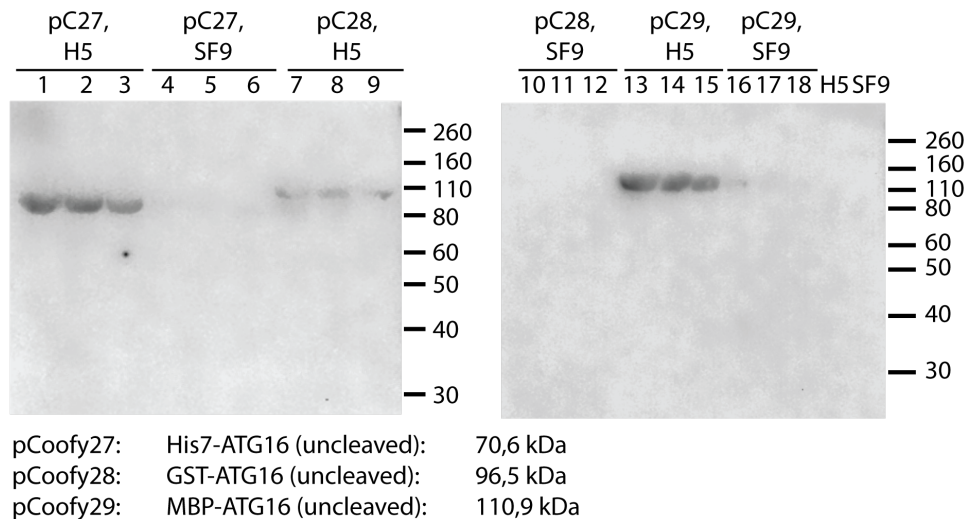


Figure A.4.: Immunoblot of ATG16 test expression results with Anti-His antibody, samples provided by the Biochemistry Core Facility. ATG16 was cloned into three vectors containing different affinity tags, suitable for insect cell expression: pCoofy27 (His-tag), pCoofy28 (GST-tag), and pCoofy29 (MBP-tag). SF9 and H5 insect cell lines were tested. Ascending numbers indicate used BIIC dilutions: 1:1000, 1:2000, 1:4000. Here, best results were obtained in H5 cells, either from pCoofy27 (lane1) or from pCoofy29 (lane13).

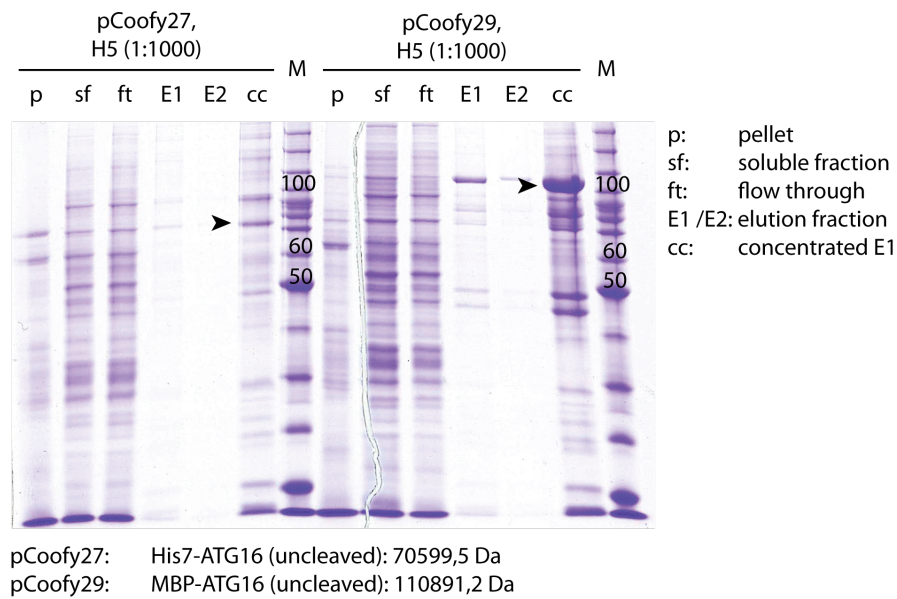


Figure A.5.: 10% SDS-PAGE gel of ATG16 medium scale test expression and pull-down from samples 1 and 13 in figure A.4. More protein was obtained from pCoofy29 expression compared to pCoofy27 (arrow heads).

A.4. Additional lipidation experiments

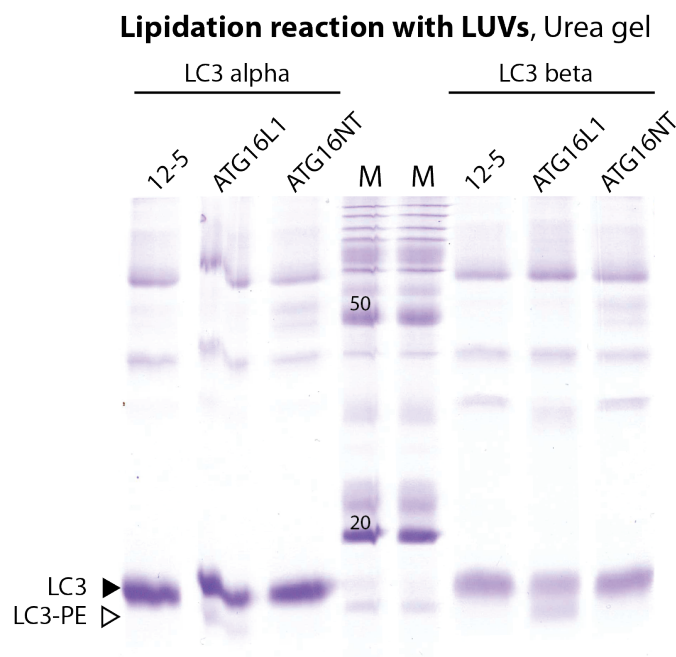


Figure A.6.: Lipidation reaction with large unilamellar vesicles (LUVs). The lower band in the reactions with ATG16L1 displays LC3-PE. However, the peptide ATG16NT(11-43) was not functional.

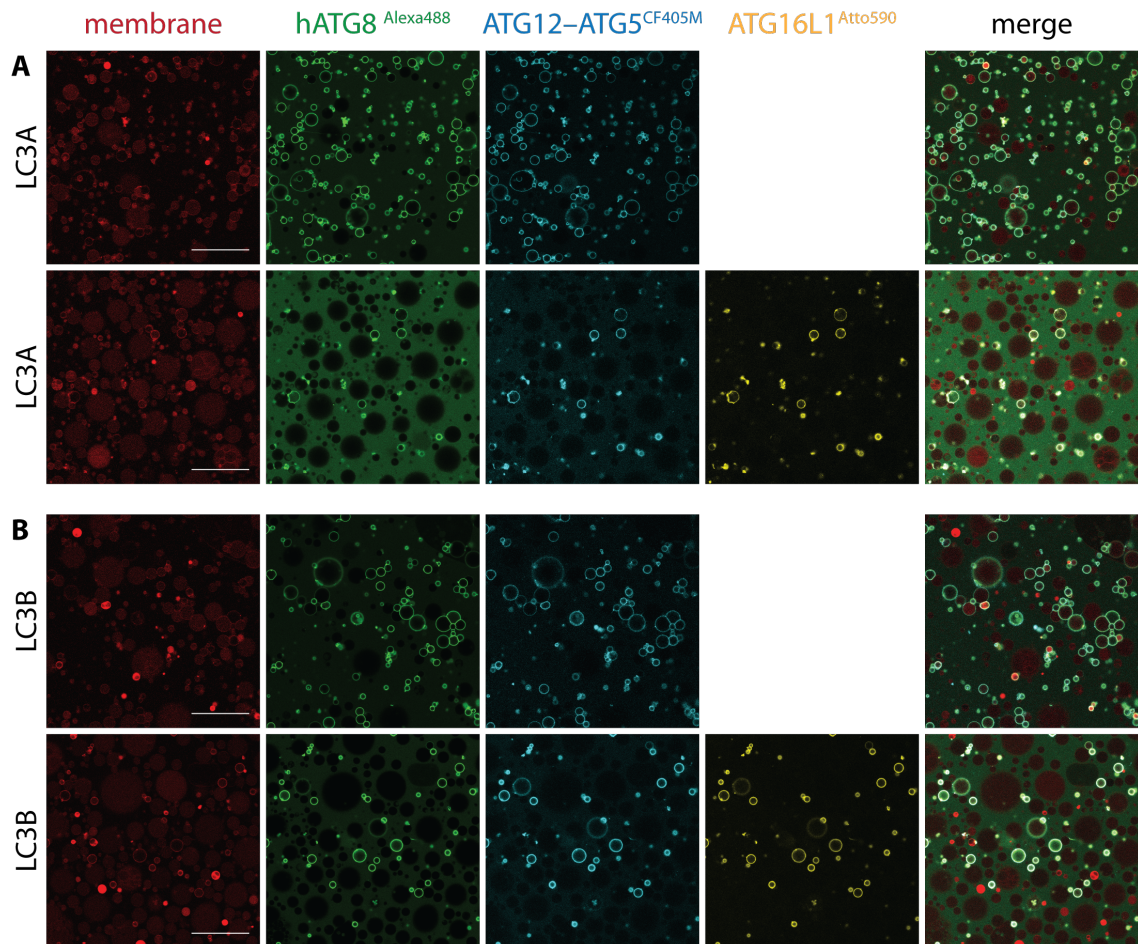


Figure A.7.: The labeling of ATG16L1 with Atto590 seemed to impair the conjugation efficiency of the reaction. The quantity of lipidated GUVs (GUVs with bright rims in merge panel) decreased in samples with labeled ATG16L1. (A) Reaction set up with LC3A, (B) reaction with LC3B. Scale bar 50 μm .

A.5. Non-starved yeast cells imaged with electron microscopy

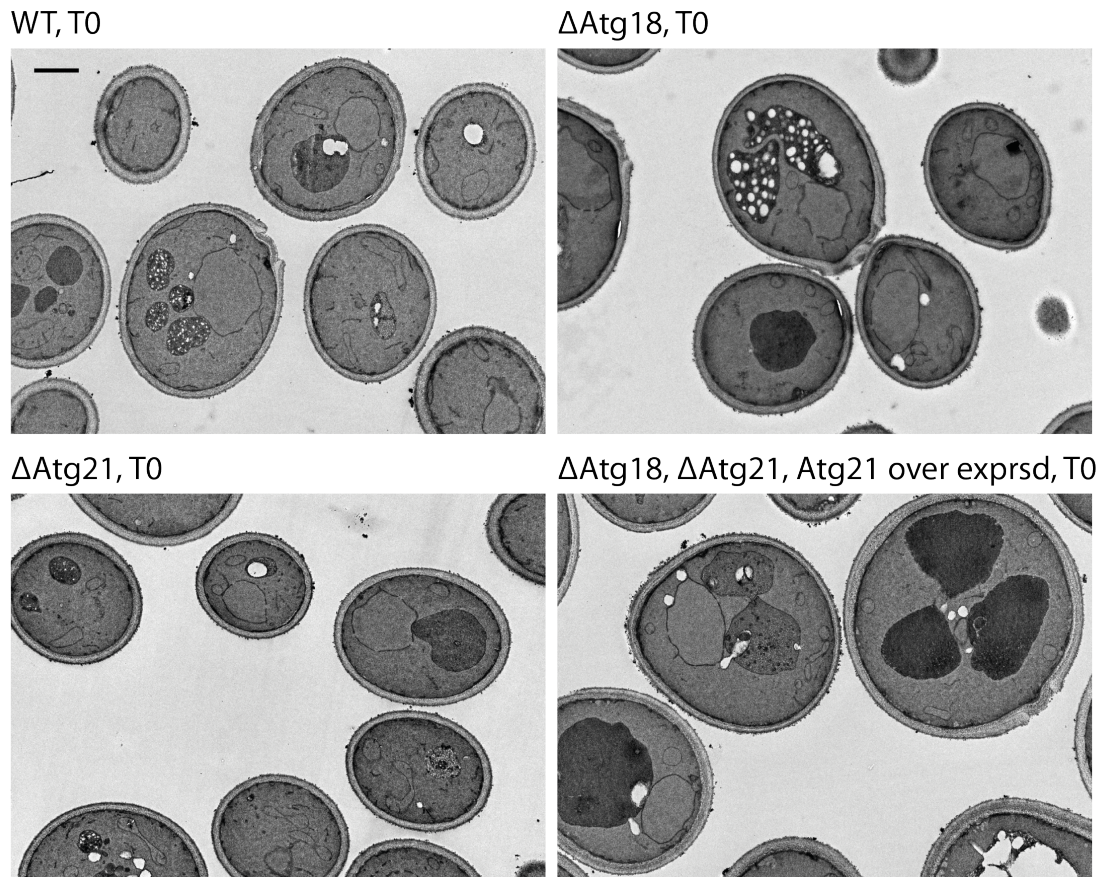


Figure A.8.: Transmission electron microscopy images of whole yeast cells with pep4 deletion in vegetative conditions, corresponding samples as in Fig. 3.7. (**WT**) Wildtype cells, carrying only the pep4 deletion. (**Δ Atg18**) cells knocked out for Atg18. Sometimes the vacuole shows accumulation of small lipid droplets (light structures). (**Δ Atg21**) Cells with Atg21 knockout (**Δ Atg18, Δ Atg21, Atg21 over exprsd**) cells with double knockout of Atg18 and Atg21, overexpressing Atg21. Scale bar 1 μ m.

References

- Alemu, E. A. et al. (2012). “ATG8 family proteins act as scaffolds for assembly of the ULK complex: sequence requirements for LC3-interacting region (LIR) motifs.” *J Biol Chem* 287.47, pp. 39275–39290.
- Axe, E. L. et al. (2008). “Autophagosome formation from membrane compartments enriched in phosphatidylinositol 3-phosphate and dynamically connected to the endoplasmic reticulum.” *J Cell Biol* 182.4, pp. 685–701.
- Baba, M., M. Osumi, S. V. Scott, D. J. Klionsky, and Y. Ohsumi (1997). “Two distinct pathways for targeting proteins from the cytoplasm to the vacuole/lysosome.” *J Cell Biol* 139.7, pp. 1687–1695.
- Balderhaar, H. J. k. and C. Ungermann (2013). “CORVET and HOPS tethering complexes - coordinators of endosome and lysosome fusion.” *J Cell Sci* 126.Pt 6, pp. 1307–1316.
- Barrowman, J., D. Bhandari, K. Reinisch, and S. Ferro-Novick (2010). “TRAPP complexes in membrane traffic: convergence through a common Rab.” *Nat Rev Mol Cell Biol* 11.11, pp. 759–763.
- Beck, R. et al. (2008). “Membrane curvature induced by Arf1-GTP is essential for vesicle formation.” *Proc Natl Acad Sci U S A* 105.33, pp. 11731–11736.
- Behrends, C., M. E. Sowa, S. P. Gygi, and J. W. Harper (2010). “Network organization of the human autophagy system.” *Nature* 466.7302, pp. 68–76.
- Bertani, G. (1951). “Studies on lysogenesis. I. The mode of phage liberation by lysogenic *Escherichia coli*.” *J Bacteriol* 62.3, pp. 293–300.
- Betaneli, V., R. Worch, and P. Schwille (2012). “Effect of temperature on the formation of liquid phase-separating giant unilamellar vesicles (GUV).” *Chem Phys Lipids* 165.6, pp. 630–637.
- Binnig, Quate, and Gerber (1986). “Atomic force microscope.” *Phys Rev Lett* 56.9, pp. 930–933.
- Boada-Romero, E. et al. (2013). “TMEM59 defines a novel ATG16L1-binding motif that promotes local activation of LC3.” *EMBO J* 32.4, pp. 566–582.
- Cann, G. M. et al. (2008). “Developmental expression of LC3alpha and beta: absence of fibronectin or autophagy phenotype in LC3beta knockout mice.” *Dev Dyn* 237.1, pp. 187–195.
- Cebollero, E., A. van der Vaart, and F. Reggiori (2012). “Understanding phosphatidylinositol-3-phosphate dynamics during autophagosome biogenesis.” *Autophagy* 8.12, pp. 1868–1870.

- Chang, C.-Y. and W.-P. Huang (2007). “Atg19 mediates a dual interaction cargo sorting mechanism in selective autophagy.” *Mol Biol Cell* 18.3, pp. 919–929.
- Chen, D. et al. (2012). “A mammalian autophagosome maturation mechanism mediated by TECPR1 and the Atg12-Atg5 conjugate.” *Mol Cell* 45.5, pp. 629–641.
- Chen, Y. and D. J. Klionsky (2011). “The regulation of autophagy - unanswered questions.” *J Cell Sci* 124.Pt 2, pp. 161–170.
- Chiantia, S., N. Kahya, and P. Schwille (2005). “Dehydration damage of domain-exhibiting supported bilayers: an AFM study on the protective effects of disaccharides and other stabilizing substances.” *Langmuir* 21.14, pp. 6317–6323.
- Coyle, J. E., S. Qamar, K. R. Rajashankar, and D. B. Nikolov (2002). “Structure of GABARAP in two conformations: implications for GABA(A) receptor localization and tubulin binding.” *Neuron* 33.1, pp. 63–74.
- De Duve, C. and R. Wattiaux (1966). “Functions of lysosomes.” *Annu Rev Physiol* 28, pp. 435–492.
- Dice, J. F. (1990). “Peptide sequences that target cytosolic proteins for lysosomal proteolysis.” *Trends Biochem Sci* 15.8, pp. 305–309.
- Djouder, N. et al. (2010). “PKA phosphorylates and inactivates AMPKalpha to promote efficient lipolysis.” *EMBO J* 29.2, pp. 469–481.
- Dooley, H. C. et al. (2014). “WIPI2 links LC3 conjugation with PI3P, autophagosome formation, and pathogen clearance by recruiting Atg12-5-16L1.” *Mol Cell* 55.2, pp. 238–252.
- Dunn Jr, W. A. et al. (2005). “Pexophagy: the selective autophagy of peroxisomes.” *Autophagy* 1.2, pp. 75–83.
- Faini, M., R. Beck, F. T. Wieland, and J. A. G. Briggs (2013). “Vesicle coats: structure, function, and general principles of assembly.” *Trends Cell Biol* 23.6, pp. 279–288.
- Faini, M. et al. (2012). “The structures of COPI-coated vesicles reveal alternate coatomer conformations and interactions.” *Science* 336.6087, pp. 1451–1454.
- Fotin, A. et al. (2004). “Molecular model for a complete clathrin lattice from electron cryomicroscopy.” *Nature* 432.7017, pp. 573–579.
- Fujioka, Y., N. N. Noda, H. Nakatogawa, Y. Ohsumi, and F. Inagaki (2010). “Dimeric coiled-coil structure of *Saccharomyces cerevisiae* Atg16 and its functional significance in autophagy.” *J Biol Chem* 285.2, pp. 1508–1515.
- Fujita, N. et al. (2008a). “An Atg4B mutant hampers the lipidation of LC3 paralogues and causes defects in autophagosome closure.” *Mol Biol Cell* 19.11, pp. 4651–4659.

- Fujita, N. et al. (2008b). “The Atg16L complex specifies the site of LC3 lipidation for membrane biogenesis in autophagy.” *Mol Biol Cell* 19.5, pp. 2092–2100.
- Fukuda, M. and T. Itoh (2008). “Direct link between Atg protein and small GTPase Rab: Atg16L functions as a potential Rab33 effector in mammals.” *Autophagy* 4.6, pp. 824–826.
- Geng, J., M. Baba, U. Nair, and D. J. Klionsky (2008). “Quantitative analysis of autophagy-related protein stoichiometry by fluorescence microscopy.” *J Cell Biol* 182.1, pp. 129–140.
- Graef, M., J. R. Friedman, C. Graham, M. Babu, and J. Nunnari (2013). “ER exit sites are physical and functional core autophagosome biogenesis components.” *Mol Biol Cell* 24.18, pp. 2918–2931.
- Guan, J. et al. (2001). “Cvt18/Gsa12 is required for cytoplasm-to-vacuole transport, pexophagy, and autophagy in *Saccharomyces cerevisiae* and *Pichia pastoris*.” *Mol Biol Cell* 12.12, pp. 3821–3838.
- Gutierrez, M. G., D. B. Munafó, W. Berón, and M. I. Colombo (2004). “Rab7 is required for the normal progression of the autophagic pathway in mammalian cells.” *J Cell Sci* 117.Pt 13, pp. 2687–2697.
- Hampe, J. et al. (2007). “A genome-wide association scan of nonsynonymous SNPs identifies a susceptibility variant for Crohn disease in ATG16L1.” *Nat Genet* 39.2, pp. 207–211.
- Hanada, T. et al. (2007). “The Atg12-Atg5 conjugate has a novel E3-like activity for protein lipidation in autophagy.” *J Biol Chem* 282.52, pp. 37298–37302.
- Hanahan, D. (1983). “Studies on transformation of *Escherichia coli* with plasmids.” *J Mol Biol* 166.4, pp. 557–580.
- Harding, T. M., K. A. Morano, S. V. Scott, and D. J. Klionsky (1995). “Isolation and characterization of yeast mutants in the cytoplasm to vacuole protein targeting pathway.” *J Cell Biol* 131.3, pp. 591–602.
- Hayashi-Nishino, M. et al. (2009). “A subdomain of the endoplasmic reticulum forms a cradle for autophagosome formation.” *Nat Cell Biol* 11.12, pp. 1433–1437.
- Heinemann, F. and P. Schwillle (2011). “Preparation of micrometer-sized free-standing membranes.” *Chemphyschem* 12.14, pp. 2568–2571.
- Huang, J. and D. J. Klionsky (2007). “Autophagy and human disease.” *Cell Cycle* 6.15, pp. 1837–1849.
- Hurley, J. H. and B. A. Schulman (2014). “Atomistic autophagy: the structures of cellular self-digestion.” *Cell* 157.2, pp. 300–311.
- Ichimura, Y. et al. (2004). “In vivo and in vitro reconstitution of Atg8 conjugation essential for autophagy.” *J Biol Chem* 279.39, pp. 40584–40592.

- Ichimura, Y. et al. (2000). “A ubiquitin-like system mediates protein lipidation.” *Nature* 408.6811, pp. 488–492.
- Ishibashi, K. et al. (2011). “Atg16L2, a novel isoform of mammalian Atg16L that is not essential for canonical autophagy despite forming an Atg12–5–16L2 complex.” *Autophagy* 7.12, pp. 1500–1513.
- Itakura, E., C. Kishi-Itakura, and N. Mizushima (2012). “The hairpin-type tail-anchored SNARE syntaxin 17 targets to autophagosomes for fusion with endosomes/lysosomes.” *Cell* 151.6, pp. 1256–1269.
- Itoh, T. et al. (2008). “Golgi-resident small GTPase Rab33B interacts with Atg16L and modulates autophagosome formation.” *Mol Biol Cell* 19.7, pp. 2916–2925.
- Jiang, P. et al. (2014). “The HOPS complex mediates autophagosome-lysosome fusion through interaction with syntaxin 17.” *Mol Biol Cell* 25.8, pp. 1327–1337.
- Juhasz, G. and T. P. Neufeld (2006). “Autophagy: a forty-year search for a missing membrane source.” *PLoS Biol* 4.2, e36.
- Jung, C. H. et al. (2009). “ULK-Atg13-FIP200 complexes mediate mTOR signaling to the autophagy machinery.” *Mol Biol Cell* 20.7, pp. 1992–2003.
- Juris, L. et al. (2015). “PI3P binding by Atg21 organises Atg8 lipidation.” *EMBO J* 34.7, pp. 955–973.
- Kabeya, Y. et al. (2004). “LC3, GABARAP and GATE16 localize to autophagosomal membrane depending on form-II formation.” *J Cell Sci* 117.Pt 13, pp. 2805–2812.
- Kabeya, Y. et al. (2000). “LC3, a mammalian homologue of yeast Apg8p, is localized in autophagosome membranes after processing.” *EMBO J* 19.21, pp. 5720–5728.
- Kang, R., H. J. Zeh, M. T. Lotze, and D. Tang (2011). “The Beclin 1 network regulates autophagy and apoptosis.” *Cell Death Differ* 18.4, pp. 571–580.
- Kihara, A., T. Noda, N. Ishihara, and Y. Ohsumi (2001). “Two distinct Vps34 phosphatidylinositol 3-kinase complexes function in autophagy and carboxypeptidase Y sorting in *Saccharomyces cerevisiae*.” *J Cell Biol* 152.3, pp. 519–530.
- Kirchhausen, T. and S. C. Harrison (1984). “Structural domains of clathrin heavy chains.” *J Cell Biol* 99.5, pp. 1725–1734.
- Kirisako, T. et al. (1999). “Formation process of autophagosome is traced with Apg8/Aut7p in yeast.” *J Cell Biol* 147.2, pp. 435–446.
- Kirisako, T. et al. (2000). “The reversible modification regulates the membrane-binding state of Apg8/Aut7 essential for autophagy and the cytoplasm to vacuole targeting pathway.” *J Cell Biol* 151.2, pp. 263–276.
- Klionsky, D. J. and Y. Ohsumi (1999). “Vacuolar import of proteins and organelles from the cytoplasm.” *Annu Rev Cell Dev Biol* 15, pp. 1–32.

- Klionsky, D. J. et al. (2003). “A unified nomenclature for yeast autophagy-related genes.” *Dev Cell* 5.4, pp. 539–545.
- Komatsu, M. et al. (2005). “Impairment of starvation-induced and constitutive autophagy in Atg7-deficient mice.” *J Cell Biol* 169.3, pp. 425–434.
- Kraft, C. et al. (2012). “Binding of the Atg1/ULK1 kinase to the ubiquitin-like protein Atg8 regulates autophagy.” *EMBO J* 31.18, pp. 3691–3703.
- Krick, R., J. Tolstrup, A. Appelles, S. Henke, and M. Thumm (2006). “The relevance of the phosphatidylinositolphosphat-binding motif FRRGT of Atg18 and Atg21 for the Cvt pathway and autophagy.” *FEBS Lett* 580.19, pp. 4632–4638.
- Kuma, A., N. Mizushima, N. Ishihara, and Y. Ohsumi (2002). “Formation of the approximately 350-kDa Apg12-Apg5-Apg16 multimeric complex, mediated by Apg16 oligomerization, is essential for autophagy in yeast.” *J Biol Chem* 277.21, pp. 18619–18625.
- Kuma, A. et al. (2004). “The role of autophagy during the early neonatal starvation period.” *Nature* 432.7020, pp. 1032–1036.
- Kuznetsov, S. A. and V. I. Gelfand (1987). “18 kDa microtubule-associated protein: identification as a new light chain (LC-3) of microtubule-associated protein 1 (MAP-1).” *FEBS Lett* 212.1, pp. 145–148.
- Le Bars, R., J. Marion, R. Le Borgne, B. Satiat-Jeunemaitre, and M. W. Bianchi (2014). “ATG5 defines a phagophore domain connected to the endoplasmic reticulum during autophagosome formation in plants.” *Nat Commun* 5, p. 4121.
- Legesse-Miller, A., Y. Sagiv, A. Porat, and Z. Elazar (1998). “Isolation and characterization of a novel low molecular weight protein involved in intra-Golgi traffic.” *J Biol Chem* 273.5, pp. 3105–3109.
- Lemasters, J. J. (2005). “Selective mitochondrial autophagy, or mitophagy, as a targeted defense against oxidative stress, mitochondrial dysfunction, and aging.” *Rejuvenation Res* 8.1, pp. 3–5.
- Levine, B. and J. Yuan (2005). “Autophagy in cell death: an innocent convict?” *J Clin Invest* 115.10, pp. 2679–2688.
- Li, M. Z. and S. J. Elledge (2007). “Harnessing homologous recombination in vitro to generate recombinant DNA via SLIC.” *Nat Methods* 4.3, pp. 251–256.
- Lum, J. J. et al. (2005). “Growth factor regulation of autophagy and cell survival in the absence of apoptosis.” *Cell* 120.2, pp. 237–248.
- Lynch-Day, M. A. et al. (2010). “Trs85 directs a Ypt1 GEF, TRAPPIII, to the phagophore to promote autophagy.” *Proc Natl Acad Sci U S A* 107.17, pp. 7811–7816.

- Manil-Ségalen, M. et al. (2014). “The *C. elegans* LC3 acts downstream of GABARAP to degrade autophagosomes by interacting with the HOPS subunit VPS39.” *Dev Cell* 28.1, pp. 43–55.
- Mann, S. S. and J. A. Hammarback (1994). “Molecular characterization of light chain 3. A microtubule binding subunit of MAP1A and MAP1B.” *J Biol Chem* 269.15, pp. 11492–11497.
- Massey, A., R. Kiffin, and A. M. Cuervo (2004). “Pathophysiology of chaperone-mediated autophagy.” *Int J Biochem Cell Biol* 36.12, pp. 2420–2434.
- Mauthe, M. et al. (2011). “Resveratrol-mediated autophagy requires WIPI-1-regulated LC3 lipidation in the absence of induced phagophore formation.” *Autophagy* 7.12, pp. 1448–1461.
- Mavrakis, M., J. Lippincott-Schwartz, C. A. Stratakis, and I. Bossis (2006). “Depletion of type IA regulatory subunit (RI α) of protein kinase A (PKA) in mammalian cells and tissues activates mTOR and causes autophagic deficiency.” *Hum Mol Genet* 15.19, pp. 2962–2971.
- McEwan, D. G. et al. (2015). “PLEKHM1 regulates autophagosome-lysosome fusion through HOPS complex and LC3/GABARAP proteins.” *Mol Cell* 57.1, pp. 39–54.
- Mijaljica, D., M. Prescott, and R. J. Devenish (2011). “Microautophagy in mammalian cells: revisiting a 40-year-old conundrum.” *Autophagy* 7.7, pp. 673–682.
- Miyata, Y., T. Shibata, M. Aoshima, T. Tsubata, and E. Nishida (2014). “The molecular chaperone TRiC/CCT binds to the Trp-Asp 40 (WD40) repeat protein WDR68 and promotes its folding, protein kinase DYRK1A binding, and nuclear accumulation.” *J Biol Chem* 289.48, pp. 33320–33332.
- Mizushima, N. (2005). “The pleiotropic role of autophagy: from protein metabolism to bactericide.” *Cell Death Differ* 12 Suppl 2, pp. 1535–1541.
- Mizushima, N., H. Sugita, T. Yoshimori, and Y. Ohsumi (1998a). “A new protein conjugation system in human. The counterpart of the yeast Apg12p conjugation system essential for autophagy.” *J Biol Chem* 273.51, pp. 33889–33892.
- Mizushima, N. (2010). “The role of the Atg1/ULK1 complex in autophagy regulation.” *Curr Opin Cell Biol* 22.2, pp. 132–139.
- Mizushima, N., B. Levine, A. M. Cuervo, and D. J. Klionsky (2008). “Autophagy fights disease through cellular self-digestion.” *Nature* 451.7182, pp. 1069–1075.
- Mizushima, N., A. Yamamoto, M. Matsui, T. Yoshimori, and Y. Ohsumi (2004). “In vivo analysis of autophagy in response to nutrient starvation using transgenic mice expressing a fluorescent autophagosome marker.” *Mol Biol Cell* 15.3, pp. 1101–1111.

- Mizushima, N. et al. (2003). “Mouse Apg16L, a novel WD-repeat protein, targets to the autophagic isolation membrane with the Apg12-Apg5 conjugate.” *J Cell Sci* 116.Pt 9, pp. 1679–1688.
- Mizushima, N. et al. (1998b). “A protein conjugation system essential for autophagy.” *Nature* 395.6700, pp. 395–398.
- Mizushima, N. et al. (2001). “Dissection of autophagosome formation using Apg5-deficient mouse embryonic stem cells.” *J Cell Biol* 152.4, pp. 657–668.
- Moreau, K., B. Ravikumar, M. Renna, C. Puri, and D. C. Rubinsztein (2011). “Autophagosome precursor maturation requires homotypic fusion.” *Cell* 146.2, pp. 303–317.
- Nair, U. et al. (2011). “SNARE proteins are required for macroautophagy.” *Cell* 146.2, pp. 290–302.
- Nair, U. et al. (2012). “A role for Atg8-PE deconjugation in autophagosome biogenesis.” *Autophagy* 8.5, pp. 780–793.
- Nakagawa, I. et al. (2004). “Autophagy defends cells against invading group A *Streptococcus*.” *Science* 306.5698, pp. 1037–1040.
- Nakatogawa, H., Y. Ichimura, and Y. Ohsumi (2007). “Atg8, a ubiquitin-like protein required for autophagosome formation, mediates membrane tethering and hemifusion.” *Cell* 130.1, pp. 165–178.
- Nakatogawa, H. and Y. Ohsumi (2012a). “SDS-PAGE techniques to study ubiquitin-like conjugation systems in yeast autophagy.” *Methods Mol Biol* 832, pp. 519–529.
- Nakatogawa, H., K. Suzuki, Y. Kamada, and Y. Ohsumi (2009). “Dynamics and diversity in autophagy mechanisms: lessons from yeast.” *Nat Rev Mol Cell Biol* 10.7, pp. 458–467.
- Nakatogawa, H. et al. (2012b). “The autophagy-related protein kinase Atg1 interacts with the ubiquitin-like protein Atg8 via the Atg8 family interacting motif to facilitate autophagosome formation.” *J Biol Chem* 287.34, pp. 28503–28507.
- Nath, S. et al. (2014). “Lipidation of the LC3/GABARAP family of autophagy proteins relies on a membrane-curvature-sensing domain in Atg3.” *Nat Cell Biol* 16.5, pp. 415–424.
- Neely, A. N., P. B. Nelson, and G. E. Mortimore (1974). “Osmotic alterations of the lysosomal system during rat liver perfusion: reversible suppression by insulin and amino acids”. *Biochimica et Biophysica Acta (BBA)-General Subjects* 338.2, pp. 458–472.

- Nemos, C. et al. (2003). “Expression of *gcl1*/GABARAPL1 versus GABARAP mRNAs in human: predominance of *gcl1*/GABARAPL1 in the central nervous system.” *Brain Res Mol Brain Res* 119.2, pp. 216–219.
- Noda, N. N. et al. (2008). “Structural basis of target recognition by Atg8/LC3 during selective autophagy.” *Genes Cells* 13.12, pp. 1211–1218.
- Noda, T. et al. (2000). “Apg9p/Cvt7p is an integral membrane protein required for transport vesicle formation in the Cvt and autophagy pathways.” *J Cell Biol* 148.3, pp. 465–480.
- Obara, K., T. Noda, K. Niimi, and Y. Ohsumi (2008). “Transport of phosphatidylinositol 3-phosphate into the vacuole via autophagic membranes in *Saccharomyces cerevisiae*.” *Genes Cells* 13.6, pp. 537–547.
- O’Sullivan, G. A., M. Kneussel, Z. Elazar, and H. Betz (2005). “GABARAP is not essential for GABA receptor targeting to the synapse.” *Eur J Neurosci* 22.10, pp. 2644–2648.
- Otomo, C., Z. Metlagel, G. Takaesu, and T. Otomo (2013). “Structure of the human ATG12 ATG5 conjugate required for LC3 lipidation in autophagy.” *Nat Struct Mol Biol* 20.1, pp. 59–66.
- Pankiv, S. et al. (2007). “p62/SQSTM1 binds directly to Atg8/LC3 to facilitate degradation of ubiquitinated protein aggregates by autophagy.” *J Biol Chem* 282.33, pp. 24131–24145.
- Pankiv, S. et al. (2010). “FYCO1 is a Rab7 effector that binds to LC3 and PI3P to mediate microtubule plus end-directed vesicle transport.” *J Cell Biol* 188.2, pp. 253–269.
- Pattingre, S. et al. (2005). “Bcl-2 antiapoptotic proteins inhibit Beclin 1-dependent autophagy.” *Cell* 122.6, pp. 927–939.
- Paz, Y., Z. Elazar, and D. Fass (2000). “Structure of GATE-16, membrane transport modulator and mammalian ortholog of autophagocytosis factor Aut7p.” *J Biol Chem* 275.33, pp. 25445–25450.
- Polson, H. E. J. et al. (2010). “Mammalian Atg18 (WIPI2) localizes to omegasome-anchored phagophores and positively regulates LC3 lipidation.” *Autophagy* 6.4, pp. 506–522.
- Proikas-Cezanne, T., Z. Takacs, P. Dönnies, and O. Kohlbacher (2015). “WIPI proteins: essential PtdIns3P effectors at the nascent autophagosome.” *J Cell Sci* 128.2, pp. 207–217.
- Ragusa, M. J., R. E. Stanley, and J. H. Hurley (2012). “Architecture of the Atg17 complex as a scaffold for autophagosome biogenesis.” *Cell* 151.7, pp. 1501–1512.

- Rioux, J. D. et al. (2007). “Genome-wide association study identifies new susceptibility loci for Crohn disease and implicates autophagy in disease pathogenesis.” *Nat Genet* 39.5, pp. 596–604.
- Roberts, P. et al. (2003). “Piecemeal microautophagy of nucleus in *Saccharomyces cerevisiae*.” *Mol Biol Cell* 14.1, pp. 129–141.
- Saitoh, T. et al. (2008). “Loss of the autophagy protein Atg16L1 enhances endotoxin-induced IL-1beta production.” *Nature* 456.7219, pp. 264–268.
- Schindelin, J. et al. (2012). “Fiji: an open-source platform for biological-image analysis.” *Nat Methods* 9.7, pp. 676–682.
- Scholz, J., H. Besir, C. Strasser, and S. Suppmann (2013). “A new method to customize protein expression vectors for fast, efficient and background free parallel cloning.” *BMC Biotechnol* 13, p. 12.
- Scott, S. V. et al. (2000). “Apg13p and Vac8p are part of a complex of phosphoproteins that are required for cytoplasm to vacuole targeting.” *J Biol Chem* 275.33, pp. 25840–25849.
- Sekito, T., T. Kawamata, R. Ichikawa, K. Suzuki, and Y. Ohsumi (2009). “Atg17 recruits Atg9 to organize the pre-autophagosomal structure.” *Genes Cells* 14.5, pp. 525–538.
- Shibutani, S. T. and T. Yoshimori (2014). “A current perspective of autophagosome biogenesis.” *Cell Res* 24.1, pp. 58–68.
- Shpilka, T., H. Weidberg, S. Pietrokovski, and Z. Elazar (2011). “Atg8: an autophagy-related ubiquitin-like protein family.” *Genome Biol* 12.7, p. 226.
- Smith, T. F., C. Gaitatzes, K. Saxena, and E. J. Neer (1999). “The WD repeat: a common architecture for diverse functions.” *Trends Biochem Sci* 24.5, pp. 181–185.
- Sonnleitner, A., G. J. Schütz, and T. Schmidt (1999). “Free Brownian motion of individual lipid molecules in biomembranes.” *Biophys J* 77.5, pp. 2638–2642.
- Sou, Y.-s. et al. (2008). “The Atg8 conjugation system is indispensable for proper development of autophagic isolation membranes in mice.” *Mol Biol Cell* 19.11, pp. 4762–4775.
- Stagg, S. M. et al. (2006). “Structure of the Sec13/31 COPII coat cage.” *Nature* 439.7073, pp. 234–238.
- Stephan, J. S., Y.-Y. Yeh, V. Ramachandran, S. J. Deminoff, and P. K. Herman (2009). “The Tor and PKA signaling pathways independently target the Atg1/Atg13 protein kinase complex to control autophagy.” *Proc Natl Acad Sci U S A* 106.40, pp. 17049–17054.

- Stephan, J. S., Y.-Y. Yeh, V. Ramachandran, S. J. Deminoff, and P. K. Herman (2010). “The Tor and cAMP-dependent protein kinase signaling pathways coordinately control autophagy in *Saccharomyces cerevisiae*.” *Autophagy* 6.2, pp. 294–295.
- Sugawara, K. et al. (2004). “The crystal structure of microtubule-associated protein light chain 3, a mammalian homologue of *Saccharomyces cerevisiae* Atg8.” *Genes Cells* 9.7, pp. 611–618.
- Suzuki, K., M. Akioka, C. Kondo-Kakuta, H. Yamamoto, and Y. Ohsumi (2013). “Fine mapping of autophagy-related proteins during autophagosome formation in *Saccharomyces cerevisiae*.” *J Cell Sci* 126.Pt 11, pp. 2534–2544.
- Suzuki, K., C. Kondo, M. Morimoto, and Y. Ohsumi (2010). “Selective transport of alpha-mannosidase by autophagic pathways: identification of a novel receptor, Atg34p.” *J Biol Chem* 285.39, pp. 30019–30025.
- Suzuki, K., Y. Kubota, T. Sekito, and Y. Ohsumi (2007). “Hierarchy of Atg proteins in pre-autophagosomal structure organization.” *Genes Cells* 12.2, pp. 209–218.
- Suzuki, K. et al. (2001). “The pre-autophagosomal structure organized by concerted functions of APG genes is essential for autophagosome formation.” *EMBO J* 20.21, pp. 5971–5981.
- Szalai, P. et al. (2015). “Autophagic bulk sequestration of cytosolic cargo is independent of LC3, but requires GABARAPs.” *Exp Cell Res* 333.1, pp. 21–38.
- Tai, H.-C. and E. M. Schuman (2008). “Ubiquitin, the proteasome and protein degradation in neuronal function and dysfunction.” *Nat Rev Neurosci* 9.11, pp. 826–838.
- Takáts, S. et al. (2013). “Autophagosomal Syntaxin17-dependent lysosomal degradation maintains neuronal function in *Drosophila*.” *J Cell Biol* 201.4, pp. 531–539.
- Takáts, S. et al. (2014). “Interaction of the HOPS complex with Syntaxin 17 mediates autophagosome clearance in *Drosophila*.” *Mol Biol Cell* 25.8, pp. 1338–1354.
- Tan, S. (2001). “A modular polycistronic expression system for overexpressing protein complexes in *Escherichia coli*.” *Protein Expr Purif* 21.1, pp. 224–234.
- Tartoff, K. and C. Hobbs (1987). “Improved media for growing plasmid and cosmid clones”. *Bethesda Res. Lab. Focus* 9.2, p. 12.
- Thumm, M. et al. (1994). “Isolation of autophagocytosis mutants of *Saccharomyces cerevisiae*.” *FEBS Lett* 349.2, pp. 275–280.
- Travassos, L. H. et al. (2010). “Nod1 and Nod2 direct autophagy by recruiting ATG16L1 to the plasma membrane at the site of bacterial entry.” *Nat Immunol* 11.1, pp. 55–62.

- Tsukada, M. and Y. Ohsumi (1993). “Isolation and characterization of autophagy-defective mutants of *Saccharomyces cerevisiae*.” *FEBS Lett* 333.1-2, pp. 169–174.
- von Muhlinen, N. et al. (2012). “LC3C, bound selectively by a noncanonical LIR motif in NDP52, is required for antibacterial autophagy.” *Mol Cell* 48.3, pp. 329–342.
- Wang, H., F. K. Bedford, N. J. Brandon, S. J. Moss, and R. W. Olsen (1999). “GABA(A)-receptor-associated protein links GABA(A) receptors and the cytoskeleton.” *Nature* 397.6714, pp. 69–72.
- Weidberg, H. et al. (2010). “LC3 and GATE-16/GABARAP subfamilies are both essential yet act differently in autophagosome biogenesis.” *EMBO J* 29.11, pp. 1792–1802.
- Weidberg, H. et al. (2011). “LC3 and GATE-16 N termini mediate membrane fusion processes required for autophagosome biogenesis.” *Dev Cell* 20.4, pp. 444–454.
- Weiergräber, O. H., D. Willbold, and J. Mohrlüder (2013). *Atg8 Family Proteins—Autophagy and Beyond*. INTECH Open Access Publisher.
- Wilkinson, D. S. et al. (2015). “Phosphorylation of LC3 by the Hippo kinases STK3/STK4 is essential for autophagy.” *Mol Cell* 57.1, pp. 55–68.
- Wright, R. (2000). “Transmission electron microscopy of yeast.” *Microsc Res Tech* 51.6, pp. 496–510.
- Xie, Z., U. Nair, and D. J. Klionsky (2008a). “Atg8 controls phagophore expansion during autophagosome formation.” *Mol Biol Cell* 19.8, pp. 3290–3298.
- Xie, Z., U. Nair, and D. J. Klionsky (2008b). “Dissecting autophagosome formation: the missing pieces.” *Autophagy* 4.7, pp. 920–922.
- Xin, Y. et al. (2001). “Cloning, expression patterns, and chromosome localization of three human and two mouse homologues of GABA(A) receptor-associated protein.” *Genomics* 74.3, pp. 408–413.
- Xu, Z., L. Yang, S. Xu, Z. Zhang, and Y. Cao (2015). “The receptor proteins: pivotal roles in selective autophagy.” *Acta Biochim Biophys Sin (Shanghai)*.
- Yamamoto, H. et al. (2012). “Atg9 vesicles are an important membrane source during early steps of autophagosome formation.” *J Cell Biol* 198.2, pp. 219–233.
- Zheng, H. et al. (2004). “Cloning and analysis of human Apg16L.” *DNA Seq* 15.4, pp. 303–305.

Acknowledgements

I would like to thank Barbara Conradt, who kindly agreed to be my Ph. D. supervisor, for being an enthusiastic TAC member, extremely helpful with all LMU-related issues, and for being a role model as passionate female scientist. Also I would like to thank Prof. Ott, who took the burden to be second reviewer for this thesis.

I would like to thank Thomas Wollert, for accepting me as his Ph. D. student, even though I was working in a quite unrelated field before. Thanks to his exceptional supervision, I had a fast start theoretically and methodologically in the field of autophagy and protein purification. Furthermore, his ability to see the full potential of scientific methods and data made the results presented here possible.

I would like to thank Henri for the great collaboration on AFM, especially for all the helpful tips on experiment conduction and moral support during late night experiments. Additionally, I would like to thank Lisa for her scientific contributions to the human autophagic protein systems, and the whole lab for suggestions on improving protein productions, as well as for company during lunch in Mensa.

Finally, I'm deeply grateful to Fabian, who put up with me during all the hard but also happy times during the last years. I'm very much looking forward to a long, joyful, and hopefully a bit more relaxed future with you.

Curriculum vitae

Anna Kaufmann

Nationality German
Date of birth 23rd of August 1983, Dresden, DE

Education

- 2012 - present **PhD student**, Max Planck Institute (MPI) of Biochemistry, Martinsried, DE;
Department for Molecular Membrane and Organelle Biology (Wollert);
Thesis title: *“In vitro reconstitution of the autophagic membrane scaffold”*
- 2010 - 2012 **PhD student**, MPI of Molecular Cell Biology and Genetics (MPI-CBG), Dresden;
Department for Quantitative Microscopy of Zebrafish Organogenesis (Huisken);
“Multi-layer mounting for Selective Plane Illumination Microscopy (SPIM)”
- 2005 - 2010 **Diploma in biology**, University of Bremen, DE; GPA: 1,0 with honors;
Specialized in cell biology, biophysics, microbiology & marine biology;
Diploma thesis: *“Influence of mutated Lamin A on nuclear mechanics investigated by Atomic Force Microscopy”*
- 2003 - 2005 **Prediploma in biology**, Eberhard Karls University, Tübingen, DE
1993 - 2003 **High school**, Dossenberger Gymnasium Günzburg, DE, GPA: 1,6

International Experience

- 08 / 2011 **Woods Hole, MA, U.S.A.**, *Zebrafish Development & Genetics course*
- 05 / 2011 **Oeiras, Portugal**, EMBO Workshop, *Biophysical Mechanisms in Development*
- 1999 / 2000 **Sacramento, CA, U.S.A.**, Student exchange year (Foothill High School)

Languages

German (native speaker), **English** (fluent oral and written), **French** (basic), **Latinum**

Further Work and Research Experience

10/2009-02/2010	Student assistant (lecture administration & tutor), University of Bremen
09/2007-06/2008	Student laboratory assistant , MPI of Marine Microbiology, Bremen
05/2007-07/2007	Student laboratory assistant , Biophysics Institute, University of Bremen
10/2007-02/2008	Math tutor for biology students, University of Bremen
10/2006-02/2007	Math tutor for biology students, University of Bremen
03/2006-05/2006	Student laboratory assistant , Alfred-Wegener-Institute, Bremerhaven

Awards & Honors

2014	1st Prize Roche pRED Oncology Award
2014	Merck Serono Innovation Cup (abstract selected from 700 applicants)
2014	Poster prize at conference “Interact 2014”
2011	Travel award Woods Hole, provided by Marine Biological Laboratory
2010	Membership international PhD program at MPI-CBG (5 % success rate)
1999	Arthur-Walter scholarship for exchange year in U.S.

Technical courses

01/2011	Statistics , MPI-CBG
2010	Biomaterials, Theoretical Biophysics, Developmental Genetics, Characterization of conditional knockout mice , Predoc Course, TU, Biotec & MPI-PKS, Dresden
12/2010	Introduction to Matlab Image Processing Toolbox , MPI-CBG
10/2010	Microscopy, Modeling & Biophysical Methods , EMBO Course, Heidelberg

Main methods

Molecular Biology & Biochemistry	Cloning, gel electrophoresis, Western Blot, recombinant protein expression and purification, chromatography, DLS, artificial membrane systems
Microscopy	Fluorescence confocal & light sheet microscopy (SPIM), FRAP, Atomic Force & Electron Microscopy

Work-related responsibilities

08/2013-12/2014	PhD representative at MPI of Biochemistry graduate school
2012-2014	Supervisor of master student, Organizer for open day
09/2011-02/2012	Mentor for high school students

Publications

Publications with published thesis parts

Anna Kaufmann, Viola Beier, Henri G. Franquelim, Thomas Wollert
“Molecular Mechanism of Autophagic Membrane-Scaffold Assembly and Disassembly”
Cell, 2014 (156), 469-81

Anna Kaufmann, Thomas Wollert
“Scaffolding the expansion of autophagosomes”
Autophagy, 2014 (10), 1343-45

Other publications

Anna Kaufmann*, Michaela Mickoleit*, Michael Weber*, Jan Huisken
“Multi-layer mounting enables long-term imaging of zebrafish development in a light sheet microscope”
Development, 2012 (139), 3242-47, *equal contribution

Anna Kaufmann, Fabian Heinemann, Manfred Radmacher, Reimer Stick
“Amphibian nuclei expressing lamin A with the progeria mutation E145K exhibit an increased elastic modulus”
Nucleus, 2011 (2), 310-19

F. Heinemann, M. Prabhune, **Anna Kaufmann**, M. Radmacher
“Cellular and Nuclear Mechanics Studied by Atomic Force Microscopy”
Imaging & Microscopy, 2010 (4), 22-24

H. Ploug, A. Terbruggen, **Anna Kaufmann**, D. Wolf-Gladrow, U. Passow
“A novel method to measure particle sinking velocity in vitro, and its comparison to three other in vitro methods”
Limnology and Oceanography: Methods, 2010 (8), 386-93